THEORY OF LATTICE EFFECTS ON
MAGNETIC INTERACTIONS IN SOLIDS

A Dissertation

presented to

the Faculty of the Graduate School

University of Missouri-Columbia

In Partial Fulfillment

of the Requirements for the Degree

of Doctor of Philosophy

by

Hakim Meskine

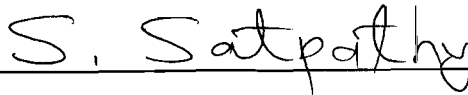Dr. Sashi Satpathy,   Dissertation Supervisor

DECEMBER 2005

The undersigned, appointed by the Dean of the Graduate School, have examined the dissertation entitled:

THEORY OF LATTICE EFFECTS ON
MAGNETIC INTERACTIONS IN SOLIDS

presented by Hakim Meskine
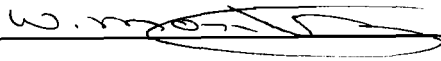
a candidate for the degree of Doctor of Philosophy

and hereby certify that in their opinion it is worthy of acceptance.
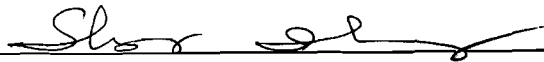
_____

Dr. Sashi Satpathy

_____

Dr. Asma Harcharras

_____

Dr. Wouter Montfrooij

_____

Dr. Carlos Wexler

_____

Dr. Shufeng Zhang

ACKNOWLEDGMENTS

Many people have shared the heavy burden of helping me obtain my doctoral degree. Foremost among them is my outstanding adviser, Professor Satpathy, whose constant encouragements have egged me forward. He has earned my respect and gratitude as a mentor, a researcher, as well as personal friend. I also wish to thank all the members of my committee for their very helpful questions and remarks, as well as their careful and patient reading of this document at various stages of its completion.

I must thank Dr. Zoran S. Popovic for his patience and helpfulness. Without Zoran's help learning the fundamentals of electronic structure theory would have been a much less enjoyable task. I am happy to count Zoran among my colleagues, but more importantly I consider him a friend.

My parents must come next, and in particular my father, Mr. Abderrahmane Meskine, whose example has always inspired me to excel. Their help in all areas of my life has forged my personality and I am deeply indebted to them. Their financial and emotional support, as well as honest and pointed advice, during the most difficult stages of my graduate life have been instrumental to my completing my degree.

Next, I wish to thank my partner, Dr. Leah Dudley, who has agreed to share my life as well as take on the duty of being the editor for this dissertation as well as for many of the papers I contributed to in the last two years. During this period Leah has provided me with companionship and, more importantly, the necessary environment to see this work through.

I wish to thank the Department of Physics and Astronomy of the University of Missouri, Columbia for its financial and moral support. I have found a home here as well as many friends. And finally I would like to thank the US Department of Energy for its financial support.

Contents

List of Tables

List of Figures

ABSTRACT

The focus of this dissertation is the study of lattice oscillations on the magnetic properties of two families of materials. One class of materials is the $La_{1-x}Ca_xMnO_3$ series of manganites which exhibit colossal magnetoresistance in some regions of their phase diagram. The second consists of $Li_{1-x}Na_xNiO_2$ series of nickelate materials which may display unusual magnetic and orbital properties. Both these classes of materials have attracted considerable attention in recent years for their possible industrial applications, the manganites for their use as base materials for read heads in hard-drives and the nickelate as rechargeable battery storage materials.

This work is divided into five main parts: Introduction, Methods, EPC in a two-site system, Magnetism in $NaNiO_2$, and self-trapped magnetic polaron. Chapter 1 is the introduction to the dissertation, while Chapter 2 discusses the numerical and analytical methods used. In Chapter 3, the issue of the electron-lattice coupling is examined in a two-site model of the $LaMnO_3$, and the magnitude of the isotope effect on the critical temperature T_c is estimated. The electron-phonon coupling is shown to decrease the magnetic exchange from its Anderson-Hasegawa upper limit of $t \cos \theta / 2$, and the oxygen isotope shift in T_c is estimated and found to agree well with experiments. Chapter 4 discusses the electronic structure and magnetism in $NaNiO_2$. The Variational Lang-Firsov method as well as exact diagonalization methods are used to show that inter-planar exchange is reduced by lattice coupling. The issue of different magnetic properties of $LiNiO_2$ compared to those of $NaNiO_2$ is discussed. Chapter 5 of the dissertation examines the magnetic polaron problem in a three dimensional lattice. The effect of the static Jahn-Teller coupling on the binding energy of the magnetic polaron is computed, as well as the effect of the next-nearest-neighbor hopping. The former is found to further stabilize the MP, while the latter has the opposite effect.

Chapter 1

Introduction

The subject of this dissertation is the study of the effect of the interactions between crystal lattice vibrations and electronic wave functions on the magnetic properties of certain solids. I focus in this work on the oxides and in particular, on the manganite and nickelate families of materials.

This coupling between electronic wave function and lattice oscillations, often referred to as the electron-phonon coupling (EPC), is a central phenomenon in solid-state physics and is found to play an important role in many of today's important problems such as the so-called colossal magnetoresistance (CMR) effect in transition-metal oxides, superconductivity and many others. In the case of the CMR effect for instance it was shown by Millis *et al.*[7] that, in order to reproduce the observed magnetoresistance, the double-exchange model should be corrected by including the EPC. It was also demonstrated that in several doped manganites, polaron formation tends to drive the system towards a first order phase transition. (see reference [8] for a review).

In order to gain a deeper understanding of many of these phenomena, it has therefore become increasingly important to determine to what extent the EPC coupling affects the magnetic properties of certain materials. Because of their unusual magnetic properties, we shall focus in particular on the series of transition metal (TM) oxides: $La_{1-x}Ca_xMnO_3$ and
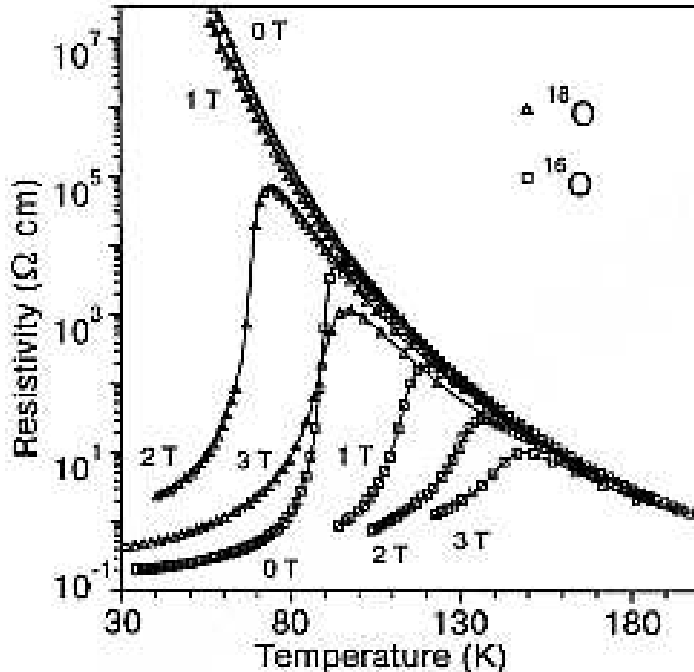
Figure 1.1: Temperature dependence of the resistivity of $La_{0.175}Pr_{0.525}Ca_{0.3}MnO_3$ for several magnetic fields. The magnetic field of 2T suppresses the [Charge-Ordered] State of the ^{18}O sample, resulting in the metal-insulator transition. (Babushkina N. A. *et al.*, *Nature* **391**, 159 (1998))

$Li_{1-x}Na_xNiO_2$.

Magnetic phenomena in transition metal oxides—Transition metal oxides show a very rich and complex phase diagram. This is presumably due the simultaneous interplay of electronic, spin, and lattice degrees of freedom. In this dissertation we focus primarily on two families of materials; Lanthanum-Calcium manganites and its relatives, and Lithium-Sodium Nickelates.

Consider first the family of materials $La_{1-x}Ca_xMnO_3$, where x is the electron doping. These materials were discovered[9] many years ago and the complex magnetic ordering in these systems was well known ever since the excellent series of experiments by Wollan and Koehler[10]. The observation of the CMR effect however, has lead to the re-discovery of this particular family of manganites. The ensuing years have seen an intense area of research develop around the manganites. Much work was done to explain the complex mag-

netic orderings in the LCMO system, culminating in the so-called Goodenough-Kanamori-Anderson[11, 12] (GKA) rules which we now state:

Rule 1. The 180° exchange between half-filled orbitals (one electron per orbital) is relatively strong and *antiferromagnetic.*

Rule 2. The 90° exchange between half-filled orbitals is *ferromagnetic* and relatively weak.

Rule 3. The exchange between a half-filled and an empty orbital is ferromagnetic and weak(irrespective of the orientation of the bond).

It should be noted that while these phenomenological rules have proved very effective in describing the simplest cases, there is no general theory that describes the magnetic ordering in LCMO for an arbitrary doping x from first-principles. In this work we have computed the ground-state energy for several model Hamiltonian and computed the exchange interaction for several materials, correctly describing their magnetic ordering. We describe this technique, as well as the associated computer code in much detail in the *Methods* section.

Cooperative Jahn-Teller effect—In transition-metal oxides, the Jahn-Teller (JT) effect is the principal driving force of the coupling between lattice distortions and electronic wave function. and may be explained simply as the response of the lattice to a local change in electric charge. The coupling between electronic and lattice degrees of freedom in these materials takes place via the Coulomb interaction. This effect can be understood easily if we consider the simple model of a solid shown in Fig. 1.2. A crystalline solid may be viewed as a background of positive charges with electrons free to move around in the lattice. If we focus on a single itinerant electron, the Coulomb interaction between the negatively charged electron and the surrounding positive ions will cause a distortion of the crystal lattice, while at the same time lowering the kinetic energy of the electron. This model however, has proven too simplistic as the situation in transition metal oxides is much more complex. Indeed, the coupling between electrons and lattice in these systems takes place via the so-called Jahn-Teller effect which we now discuss.
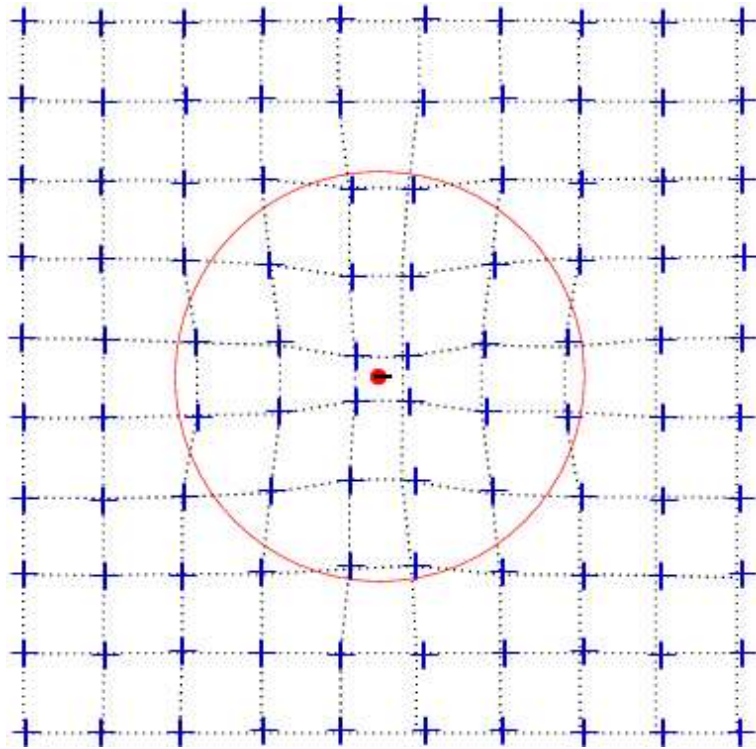
Figure 1.2: Simple picture of the electron-phonon coupling in solids. The positive signs represent the nuclei of the atoms in the lattice while the negative sign is the electron.

When solving the Schrödinger equation in a crystal one expects the resulting electronic wave functions φ_i to be highly degenerate due to the symmetric nature of the system. However, some of these degeneracies will be lifted by the lattice distortions. The Jahn-Teller effect may generally be described as the lifting of some of the degeneracies of the electronic wave functions in response to the lattice distortions. Consider for example the ideal perovskite structure as it occurs in $CaMnO_3$. In this crystal, a manganese ion is surrounded by six oxygen atoms. If we dope this system using for example La, additional electrons are introduced in the system, thus changing the local valence. The itinerant electrons will then occupy one of the empty e_g orbitals, thus lifting the degeneracy of the electronic orbitals. This has been shown from Density Functional calculations[13] where the electronic wave functions around the Fermi energy have $Mn(d)$ character with strong hybridization with the $O(p)$ orbitals(see Fig.1.3). The presence of the itinerant electron will cause the degeneracy of the e_g orbitals to be lifted, which is associated with a lowering of the symmetry of the crystal from cubic to orthorhombic.

Effect of the EPC on magnetism−A useful experimental probe of the electron-phonon coupling in oxides is the isotope effect, where vibronic coupling is modified by the substitution of ^{16}O by its heavier isotope ^{18}O. The observation of an isotope effect[14, 15] on the charge-ordering critical temperature of certain CMR materials indicated the involvement of the lattice in the magnetic properties of these important compounds. The isotope effect requires for its interpretation a description of the physics involving the quantum- mechanical nature of the nuclear wave function. That is we must consider the dynamics of the lattice and use the quantum mechanical description (phonons) of lattice vibrations.

While no single model describing the physics exists, it is now generally believed[16] that such an effect arise from complex interactions between different degrees of freedom. What makes this problem difficult is that no single degree of freedom seems to dominate the physics, so that traditional methods such as perturbation theory, have largely failed to describe the experimental observations. It has now become clear that in order to make
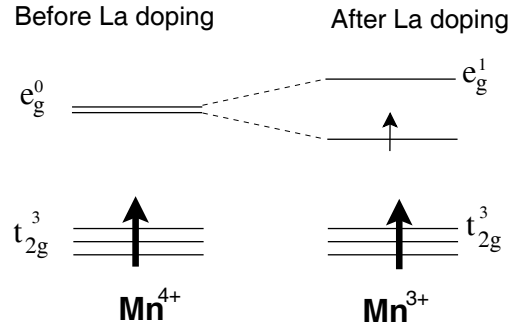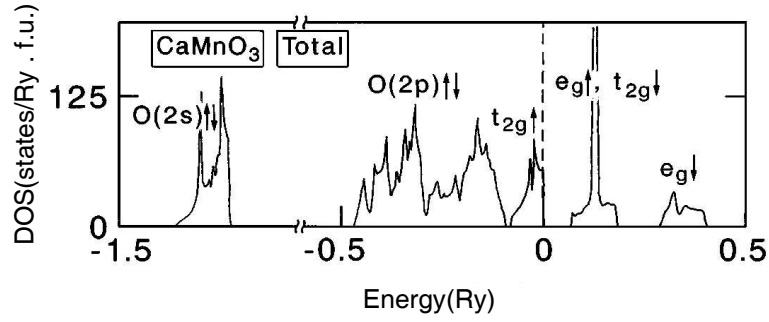
Figure 1.3: Density of state of $CaMnO_3$ calculated using Local Spin-Density Approximation to density functional theory. The diagram shows the $Mn(d$) orbitals with their occupation. The large arrows correspond to the t_{2g} electrons, while the smaller one corresponds to the single doped electron.

progress in this area of condensed matter we must develop methods that are able to treat the different interactions on an equal footing. In this work, and in order to compute the magnetic exchange, we make use of the Variational Lang-Firsov method which is shown to give good results for a wide range of the electron-phonon coupling strength.

Organization of the Thesis − In chapter two the methods used in this dissertation are discussed in detail. In particular, we give a detailed description of the Variational Lang-Firsov Method, and apply it to a simple Hamiltonian. We also explain the use of the *Cluster* program which is a code we developed and whose purpose is to compute the ground-state of a system of N atoms with N atoms and M orbitals per site. An example of how to use the code is also presented.

In chapter three we study the electron-phonon coupling as well as the isotope effect in a two-site system. The problem is discussed based on a two-site Hamiltonian and it is shown that the coupling significantly decreases the magnetic exchange. In chapter two, the effect of the dynamical Jahn-Teller coupling on the Anderson-Hasegawa double exchange in the manganites is studied in a two-site model taking into account the double degeneracy of the e_g orbitals and their coupling to three of the MnO_6 octahedron vibrational modes (Q_1, Q_2, and Q_3). Both exact diagonalization and the Lang-Firsov variational method approaches are used. We find that the coupling to the Q_2 and Q_3 vibrational modes reduces the double exchange, while the Q_1 mode is ineffective. The isotope dependence of the double exchange interaction is also found to be consistent with experiments.

In chapter four the electronic structure and magnetism in $NaNiO_2$ are studied from density-functional calculations and by solving model Hamiltonians, suggested from the density-functional results, to understand the magnetic exchange. The density-functional calculations within the "LSDA+U" approach yields a layered antiferromagnetic solution with ferro-orbital ordering of the Ni(d) orbitals arising from the Jahn-Teller distortion around the Ni^{3+} ion in agreement with the orbital ordering inferred from neutron diffraction. The weak ferro-magnetic interaction within the layer ($J_F \approx 1$ meV) is caused by the 90° Ni-O-Ni exchange

following the Goodenough-Kanamori-Anderson rules, while the weaker antiferromagnetic interaction between the layers ($J_{AF} \approx -0.1$ meV) is mediated via a long Ni-O-Na-O-Ni superexchange path. In order to shed light on the differences between $NaNiO_2$ and $LiNiO_2$, which show very different magnetic behaviors in spite of the similarity of their crystal structures, we examine the effect of the coupling of the alkali atom (Na) motion to the electronic degrees of freedom on the inter-layer exchange J_{AF}. A model Hamiltonian is proposed and solved by exact diagonalization and by using the variational Lang-Firsov method. We find that reducing the mass by going from Na to Li does reduce the strength of the magnetic exchange, but only by a small amount, so that the difference in mass alone can not describe the differences in magnetic behavior between the two compounds.

In chapter five We study the energetics of the self-trapped magnetic polaron (electron plus the distorted local magnetization cloud) in the electron doped manganites, e.g., $Ca_{1-x}La_xMnO_3$ with small x. A single electron moving in a cubic lattice of antiferromagnetic t_{2g} core spins, as appropriate for the manganites, is examined, taking into account the effects of the nearest and the next-nearest neighbor hoppings, the Anderson-Hasegawa double-exchange, as well as the Jahn-Teller interaction. We compute the ground state energy and the wave function of the system using a set of self-consistent equations. While we show that the next-nearest-neighbor hopping significantly reduces the binding energy of the magnetic polaron, this reduction is not enough to destabilize the self-trapped state. The ground-state of the polaron is found to be a seven-site ferromagnetic region, comprising the central spin and the six nearest neighbors, with a net magnetic moment of approximately 7 μ_B in qualitative agreement with the experiments. We argue that the polaron should exhibit an activated hopping an seen in the experiments, and estimate an activation energy of about 40 meV.

The results of the dissertation are then briefly summarized again in the conclusion section.

Chapter 2

Methods

In order to study the problem of the electron-phonon coupling and its effect on the magnetism various numerical and analytical techniques were used in this work. The most interesting methods used here are exact diagonalization (ED) and the semi-analytical method known as the Variational Lang-Firsov (VLF) method. However, first-principle electronic structure calculations based on Density Functional Theory (DFT) were also used, as well fourth order non-degenerate perturbation theory. Extensive use was also made of the "*Cluster*" computer code developed for the purpose of forming the Hamiltonian matrix of a system with N_s sites (M orbitals per site) and N_e electrons of both spins. This chapter gives an introduction to the various methods used to solve some of the problems of this thesis.

2.1 Computation of the magnetic exchange

Because the exchange interaction in Oxides usually takes place via an intermediate oxygen ion, it is necessary to resort to fourth order perturbation to compute the ground-state energy. Based on the Heisenberg Hamiltonian

$$H_S = -\frac{J}{2} \sum_{\langle ij \rangle} \vec{S}_i \vec{S}_j, \tag{2.1}$$

9

the exchange interaction is then defined as the energy difference between the ferromagnetic and anti-ferromagnetic spin configurations

$$J = E_{\uparrow\downarrow} - E_{\uparrow\uparrow}. \tag{2.2}$$

We use this definition of the exchange interaction throughout this thesis. In this section section we discuss in detail how the exchange is obtained from perturbation theory where the first four orders in perturbation theory are given by [17]

$$
\begin{aligned}
E_n^{(4)} &= \sum_{i,j,k \neq n} \frac{V_{ni} V_{ij} V_{jk} V_{kn}}{(\epsilon_n - \epsilon_i)(\epsilon_n - \epsilon_j)(\epsilon_n - \epsilon_k)} - \sum_{i,j \neq n} \frac{|V_{ni}|^2 |V_{jn}|^2}{(\epsilon_n - \epsilon_i)(\epsilon_n - \epsilon_j)} \frac{1}{\epsilon_n - \epsilon_i} \\
&+ \sum_{i \neq n} \frac{|V_{nn}|^2 |V_{ni}|^2}{(\epsilon_n - \epsilon_i)^3} - \sum_{i,j \neq n} \frac{V_{ni} V_{ij} V_{jn} \cdot V_{nn}}{(\epsilon_n - \epsilon_i)(\epsilon_n - \epsilon_j)} \left[\frac{1}{\epsilon_n - \epsilon_i} + \frac{1}{\epsilon_n - \epsilon_j} \right].
\end{aligned} \tag{2.3}
$$

The matrix elements V_{ij} are the off-diagonal elements of the perturbation Hamiltonian, and ϵ_i is the $i-$th diagonal matrix element of the unperturbed Hamiltonian. The first, second, and third terms of the expansion are given in the appendix for completeness.

As an example of computing the exchange based on fourth-order non-degenerate perturbation theory consider a three sites Mn-O-Mn system as shown in Fig. 2.1. For the sake of simplicity we assume that only one e_g orbital per Mn atom is involved in the hopping, and take the Hund's rule coupling to be infinity. This model is probably inappropriate to describe any meaningful physics in the manganites, but it is nevertheless useful in illustrating some of the methods developed in this thesis. The on-site Coulomb interaction at the O site is denoted by U, the $p - d$ hopping by t, and the charge-transfer energy cost by Δ.

The Hamiltonian for this system may be written

$$H = \sum_{\sigma} \left[t(c_{1\sigma}^{\dagger} c_{p\sigma} + c_{2\sigma}^{\dagger} c_{p\sigma} + \text{h.c.}) + \Delta n_{p\sigma} \right] + U n_{p\uparrow} n_{p\downarrow}, \tag{2.4}$$

where $c_{i\sigma}^{\dagger} (c_{i\sigma})$ are the creation (annihilation) operator for an electron of spin σ at Mn site

10

e_g^1 t e_g^1

Δ

t_{2g}^3 t_{2g}^3

Mn(1)   O   Mn(2)
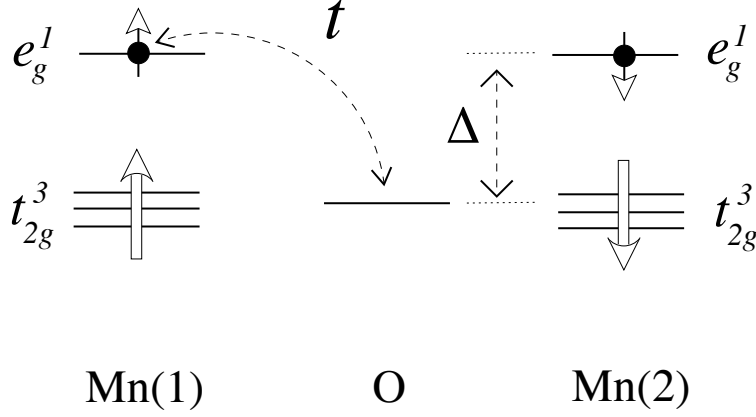
Figure 2.1: Schematic representation of the hopping in a three-levels system with two electrons. The Hund's exchange coupling on the Mn is assumed infinite for the sake of simplicity.

$i = 1$ or 2, while $c_{p\sigma}^{\dagger}(c_{p\sigma})$ are the creation (annihilation) on the O site. The occupation number operators are then defined as $n_{i\sigma} = c_{i\sigma}^{\dagger}c_{i\sigma}$. In order to compute the exchange J using Equation 2.2 we must first compute the Hamiltonian matrices in the occupation number representation for both the ferromagnetic and anti-ferromagnetic arrangements of the t_{2g}spins(see Figure 2.1. For example the ordered basis set for the anti-ferromagnetic case is written $\{|(100)_{\uparrow}(001)_{\downarrow}\rangle, |(100)_{\uparrow}(010)_{\downarrow}\rangle, |(010)_{\uparrow}(001)_{\downarrow}\rangle, |(010)_{\uparrow}(010)_{\downarrow}\rangle\}$. We then compute the matrix elements for the Hamiltonian Eq. 2.4. For instance, the matrix element between the two states $|(100)_{\uparrow}(001)_{\downarrow}\rangle$ and $|(100)_{\uparrow}(010)_{\downarrow}\rangle$ is $\pm t$ (hopping of the spin $\downarrow$ from site 3 to site 2). The exact sign is determined according to the fermion commutation relations (see the appendix for a discussion of the fermion sign issue).

The respective Hamiltonians for the ferromagnetic and antiferromagnetic configurations are then written

$$H_{\uparrow\uparrow} = \begin{pmatrix} \Delta & t & 0 \\ t & 0 & t \\ 0 & t & \Delta \end{pmatrix}, \text{ and } H_{\uparrow\downarrow} = \begin{pmatrix} 0 & t & t & 0 \\ t & \Delta & 0 & t \\ t & 0 & \Delta & t \\ 0 & t & t & U + 2\Delta \end{pmatrix}. \tag{2.5}$$

Note that neither of the above Hamiltonians is degenerate. If they were, then the use of the energy expansion given by Eq. 2.3 is wrong. This is nevertheless frequently encountered in the literature. An example of the proper treatment of the degenerate case is discussed in section 4.3.2. In this case however, the exchange is fund trivially by carrying out the expansions of the ferromagnetic and antiferromagnetic ground-state energies up to fourth order and taking the difference. In this case we find

$$J = \frac{-4t^4}{\Delta^2(U + 2\Delta)}.$$
(2.6)

The fourth-order perturbative method is useful provided the dimension of the Hilbert space is small enough that one can compute the matrix elements of the Hamiltonian by hand. However, for many of the systems encountered throughout this thesis the Hilbert space is often prohibitively large. It is for this purpose that the "*Cluster*" computer code was developed.

2.2 "*Cluster*" computer program

The general problem the *Cluster* computer code solves is that of an N_s - sites system with $M(i)$ orbitals per site and N_e electrons present in the system. Both the on-site Coulomb and the Hund's rule exchange interactions are taken into account. The hopping between the different orbitals is computed using the tight-binding matrix elements as given in Harrison's book[2]. Some of these matrix elements are shown for reference in Appendix A. The model Hamiltonian used is given by

$$H \;=\; H_1 + H_2 + H_3 + H_4,$$
(2.7)

where

$$H_1 = \sum_{\langle i,j \rangle} \sum_{\alpha\beta} t_{ij}^{\alpha\beta} \sum_{\sigma} c_{i\alpha\sigma}^{\dagger} c_{j\beta\sigma} + \text{h.c.} \tag{2.8}$$

$$H_2 = \sum_{i} \sum_{\alpha} \varepsilon_{i\alpha} \sum_{\sigma} n_{i\alpha\sigma} \tag{2.9}$$

$$H_3 = \sum_{i} \frac{1}{2} U_i^C \sum_{\alpha\beta}{}' \sum_{\sigma\sigma'} n_{i\alpha\sigma} n_{i\beta\sigma'} \tag{2.10}$$

$$H_4 = \sum_{i} \frac{1}{2} J_i^H \sum_{\alpha\beta}{}' \sum_{\sigma} (n_{i\alpha\sigma} n_{j\beta,-\sigma} - n_{i\alpha\sigma} n_{j\beta\sigma}). \tag{2.11}$$

The definition of the various terms of the above Hamiltonian is as usual and the primed sums are, by definition, such that the arguments are distinct: $\sum_{\alpha\beta}' \equiv \sum_{\alpha\neq\beta}$. The Koster-Slater tight-binding matrix elements $t_{ij}^{\alpha\beta}$ are determined from reference [2]. The on-site energy of an electron in orbital α at site i is denoted $\varepsilon_{i\alpha}$, while the on-site Coulomb and Hund's rule exchange interactions are denoted U_i^C and J_i^C, respectively.

In order to compute the exchange interaction J_{ex}, the *Cluster* program computes the ground-state energies for the ferromagnetic and antiferromagnetic configurations separately, then takes the difference. The two configurations usually only differ in the number of electrons of each spin. For example in the example above, the number of electrons for the antiferromagnetic configuration is the same for either spins ($N_e^{\uparrow} = 1$, $N_e^{\downarrow} = 1$), while for the ferromagnetic configuration there are no spin$\downarrow$ electrons ($N_e^{\uparrow} = 2$, $N_e^{\downarrow} = 0$).

The information about the number of electrons, the number of sites, etc. is stored in a pair of input files (one for each magnetic configuration, MN.TPaf and MN.TPfm). The information about the hopping must be supplied "by hand" by editing the file "edit.f90" before recompiling and running the program. The algorithm for the *Cluster* program is summarized in the flowchart shown in Fig. 2.2. The procedure is as follows:

1. *Cluster* asks for the value of $V_{pd\sigma}$

2. From the Input Files (MN.TPaf and MN.TPfm) read the following

```
                    ┌──────────────────┐
                   ╱   Enter Vpdσ     ╱
                  ╱──────────────────╱
                          │
                          ▽
                 ╱──────────────────╲
                ╱  Read Input Files  ╲
               ╱──────────────────────╲
                          │
                          ▽
                 ┌──────────────────┐
                 │   Form Basis Set │
                 └──────────────────┘
                          │
                          ▽
                 ┌──────────────────┐
                 │  Form Hamiltonian│
                 └──────────────────┘
                          │
                          ▽
                 ┌──────────────────┐
                 │  Find Ground State│
                 └──────────────────┘
```
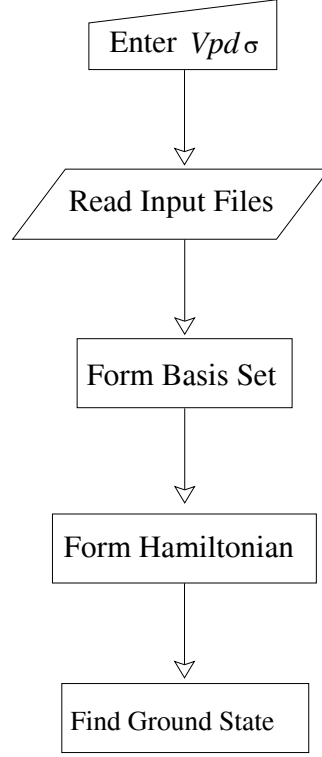
Figure 2.2: Flowchart diagram for the *Cluster* program.

(a) N_s, $M(i)$, $N_e^\uparrow$, $N_e^\downarrow$

(b) On-site energies

(c) Coulomb and Hund's rule

3. Form the Basis Set in the occupation number representation

4. Form the Hamiltonian H (Eqs. 2.8-2.11)

5. Find the Ground State by using either Lanczos Diagonalization or Fourth-Order non-degenerate perturbation theory.

2.3   Exact Diagonalization

Exact diagonalization (ED) methods are the "brute-force" methods of solving the problem of the electron-phonon coupling. The Lanczos diagonalization scheme is simply a method to

bring a symmetric matrix into tridiagonal form. The advantage in finding a basis set where a matrix is tridiagonal is two-fold; The memory storage required is considerably reduced compared to that of the initial matrix; one only needs to remember $2n - 1$ numbers instead of $n(n+1)/2$. In the appendix we give a brief description of the Lanczos numerical scheme. The Lanczos method consists of constructing a basis where the initial symmetric matrix is brought into tridiagonal form. We consider a set of orthonormal states $|\phi_j\rangle$, for $j = 1, \cdots, n$, it is then to write each tridiagonal state $|\psi_i\rangle$ as a linear combination of $|\phi_j\rangle$:

$$|\psi_i\rangle = \sum_{j=1}^{n} c_{i,j} |\phi_j\rangle. \tag{2.12}$$

Now consider the Hamiltonian of the system in the form

$$H = H_0 + H_1 \tag{2.13}$$

such as the $|\phi_j\rangle$ are the eigenfunctions of H_0. If we now consider H_1 as a perturbation, it may be possible to approximate the true ground-state using a linear combination of only a few $|\phi_j\rangle$. For a more detailed description see Reference[18].

2.4   Variational Lang-Firsov Method

In general the electron-phonon coupling problem is not soluble, save for very simple models since excited states of the lattice are bosons, which gives rise to infinite-size Hamiltonians that are, in general, impossible to diagonalize via "brute-force". A possible solution to this dilemma is to truncate the Hilbert space basis, then diagonalize the smaller matrices. This has the drawback that the accuracy will depend on the problem at hand, an that for complex systems there is no hope for this method to achieve reasonable accuracy. It is possible in some case to diagonalize very large matrices using the Lanczos algorithm described earlier, but there still remains a fundamental limit to exact diagonalization methods.

It is therefore necessary to approach the problem from a different angle. The Variational Lang-Firsov method is the combination of the variational method with a unitary transformation of the many-body Hamiltonian. Let's consider the simplest Hamiltonian with electron-phonon coupling

$$H = H_{el} + H_{EP} \tag{2.14}$$

where

$$H_{el} = t \sum_{\langle ij \rangle} c_i^\dagger c_j + \text{h.c.} \tag{2.15}$$

$$H_{EP} = \hbar\omega(\sum_i b_i^\dagger b_i + \frac{1}{2}) + \lambda \sum_i c_i^\dagger c_i(b_i + b_i^\dagger). \tag{2.16}$$

The program of the VLF is to find the unitary transformation U which diagonalizes H_{EP}, then applying U to H_{el} we find the total transformed Hamiltonian $\tilde{H} = U^\dagger H U$. An appropriate variational state of the form $|\Psi\rangle_V = |0\rangle_{ph}$ is then chosen, where $|0\rangle_{ph}$ is the phonon vacuum, and the resulting Hamiltonian $\bar{H}$ is then minimized with respect to some variational parameter. We now apply such a method to the above Hamiltonian.

We shall look for unitary transformations of the form

$$U = e^S \tag{2.17}$$

where S is an anti-Hermitian operator ($S^\dagger = -S$). It is easily shown that an arbitrary operator A will transform as

$$\tilde{A} = e^{-S} S e^S = A + [A, S] + \frac{1}{2!}[[A, S], S] + \frac{1}{3!}[[[A, S], S], S] + \dots \tag{2.18}$$

We choose the form

$$S = \alpha \frac{\lambda}{\hbar\omega} \sum_i (b - b_i^\dagger) c_i^\dagger c_i \tag{2.19}$$

where α is a variational parameter, and apply Eq.2.18 to the phonon operator b, and we find

$$\tilde{b} = b - \alpha\frac{\lambda}{\hbar\omega}\sum_i c_i^\dagger c_i \equiv b - \alpha\frac{\lambda}{\hbar\omega}n \qquad (2.20)$$

where we use the condensed notations $n = \sum_i n_i = \sum_i c_i^\dagger c_i$. The transformed of the electron-phonon Hamiltonian is then

$$\tilde{H}_{EP} = \hbar\omega(\sum_i b_i^\dagger b_i + \frac{1}{2}) + \lambda(1-\alpha)\sum_i n_i(b_i + b_i^\dagger) + \frac{\lambda^2}{\hbar\omega}(\alpha^2 - 2\alpha)n^2. \qquad (2.21)$$

Note that for a $\alpha = 1$, the above transformation does indeed diagonalize the electron-phonon Hamiltonian. If we now use the same method to calculate the transformed electronic Hamiltonian we find $\tilde{c}_i = c_i e^{-\alpha\frac{\lambda}{\hbar\omega}(b_i - b_i^\dagger)}$, and

$$\tilde{H}_{el} = t\sum_{\langle ij\rangle} c_i^\dagger c_j e^{\alpha\frac{\lambda}{\hbar\omega}(b_i - b_i^\dagger)}e^{-\alpha\frac{\lambda}{\hbar\omega}(b_j - b_j^\dagger)}.$$

The next step in the Variational Lang-Firsov program is to take the average over the variational state $|\Psi\rangle_V$

$$\bar{H} = te^{-\alpha^2\frac{\lambda^2}{2\hbar\omega^2}}\sum_{\langle ij\rangle} c_i^\dagger c_j + \frac{\hbar\omega}{2} + \frac{\lambda^2}{\hbar\omega}(\alpha^2 - 2\alpha)n^2 \qquad (2.22)$$

and minimize the corresponding ground-state energy with respect to the variational parameter λ.

As the above transformation diagonalizes the electron-phonon Hamiltonian for $\alpha = 1$ it may be considered exact in the limit where $t \to 0$, and is therefore a good approximation in the strong coupling limit (the so called anti-adiabatic limit). However, in the weak-coupling or adiabatic limit it is not clear that S alone gives a suitable approximation to the ground-state energy. When a greater accuracy is required of the simple transformation S is often supplemented by two additional unitary transformations S_2 and S_3. References [19, 20] discusses this case in much more detail in the context of the Holstein model.

The first transformation is often taken

$$S_2 = \xi \sum_i \Delta_i (b - b^\dagger) \qquad (2.23)$$

where ξ is a dimensionless constant and Δ_i are variational parameters usually interpreted as uniform lattice displacements. The above transformation describes the system well in the adiabatic regime where the electron-phonon coupling is weak compared to the hopping t. To understand that we note that the electron's creation/destruction commute with S_2 and are therefore not affected by the unitary transformation. The phonon operator on the other hand are rescaled as

$$\tilde{b}_i = b_i - \xi \Delta_i. \qquad (2.24)$$

The transformed Hamiltonian (under S_2 alone) is then

$$\tilde{H} = H_{el} + \tilde{H}_{EP} \qquad (2.25)$$

which will be a good approximation only if $\tilde{H}_{EP}$ is small compared to H_{el}, that is in the small coupling limit.

Another transformation that is often used is the so-called "squeezed" phonon state transformation S_3 and has the form

$$S_3 = \zeta \sum_i n_i (b_i b_i - b_i^\dagger b_i^\dagger) \qquad (2.26)$$

which describes the physics for the intermediate strength of the electron-phonon coupling . A detailed discussion is beyond the scope of this thesis and we again refer the reader to References [19, 20] for a more sophisticated discussion of the Variational Lang-Firsov Method.

2.5 Density Functional Theory

First principle or *ab initio* methods of computing the electronic structure of crystalline solids have been in use for a long time. Recently, and with the explosion of computational power, these methods have become quite popular. The focus of this dissertation, however, is not on electronic structure so I will limit the description of such methods to the most general introduction to Density Functional Theory(DFT). This theory provides a general method to solve, in principle, the problem of infinitely-many interacting fermions. There are , however, difficulties such as the fundamental impossibility to exactly determine the exchange-correlation energy. In order to solve the equations of DFT it is often necessary to resort to drastic approximations such as the Local Density Approximation (LDA) where the density is assumed to vary slowly enough that it may be considered constant locally. This, surprisingly, has not kept DFT from becoming a very powerful tool when studying the electronic structure of relatively complex materials.

As proved by Hohenberg and Kohn[21] the ground-state energy of a system of interacting electrons can be found by minimizing the following functional of the one-electron density $n(\mathbf{r})$

$$E_v[n(\mathbf{r})] = \int v(\mathbf{r})n(\mathbf{r})d\mathbf{r} + F[n(\mathbf{r})] \tag{2.27}$$

where T and V are the kinetic and potential energies, $v(\mathbf{r})$ is a static external potential, and $|\Psi\rangle$ is the many-body wavefunction. The quantity

$$F[n(\mathbf{r})] = \langle\Psi|\,(T+V)\,|\Psi\rangle \tag{2.28}$$

is universal functional of the density and can be shown to be independent of the both the number of electron, and the external potential. It is convenient to separate the above functional into three separate terms: the classical Coulomb energy $\frac{1}{2}\int n(\mathbf{r}')n(\mathbf{r})/\left|\mathbf{r}-\mathbf{r}'\right|d\mathbf{r}d\mathbf{r}'$, the kinetic energy $T_s[n(\mathbf{r})]$ of a non-interacting electron gas with same density $n(\mathbf{r})$, and

the Kohn-Sham[22] exchange-correlation energy $E_{xc}[n(\mathbf{r})]$ of the interacting electron system. The energy functional then takes the form

$$F[n(\mathbf{r})] = \int v(\mathbf{r})n(\mathbf{r})d\mathbf{r} + \frac{1}{2}\int \frac{n(\mathbf{r}')n(\mathbf{r})}{|\mathbf{r} - \mathbf{r}'|}d\mathbf{r}d\mathbf{r}' + T_s[n(\mathbf{r})] + E_{xc}[n(\mathbf{r})]. \qquad (2.29)$$

The one-electron density $n(\mathbf{r})$ is then expanded in term of one-electron orbitals $\Phi_\sigma(\mathbf{r})$, and the above functional is minimized subject to the normalization condition

$$\sum_\sigma \int \Phi_\sigma^*(\mathbf{r})\Phi_\sigma(\mathbf{r})d\mathbf{r} = 1. \qquad (2.30)$$

This result in a set of coupled equation which are then solved self-consistently.

The method described above is in general exact, as no approximation have been made so far. However, determining the exchange-correlation energy E_{xc} is a non-trivial many-body problem in its own right. Various approximations (LDA, GGA,...) are in use today in order to a solve the self-consistent equations thus obtained.

Chapter 3

Electron-Phonon coupling and isotope effect in a two-site system

3.1 Introduction

The lanthanum manganites are mixed valence systems with a mixture of Mn^{3+} which is a Jahn-Teller (JT) ion and Mn^{4+} which is not. The excess electron therefore tends to carry the local JT distortion of the MnO_6 octahedron along with it as it moves about in the lattice. The way this coupled motion affects the phenomenology of the manganites has been addressed by several authors [23, 24]. The recent discovery of the isotope effect indicates the involvement of the lattice in the magnetic properties [25]. The isotope effect requires for its explanation the quantum mechanical nature of the nuclear wave function. In fact, it has been shown earlier from a simple model with non-degenerate electron states that the double exchange (DE) interaction[26, 27] is modified in two important ways by coupling to the lattice: *1.* the magnitude of the DE is reduced sharply from the Anderson-Hasegawa $t\cos(\theta/2)$ value, and *2.* the coupling to the oxygen motion leads to an oxygen-mass-dependent DE. On the other hand, the double degeneracy of the e_g electrons and their characteristic coupling to the JT distortions of the MnO_6 octahedron has been shown to

lead to interesting consequences. In this chapter, we include the effects of double degeneracy and the appropriate JT coupling within a two-site Van Vleck-Kanamori Hamiltonian[28, 29] which we solve by Lanczos diagonalization.

3.2   Electron-Phonon coupling in a two-site model

The relevant orbitals for the itinerant electron motion in $La_{1-x}Ca_xMnO_3$ are the $Mn(e_g)$ orbitals, which couple to the vibrational mode of the MnO_6 octahedra via the JT interaction. There are three important vibrational modes[30] (i) the breathing mode Q_1, (ii) the in-plane distortion mode Q_2, and (iii) the apical stretching mode Q_3. Taking the symmetric MnO_6 octahedron with the average $Mn-O$ bond length as the reference, the amplitudes of the Q_2 and the Q_3 distortions in $LaMnO_3$ are 0.20 Å and 0.02 Å, respectively, resulting in the three $Mn-O$ bond lengths of 1.91, 2.19, and 1.96 Å. The amplitude of the Q_1 distortion is zero by definition. The three normal modes are shown in Fig. 3.1. Q_1, Q_2 and Q_3 are given by[29]

$$\begin{aligned}
Q_1 &= (-X_1 + X_2 - Y_3 + Y_4 - Z_5 + Z_6)/\sqrt{6} \\
Q_2 &= (-X_1 + X_2 + Y_3 - Y_4)/2 \\
Q_3 &= (-X_1 + X_2 - Y_3 + Y_4 + 2Z_5 - 2Z_6)/\sqrt{12}
\end{aligned}$$

where X_1, X_2, Y_3, Y_4, Z_5 and Z_6 are the positions of the oxygen atoms in the MnO_6 octahedron.

If we now consider two MnO_6 octahedra sharing a common vertex such that one of the Mn ions has the valence d^3 while the other has the valence d^4, so as to correctly reproduce the valence in $La_{0.5}Ca_{0.5}MnO_3$, then the Hamiltonian of the system may be written as

$$H = H_e + H_{ph} + H_{JT} \tag{3.1}$$

where the first term represents the kinetic energy of the itinerant electron , the second term

the lattice distortion, and the third term represents the electron-phonon coupling due to the Jahn-Teller effect. These three terms may be written

$$
\begin{aligned}
H_{\mathrm{e}} &= \sum_{\langle ij \rangle \sigma} \sum_{a,b} t_{ij}^{ab} c_{ia\sigma}^{\dagger} c_{ib\sigma} - J_H \sum_{i,a} \vec{S}_i . \vec{\sigma}_{ia} \\
H_{\mathrm{ph}} &= \sum_{i\alpha} -\frac{\hbar^2}{2M} \frac{d^2}{dQ_{i\alpha}^2} + \frac{K}{2} Q_{i\alpha}^2 \\
H_{\mathrm{JT}} &= \sum_{i\sigma} \left(c_{i1\sigma}^{\dagger}, c_{i2\sigma}^{\dagger} \right) [g' Q_{i1} 1_u - g(Q_{i2}\tau_x + Q_{i3}\tau_z)] \begin{pmatrix} c_{i1\sigma} \\ c_{i2\sigma} \end{pmatrix}
\end{aligned}
\tag{3.2}
$$

This Hamiltonian is referred to in the literature as the Van Vleck-Kanamori Hamiltonian[29, 28]. The operator $c_{ia\sigma}^{\dagger}$ ($c_{ib\sigma}$) creates (destroys) an electron of spin σ at the ith site in orbital α, where $\alpha = 1$ corresponds to the $z^2 - 1$ orbital, while $\alpha = 2$ corresponds to the $x^2 - y^2$ orbital. The matrix elements t_{ij}^{ab} are the Koster-Slater[2] tight-binding hopping integrals between the different pairs of e_g orbitals and are given by the matrix

$$
t_{ij} = \begin{pmatrix} t_{ij}^{1,1} & t_{ij}^{1,2} \\ t_{ij}^{2,1} & t_{ij}^{2,2} \end{pmatrix} = \begin{pmatrix} 1 & -\sqrt{3} \\ -\sqrt{3} & 3 \end{pmatrix} \frac{V_{dd\sigma}}{4} \cos(\theta/2).
\tag{3.3}
$$

The angle θ is the angle between the two net t_{2g} which we consider here to be classical and denote by the vectors $\vec{S}_{i\alpha}$. The spin of the itinerant electron at (i, α) is referred to as $\vec{\sigma}_{i\alpha}$, and $Q_{i\beta}$ is the βth normal mode of the $\mathrm{MnO_6}$ octahedron. The respective Pauli spin-matrices $\tau_{x,z}$ are given by

$$
\tau_x = \begin{pmatrix} 0 & 1 \\ 1 & 0 \end{pmatrix} \text{ and } \tau_z = \begin{pmatrix} 1 & 0 \\ 0 & -1 \end{pmatrix}
$$

The constants K, g, and g' respectively represent the lattice stiffness, the electron-phonon coupling to the $Q_{2,3}$ modes, and the electron-phonon coupling to the Q_1 mode. Moreover, the Hund's rule coupling is here assumed to be infinite ($J_H = \infty$), which in effect allows

one to consider only spin orientation, and the Hamiltonian Eq. (3.1) will not depend on the spin-index σ.

It can be shown by seeking the ground-state of $H_\text{ph} + H_\text{JT}$, where we assume that the lattice distortion is not quantized (i.e. static Jahn-Teller distortion), that the e_g levels are split by the lattice distortion, and that the addition of the kinetic energy term H_e further lowers the energy by forming a band electron.[31]

Before carrying the second quantization of the Hamiltonian Eq. (3.1), we estimate the parameters as follows: (i)$V_{dd\sigma} \approx -0.3 - 0.4$ eV from the calculated band-width and taking into account the appropriate orbital ordering.[13] (ii)The electron-phonon coupling constant $g \approx 3 - 4$ eV/Åas estimated from tight-binding fits to the density functional e_g bands with varying octahedral distortions.[31] (iii) The stiffness constant is then estimated from $K = g/\sqrt{Q_2^2 + Q_3^2}$ to be about 15-20 eV/Å^2.

The dynamical problem may be solved by quantizing the lattice degrees of freedom in Eq. 3.2; we take

$$
\begin{aligned}
Q_{i\alpha} &= \left(\frac{\hbar}{2M\omega}\right)^{1/2} \left(b_{i\alpha}^\dagger + b_{i\alpha}\right) \\
P_{i\alpha} &= -i\hbar\frac{d}{dQ_{i\alpha}} = \left(\frac{M\hbar\omega}{2}\right)^{1/2} \left(b_{i\alpha}^\dagger - b_{i\alpha}\right)
\end{aligned}
$$

which in this case gives the following Hamiltonian

$$
H = H_\text{e} + H_\text{ph} + H_\text{JT} \tag{3.4}
$$
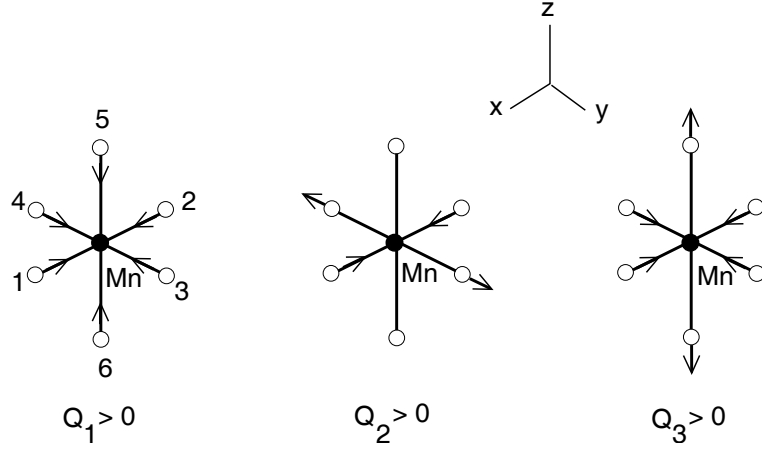
Figure 3.1: The three relevant normal modes of vibration for the MnO_6 octahedron with their eigenvectors $|Q_1\rangle$, $|Q_2\rangle$ and $|Q_3\rangle$.
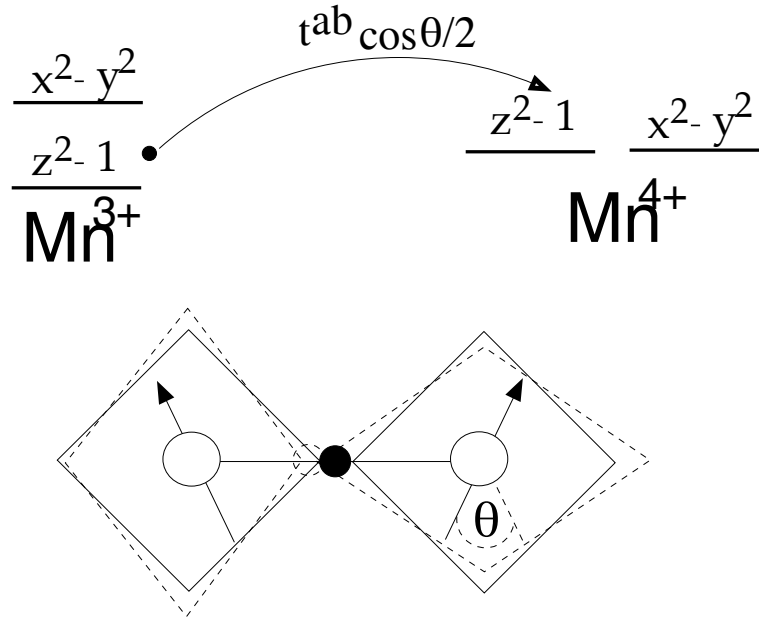
Figure 3.2: Mn-O-Mn bonds and angle-dependent hopping in $La_{1/2}Ca_{1/2}MnO_3$.

where

$$
\begin{aligned}
H_{\text{e}} &= \sum_{\langle ij \rangle} \sum_{a,b} t_{ij}^{ab} c_{ia}^{\dagger} c_{jb} + \text{h.c.} \\
H_{\text{ph}} &= \sum_{i\alpha} \hbar\omega (b_{i\alpha}^{\dagger} b_{i\alpha} + \frac{1}{2}) \\
H_{\text{JT}} &= \sum_{i} \xi' n_i (b_{i1}^{\dagger} + b_{i1}) + \xi(c_{i1}^{\dagger} c_{i2} + \text{H.c.})(b_{i2}^{\dagger} + b_{i2}) + \xi(n_{i1} - n_{i2})(b_{i3}^{\dagger} + b_{i3})
\end{aligned} \tag{3.5}
$$

where $c_{ia}^{\dagger}$ (c_{ia}) creates (destroys) an electron at site i in the orbital a, $b_{i\alpha}^{\dagger}$ $(b_{i\alpha})$ creates (destroys) a phonon of type α at the ith site. Again we point out that since $J_H = \infty$, the Hamiltonian is essentially spin-independent. The Koster-Slater tight-binding matrix elements t_{ij}^{ab} are given by Eq. (3.3), $\omega = \sqrt{\frac{K}{M}}$ is the phonon frequency (assumed uniform for the sake of simplicity), and $\xi(') = g(')\sqrt{\frac{\hbar}{2M\omega}}$ is the electron-phonon coupling to the Q modes. We define the double-exchange energy as the difference of the ground-state energies between the states where the two core spins are parallel and anti-parallel, i.e.

$$
J_{\text{DE}} = E_{\uparrow\downarrow} - E_{\uparrow\uparrow}
$$

In this work, we shall neglect the effect of the coupling to the Q_1 mode, as it merely introduces a shift in the total energy by an amount $N_e \times g'/2K$, where N_e is the total number of electrons. That energy shift is independent of the hopping t^{ab}, and is therefore the same for all values of θ, therefore contributing nothing to the double-exchange energy J_{DE}.

3.3 Exact diagonalization

Unlike the case of an infinite lattice, it is possible for the two-site model to use brute-force numerical methods in order to find the ground-state solution of the problem. We shall compute such a solution using exact-diagonalization and compare the results obtained from the Variational Lang-Firsov method. The ground-state energy of the Hamiltonian (3.5) is
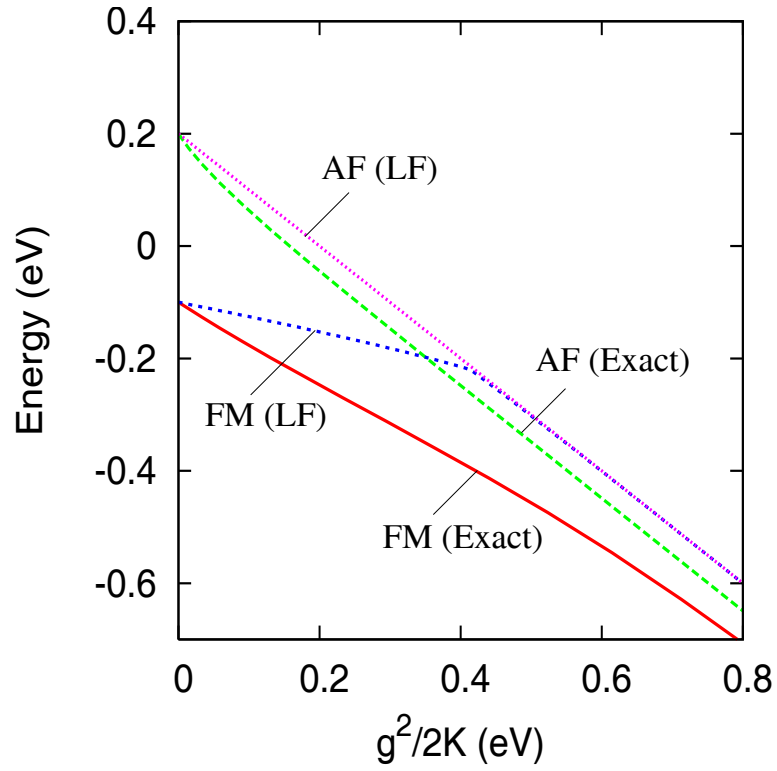
Figure 3.3: Comparison between the exact and variational Lang-Firsov (LF) energies for the ferromagnetic (FM) or antiferromagnetic (AF) alignment of the Mn core spins.

obtained by direct diagonalization in the occupation representation. An element of the basis set may be written

$$|ia\rangle \otimes |\nu_1\nu_2\nu_3\nu_4\rangle \tag{3.6}$$

where i and a are the site and orbital, and the ν's are the vibrational quantum numbers of the phonon modes at the two sites, such that ν_1 and ν_2 correspond to Q_2 and ν_3 and ν_4 correspond to Q_3. Note that while i and a are limited to to the number of sites and orbitals, the phonon indices may in general take any positive value, the phonon Hilbert space being infinite by definition. Let us calculate the matrix elements of the Hamiltonian in this basis:

$$\begin{aligned}
\langle \Psi' | H | \Psi \rangle &= \langle jb, \mu_1\mu_2\mu_3\mu_4 | H | ia, \nu_1\nu_2\nu_3\nu_4 \rangle \\
&= \langle jb, \vec{\mu} | (H_{\mathrm{e}} + H_{\mathrm{ph}} + H_{\mathrm{e\text{-}ph}}) | ia, \vec{\nu} \rangle
\end{aligned} \tag{3.7}$$

where we have adopted the following vector notation for the phonon numbers for simplicity.

$$|\vec{\nu}\rangle \equiv |\nu_1, \nu_2, \nu_3, \nu_4\rangle . \tag{3.8}$$

We compute the various terms in Eq. (3.7). A general matrix element for the kinetic energy may be written

$$\begin{aligned}
\langle jb, \vec{\mu} | H_{\mathrm{e}} | ia, \vec{\nu} \rangle &= \sum_{\alpha,\beta} t^{\alpha\beta} \langle jb, \vec{\mu} | \left(c_{1\alpha}^\dagger c_{2\beta} + c_{2\beta}^\dagger c_{1\alpha} \right) | ia, \vec{\nu} \rangle \\
&= t^{ab}\delta(\vec{\nu} - \vec{\mu}) \left[\delta_{1,i}\delta_{2,j} + \delta_{2,i}\delta_{1,j} \right] .
\end{aligned}$$

The part of the Hamiltonian representing the lattice dynamic has the following matrix element in the occupation representation

$$\langle jb, \vec{\mu} | \, H_{\mathrm{ph}} \, | ia, \vec{\nu} \rangle \;\; = \;\; \sum_{i,\sigma} \hbar\omega \delta_{ij} \delta_{ab} \langle \vec{\mu} | \left(b_{i\sigma}^{\dagger} b_{i\sigma} + 1/2 \right) | \vec{\nu} \rangle$$

$$= \;\; \hbar\omega \delta_{ij} \delta_{ab} \delta(\vec{\nu} - \vec{\mu}) \left(1 + \sum_{k=1,4} \nu_k \right),$$

whereas the electron-phonon coupling has the form

$$\langle jb, \vec{\mu} | \, H_{\mathrm{e-ph}} \, | ia, \vec{\nu} \rangle \;\; = \;\; \xi \sum_{l} \langle \mu_1 \mu_2 | \left(b_{l2}^{\dagger} + b_{l2} \right) | \nu_1 \nu_2 \rangle \, \delta_{\nu_3,\mu_3} \delta_{\nu_4,\mu_4} \langle jb | \left(c_{l1}^{\dagger} c_{l2} + c_{l2}^{\dagger} c_{l1} \right) | ia \rangle$$

$$+ \;\; \langle \mu_3 \mu_4 | \left(b_{l3}^{\dagger} + b_{l3} \right) | \nu_3 \nu_4 \rangle \, \delta_{\nu_1,\mu_1} \delta_{\nu_2,\mu_2} \langle jb | \left(c_{l1}^{\dagger} c_{l1} - c_{l2}^{\dagger} c_{l2} \right) | ia \rangle$$

$$= \;\; \xi \delta_{ij} \Big[\left(\delta_{1a} \delta_{2b} + \delta_{2a} \delta_{1b} \right) \langle \mu_j | \left(b_{j2}^{\dagger} + b_{j2} \right) | \nu_j \rangle \prod_{k \neq j} \delta_{\nu_k, \mu_k}$$

$$+ \;\; \delta_{ab} \left(\delta_{1a} - \delta_{2a} \right) \langle \mu_{j+2} | \left(b_{j3}^{\dagger} + b_{j3} \right) | \nu_{j+2} \rangle \prod_{k \neq j+2} \delta_{\nu_k \mu_k} \Big]$$

$$= \;\; \xi \delta_{ij} \Big[\left(\delta_{1a} \delta_{2b} + \delta_{2a} \delta_{1b} \right) \prod_{k \neq j} \delta_{\nu_k, \mu_k} \left(\delta_{\mu_j, \nu_j - 1} \sqrt{\nu_j} + \delta_{\mu_j, \nu_j + 1} \sqrt{\nu_j + 1} \right)$$

$$+ \;\; \delta_{ab} \left(\delta_{1a} - \delta_{2a} \right) \prod_{k \neq j} \delta_{\nu_{2+k}, \mu_{2+k}} \times$$

$$\left(\delta_{\mu_{2+j}, \nu_{2+j} - 1} \sqrt{\nu_{j+2}} + \delta_{\mu_{2+j}, \nu_{2+j} + 1} \sqrt{\nu_{2+j} + 1} \right) \Big]$$

The phonons being boson particles, there is an infinite number of phonon states in the Hilbert space, which makes it impossible to exactly diagonalize the Hamiltonian, and it is therefore necessary to truncate the phonon part of the Hilbert space such that only a maximum of M phonons per mode are kept. In which case the dimension of the Hamiltonian matrix is

$$LN(M + 1)^{qN}$$

where N is the number of lattice sites, L is the number of orbitals per site, M is the maximum number of phonon per mode, and q is the number of vibrational modes. In our case we have that $N = L = q = 2$, and the dimension of the Hilbert space in the case of our

two-site system is $4(M+1)^4$. For the calculation of the results we keep a maximum number of $M = 20$ phonons, which results in a Hamiltonian matrix of dimension 777924 that we diagonalize using the Lanczos diagonalization scheme (See Appendix B). In Fig. (3.3) we show that ground-state energy as a function of the Jahn-Teller energy $(-\Delta_{JT} = g^2/2K)$.

3.4   The Variational Lang-Firsov method

As discussed earlier, the bosonic nature of the lattice excitation gives rise to a Hilbert space with infinite dimension. It is thus not in general possible to find the true ground-state of the system, except for simple mode systems. Numerous authors[cite Feynman] have outlined the difficulties of solving the general electron-phonon problem, and it is clear that in order to handle more realistic systems different methods must be developed. Methods based on Unitary transformations have proven to be quite powerful in that respect, where such methods allow for an exact diagonalization of the problem when the Hamiltonian is quadratic in the boson or fermion operators. Unfortunately, the Hamiltonian Eq. 3.5 does not belong to this class of problems.

It is possible, however, to devise a method which makes use of the power of the variational principle and that is based on a unitary transformation. The Variational Lang-Firsov approximation has the following simple program: *1.* Find a transformation that diagonalizes the phonon and electron-phonon parts of the Hamiltonian. *2.* Continuously vary the expectation value of the transformed Full Hamiltonian.

In this section we use the Variational Lang-Firsov (VLF) method to compute the ground-state energy of the Hamiltonian 3.5 and compare our results to the exact diagonalization. We consider the anti-Hermitian operator

$$S = \sqrt{\Delta_{\text{JT}}/\hbar\omega} \times \sum_i n_i \left[\gamma_1(b_{i2}^\dagger - b_{i2}) + \gamma_2(b_{i3}^\dagger - b_{i3})\right]$$

where γ_1 and γ_2 are variational parameters and transform the quantized VVK Hamiltonian of
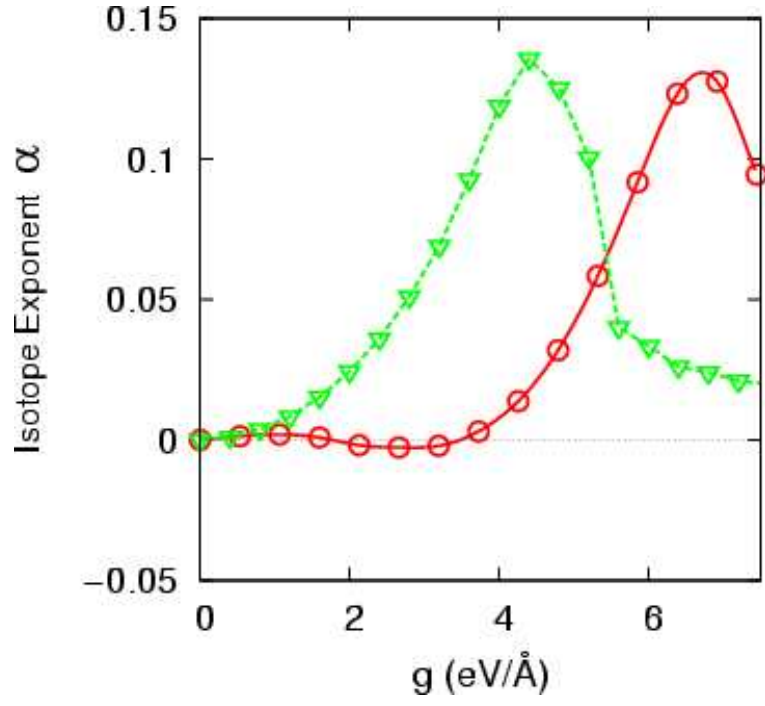
Figure 3.4: Isotope exponent in terms of the electron-phonon coupling constant g. The two curves correspond to the exact result with only the Q_2 mode (green line), or both Q_2 and Q_3 retained in the total Hamiltonian. The lines are a smoothed fit to the data.

Eq. (3.4) such that the transformed Hamiltonian is given by $\tilde{H} = e^S H e^{-S}$. From Appendix A, the transformed annihilation operators for electron and phonons are given by

$$\tilde{c}_{ia} = c_{ia} e^{\sqrt{\frac{\Delta_{JT}}{\hbar\omega}} \sum_\alpha \gamma_\alpha (b_{i\alpha} - b_{j\alpha}^\dagger)}$$

$$\tilde{b}_{i\alpha} = b_{i\alpha} + \sqrt{\frac{\Delta_{JT}}{\hbar\omega}} \gamma_i n_i$$

where i refers to the ith lattice site, a refers to the orbital occupied by the electron at that site, and α corresponds to the phonon mode(either Q_2 or Q_3). The transformed Hamiltonian then takes the form

$$\tilde{H} = \tilde{H}_{\text{e}} + \tilde{H}_{\text{ph}} + \tilde{H}_{\text{e}-\text{ph}}$$

where

$$\tilde{H}_{\text{e}} = \sum_{\langle i,j \rangle ab} t_{ij}^{ab} e^{-\sqrt{\frac{\Delta_{JT}}{\hbar\omega}} \sum_\alpha \gamma_\alpha (b_{i\alpha} - b_{i\alpha}^\dagger)} e^{\sqrt{\frac{\Delta_{JT}}{\hbar\omega}} \sum_\alpha \gamma_\alpha (b_{j\alpha} - b_{j\alpha}^\dagger)} c_{ia}^\dagger c_{jb}$$

$$\tilde{H}_{\text{ph}} = \hbar\omega \sum_{i\alpha} \left(b_{i\alpha}^\dagger b_{i\alpha} + \sqrt{\frac{\Delta_{JT}}{\hbar\omega}} n_i \gamma_\alpha (b_{i\alpha}^\dagger + b_{i\alpha}) + \frac{\Delta_{JT}}{\hbar\omega} n_i^2 \gamma_\alpha^2 + \frac{1}{2} \right)$$

$$\begin{aligned} \tilde{H}_{\text{e}-\text{ph}} = \xi \sum_i & \left((b_{i2}^\dagger + b_{i2} + 2\sqrt{\frac{\Delta_{JT}}{\hbar\omega}} \gamma_2 n_i)(c_{i1}^\dagger c_{i2} + c_{i2}^\dagger c_{i1}) \right. \\ & + \left. (b_{i3}^\dagger + b_{i3} + 2\sqrt{\frac{\Delta_{JT}}{\hbar\omega}} \gamma_3 n_i)(c_{i1}^\dagger c_{i1} - c_{i2}^\dagger c_{i2}) \right) \end{aligned}$$

We then approximate the ground-state by the variational state

$$\left| \tilde{\Psi} \right\rangle_{\text{V}} = \left| \tilde{\Psi} \right\rangle_{\text{e}} \otimes \left| \tilde{\Psi}_0 \right\rangle_{\text{ph}} \tag{3.9}$$

where $\left|\tilde{\Psi}_0\right\rangle_{\text{ph}}$ is the transformed phonon vacuum. The final form of the Hamiltonian is then

$$
\begin{aligned}
\bar{H} &= \sum_{\langle i,j\rangle ab} t_{ij}^{ab} e^{-\frac{\Delta_{\text{JT}}}{\hbar\omega}\sum_\alpha \gamma_\alpha^2} \left(c_{ia}^\dagger c_{jb} + \text{H.c.} \right) + \Delta_{\text{JT}} \sum_i \left(\frac{\hbar\omega}{2\Delta_{\text{JT}}} + (\gamma_1^2 + \gamma_2^2)n_i^2 \right) \\
&\quad + 2\xi\sqrt{\frac{\Delta_{\text{JT}}}{\hbar\omega}} \sum_i n_i \left[\gamma_2(c_{i1}^\dagger c_{i2} + c_{i2}^\dagger c_{i1}) + \gamma_3(n_{i1} - n_{i2}) \right]
\end{aligned}
$$

where we have calculated the average over the phonon vacuum. At this point we diagonalize the above Hamiltonian using the γ_α's as variational parameters. The results for the ground-state and exchange energy are shown in Fig. (3.3). We see that, as expected from a variational scheme, the VLF energies are indeed higher than the exact energies. Also, we note that while the VLF is exact in the adiabatic limit ($\hbar\omega \gg t$) and yields good agreement in the opposite anti-adiabatic limit (strong coupling), it is a poor approximation in the intermediate range of the electron-phonon coupling. It has however been shown[32] that by modifying the operator S to include two-phonon coherent (or squeezed) states (these are an-harmonic terms which lower the polaronic band-narrowing effect and enhance the hopping) and inhomogeneous distortion of the lattice[20], the VLF agreement with exact diagonalization is substantially improved. Furthermore, it is also possible to increase the number of phonon states one averages over via successive perturbative corrections. That is, instead of taking the variational state to be of the form given by Eq. (3.9) one could imagine taking such a variational state as

$$
\left|\tilde{\Psi}\right\rangle_{\text{V}} = \left|\tilde{\Psi}\right\rangle_{\text{e}} \otimes \left(|0\rangle_{\text{ph}} + \lambda |1\rangle_{\text{ph}} + \lambda^2 |2\rangle_{\text{ph}} + ... \right)
$$

thus effectively adding more and more phonon states to the Hilbert space. Such an approach has been used in theoretical studies of the two-site Holstein model.[33]

Chapter 4

Lattice Coupling and Magnetic Exchange in NaNiO$_2$

4.1 Introduction

It is a puzzle as to why the two compounds, NaNiO$_2$ and LiNiO$_2$, in spite of having very similar crystal structures, show very different magnetic properties. The former is a type-A antiferromagnet (ferromagnetic layers coupled antiferromagnetically; Fig. 1), while the latter shows no long-range magnetic order. Experiments [1] on NaNiO$_2$ have revealed that the antiferromagnetic exchange interaction J_{AF} between the layers is considerably weaker than the ferromagnetic exchange J_F within the layer, $J_F \approx 1$ meV and $J_{AF} \approx -0.1$ meV. It is conceivable that the superexchange path between the layers being Ni-O-Na-O-Ni, replacing Na by Li weakens the inter-planar superexchange sufficiently so as to destroy the magnetism altogether, since the two-dimensional magnetism becomes untenable by virtue of the Mermin-Wagner Theorem.[34, 35]

The reduction of the inter-planar coupling could come either through differences in the electronic parameters such as the hopping parameters and charge-transfer energy or simply through the mass difference of the intervening alkali atom, which is quite large between Na
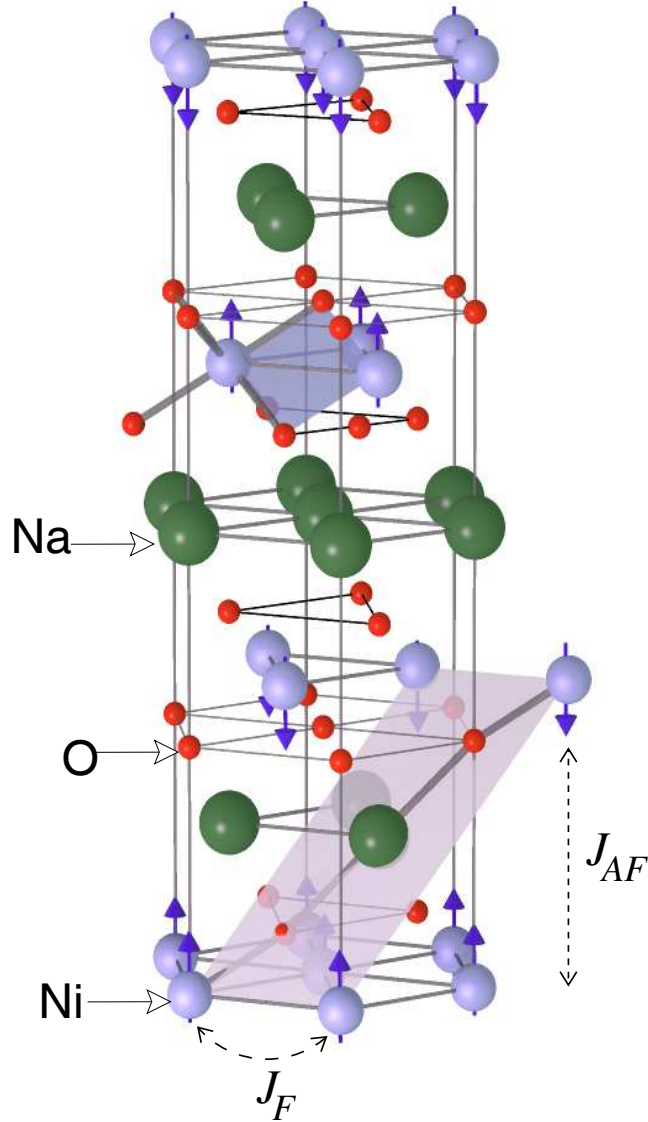
Figure 4.1: Crystal structure of $NaNiO_2$ at high temperature.[3] The low temperature structure is obtained by distorting the NiO_6 octahedra along the long Ni-O-Na-O-Ni bond shown in the figure. The magnetic ordering is anti-ferromagnetic type A and the two types of Ni-Ni exchange interactions J_F and J_{AF} are shown. The shaded plane is the plane of the charge density plot in Fig. 2. The shaded square in the upper portion of the figure shows the Ni-O-Ni-O plaquette for the 90° exchange as discussed in the text.

Table 4.1: Structural information for $NaNiO_2$ for both high and low-temperature structures.[1] The lattice parameters at low temperatures are $a = 5.311$Å, $b = 2.84$Å, $c = 5.568$Å, and $\beta = 110.4°$, while those for the high-T structure are $a = b = 2.96$Å, $c = 15.78$Å, and $\gamma = 120°$.

	Atom	x/a	y/b	z/c
	Na	0	1/2	1/2
$T \approx 10$ K	Ni	0	0	0
	O	0.2832	0	0.8047
	Na	0	0	1/2
$T > 490$ K	Ni	0	0	0
	O	0	0	0.2308

and Li. In view of the fact that isotope substitution has been known to alter the magnetic interactions, changing the magnetic transition temperature T_c in a variety of compounds such as Fe_3O_4 [36] and the manganites[14, 15, 25, 37, 30], it is important to examine the effect of the alkali mass .

In this chapter, we focus on the compound $NaNiO_2$. Starting with the density-functional band structure, we study the mechanism of the magnetic interaction as well as the effect of the sodium mass on it. We study this by proposing a model for the superexchange and solving it by a variational Lang-Firsov approach as well as by exact diagonalization and the fourth-order perturbation theory. From our model, we explain the mechanism of the exchange interactions for $NaNiO_2$, ferromagnetic within the layer and antiferromagnetic between the layers. However, we find that although there is some effect of the alkali mass on the magnetic interactions, it is not enough to describe the suppression of magnetism in $LiNiO_2$. It is suggested that differences in the electronic structure such as orbital ordering or simply the magnitudes of the Hamiltonian parameters could further reduce J_{AF}, enough to suppress the 2D magnetism in $LiNiO_2$.
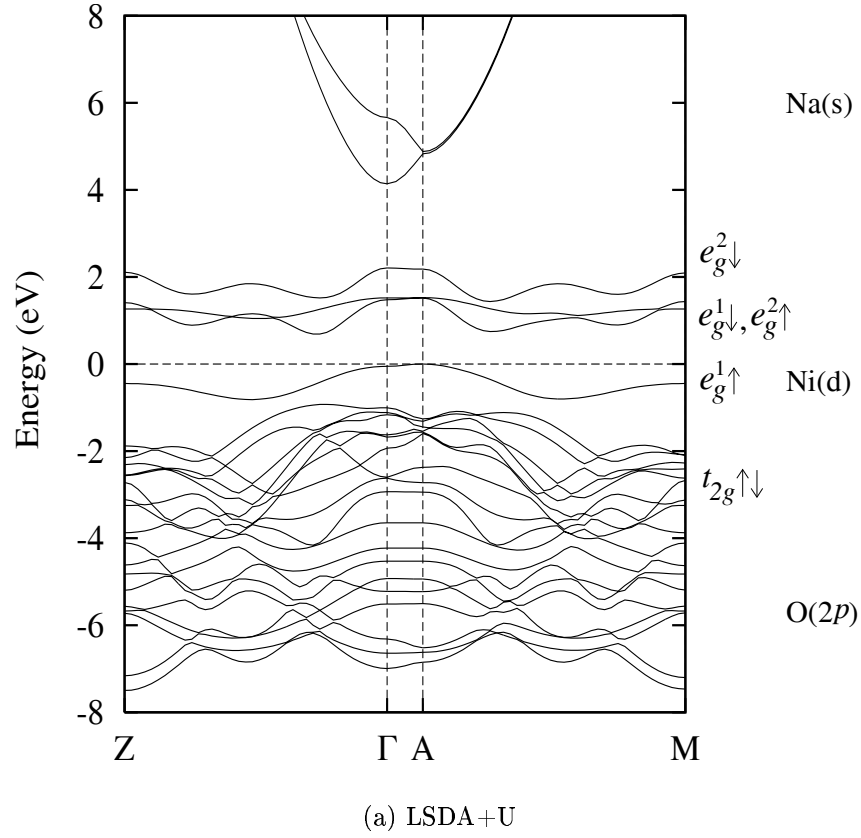
Figure 4.2: Density-functional electron bands for the antiferromagnetic NaNiO$_2$ obtained from the "LSDA+U" calculations. The low-temperature crystal structure with two formula units in the unit cell was used in the calculation. The e_g bands are split near the Fermi level due to the Jahn-Teller and exchange interactions. The LSDA calculation without the Coulomb U correction produces a similar band structure, except that the lowest e$_g$ band ($e_g^1 \uparrow$) is not completely detached from the rest of the e$_g$ bands, resulting in a metallic band structure.
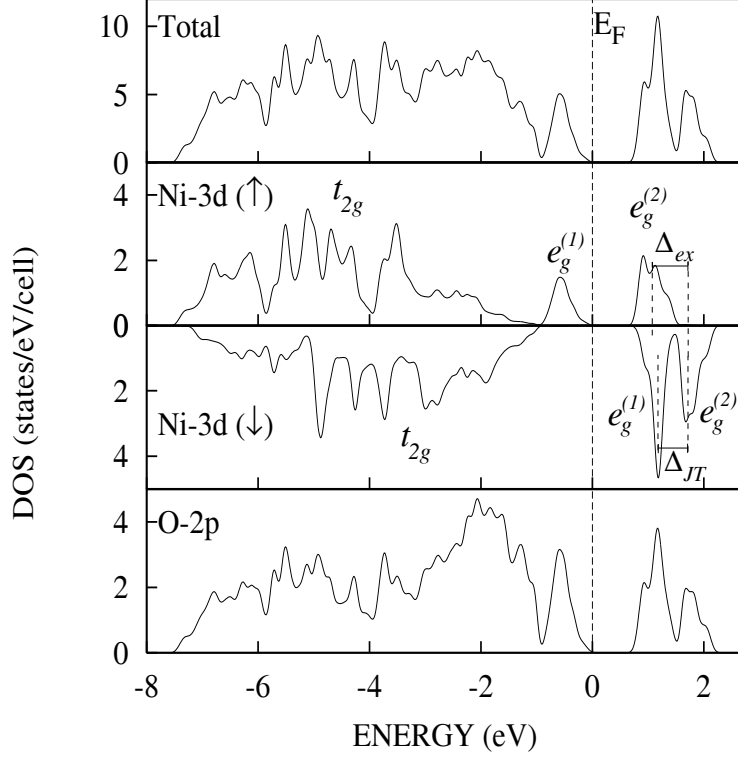
Figure 4.3: One-electron Densities-of-States for antiferromagnetic NaNiO$_2$.

4.2 Electronic Structure of NaNiO$_2$

We begin by discussing the *ab initio* electronic structure calculations based on density functional theory (DFT). At high temperature, NaNiO$_2$ has the simple hexagonal crystal structure (space group $R\bar{3}m$, no. 166) shown in Fig. 4.1, and undergoes a structural transition to a lower-symmetry monoclinic structure with the paramagnetic space group $C2/m$ (no. 12) at about 500 K [1]. This latter structure is layered and may be viewed as an arrangement of slightly elongated NiO$_6$ octahedra separated by Na sheets. The NiO$_6$ octahedra in this material are edge-sharing such that the Ni ions form a triangular lattice. There are two types of oxygen atoms due to the strong JT distortion, giving rise to two different Ni-O bond lengths: four short bonds of approximately 1.91 Å, and two long ones of 2.14 Å. The lattice parameters are taken from Ref. [1] The magnetic structure of this material is anti-ferromagnetic (AF) of type A with a Néel temperature of $T_N \approx 20$ K.[3]
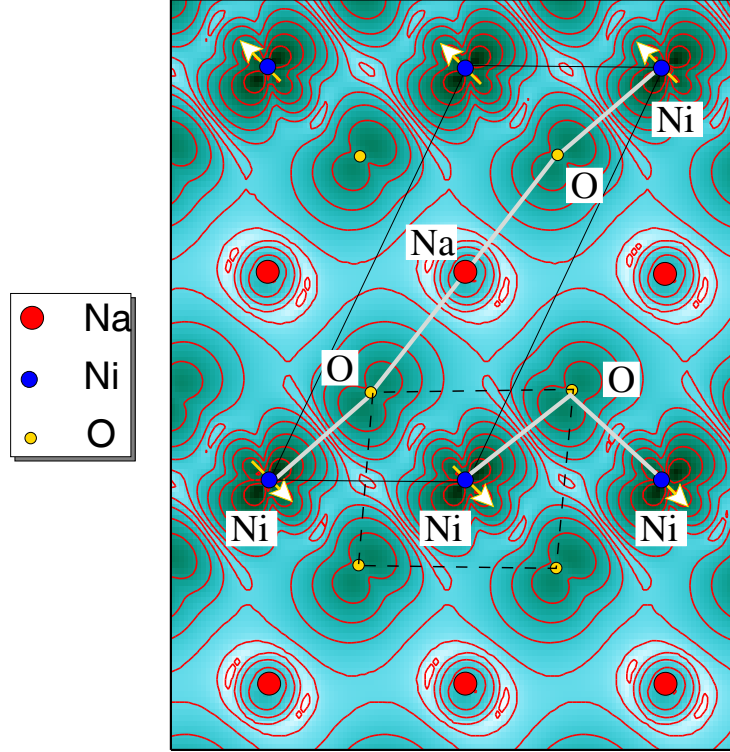
Figure 4.4: Charge-density contours for the occupied Ni(e_g) bands obtained from the local spin-density approximation and plotted on the shaded plane shown in Fig.4.1. The plane contains both the Ni-O-Na-O-Ni and the 90° Ni-O-Ni superexchange paths. The dashed-line rectangle indicates the Jahn-Teller distorted NiO$_6$ octahedron. All Ni(d) orbitals in the crystal are oriented along the same direction indicating the so-called "ferrodistorsive" orbital ordering, inferred from the neutron scattering experiments.[4, 5]

The *ab-initio* electronic structure calculations were performed for the low temperature structure using the local spin-density approximation (LSDA) to density functional theory (DFT). The self-consistent tight-binding linear muffin-tin orbitals (TB LMTO) method was used[38, 39]. In addition we made use of the "LSDA+U" correction[40] to better account for the correlation effects. The on-site Coulomb energy of $U = 5$ eV for the Ni(d) orbitals was used. In the magnetic calculation, the symmetry is not reduced further and the magnetic unit cell is also monoclinic with space group $C2/m$ with two formula units per unit cell. The calculations were scalar relativistic and the von Barth-Hedin[41] exchange-correlation potential was used.

Within the LMTO atomic sphere approximation (LMTO-ASA), the AF-A structure was found to be the ground state, lower in energy than both the ferromagnetic and paramagnetic configurations. It was found that the Ni ion is in a low spin state with the nominal occupations $t_{2g}^6 e_g^1$ and a magnetic moment $\mu \approx 0.5$ μ_B/Ni ion. The magnetic moment is significantly reduced from the expected Hund's rule value of $\mu = 1$ μ_B/Ni due to the strong hybridization of the Ni(d) and O(p) orbitals.

The band structure is shown in Fig. 4.2. The bands are consistent with a low-spin state , with the t_{2g} states being completely occupied while the e_g states are only 1/2-filled ($t_{2g}^6 e_g^1$). The t_{2g} and e_g bands are split by a strong crystal-field, while the $e_g^\uparrow$ and $e_g^\downarrow$ are split by the exchange coupling with a strength $\Delta_{ex} \approx 0.5$ eV. The Ni(d) occupation being $t_{2g}^6 e_g^1$, the atom is JT-active and the degeneracy of the e_g levels is then lifted, with a JT splitting $\Delta_{JT} \approx 0.6$ eV. The one-electron densities of states are shown in Fig. 4.3.

We have also computed the electronic charge density for an energy range which includes only the valence e_g band. In a frame of reference where the z axis points along the long Ni-O bond, we found this band to be of $3z^2 - r^2$ character. The charge-density contours are plotted in Fig. 4.4, which clearly show the "ferro-orbital ordering," where all the $3z^2 - r^2$ orbitals on all Ni atoms in the structure are oriented along the same direction, towards the elongated Ni-O bond which lies on the Ni-O-Na-O-Ni superexchange path as indicated in

40

the contour plot. Electronic structure calculations for the high-temperature structure, which has undistorted NiO_6 octahedra, were also performed and no orbital ordering was found for this structure. The DFT calculations are discussed in full detail in Ref. [42].

4.3 Magnetism in $NaNiO_2$

4.3.1 Intra-layer Exchange

The ferromagnetic exchange interaction within the plane is mediated via the oxygen atom forming the 90^0 Ni-O-Ni bond, which is weakly ferromagnetic according to the celebrated Goodenough-Kanamori-Anderson rules. The rule states that the 90^0 exchange between filled orbitals is ferromagnetic and relatively weak[11, 12].

To illustrate this for the present compound, we adopt a simple model shown in Fig. 4.5, retaining only the z^2 orbitals as the active orbital for electron transfer on the two transition metals, consistent with the orbital ordering shown in Fig. 4.4. The Ni t_{2g} orbitals are fully occupied. There are actually two 90^0 Ni-O-Ni paths forming a square plaquette as shown in Fig. 4.4, so that, considering the two paths to be independent, the exchange will be twice of the magnitude calculated for a single Ni-O-Ni path.

We assume that if two e_g electrons are present on the transition metal atom, they both will occupy the z^2 $\uparrow\downarrow$ orbitals, which is favored by the Jahn-Teller energy gain. The alternative configuration of z^2 $\uparrow$, $x^2 - y^2$ $\uparrow$ is considered to have a higher energy, because although favored by the Hund's rule, there is no JT energy gain for this state, which is important since two electrons are occupied. With this reasoning we omit the $x^2 - y^2$ orbital altogether in our model.

The magnetic interactions are best described in terms of the holes. With the oxygen shell full and the Ni z^2 orbitals occupied by one electron each, we have just two holes present in the system. Furthermore, we neglect the double occupancy of the holes on the Ni atom, which would have a much higher energy. With these simplifications, the Hamiltonian for the
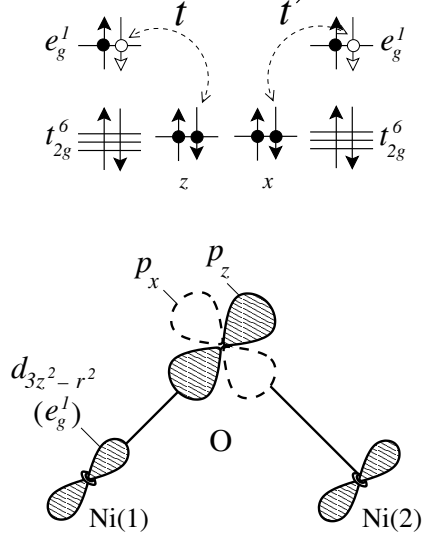
Figure 4.5: Model for the 90° Ni-O-Ni exchange interaction within the layer. Open arrows represent the holes. Double-arrowed, dashed lines indicate virtual processes with the hopping of the e_g^1 electrons from the neighboring transition-metal atoms to the oxygen atom giving rise to the ferromagnetic interaction.

holes reads

$$
\begin{aligned}
H &= \sum_{\sigma} (t d_{1\sigma}^{\dagger} c_{z\sigma} + t' d_{2\sigma}^{\dagger} c_{x\sigma} + \text{h.c.}) + \Delta \sum_{p=x,z} \sum_{\sigma} c_{p\sigma}^{\dagger} c_{p\sigma} \\
&+ \sum_{p=x,z} U_p n_{p\uparrow} n_{p\downarrow} J_H (n_{x\uparrow} n_{z\uparrow} + n_{x\downarrow} n_{z\downarrow}).
\end{aligned}
\tag{4.1}
$$

Here, the creation operator for a hole of spin σ on the oxygen in the $p = x$ or z orbital is denoted by $c_{p\sigma}^{\dagger}$, while the same for the two Ni sites are denoted by $d_{1\sigma}^{\dagger}$ and $d_{2\sigma}^{\dagger}$, respectively. The Coulomb energy and the Hund's exchange coupling on the oxygen site are denoted by U_p and J_H, while Δ is the charge transfer energy of the hole from the nickel to the oxygen site. The holes hop between Ni(1) and O(p_z) and between Ni(2) and O(p_x) orbitals, with the two hopping matrix elements being t and t', respectively. According to Harrison's tight-binding parametrization,[2] we have $t' \approx -t/2 = -V_{pd\sigma}/2$.

It is quite simple now to obtain the energies of the AF and FM states of the two holes

and take the difference to yield the exchange energy

$$J = E_{\uparrow\downarrow} - E_{\uparrow\uparrow}. \tag{4.2}$$

There are only four configurations for the two holes in both cases: $\{|\uparrow\, 00\, \uparrow\rangle,\ |0\uparrow 0\uparrow\rangle,$ $|\uparrow 0\uparrow 0\rangle,\ |0\uparrow\uparrow 0\rangle\}$ for the FM case (ferromagnetic) and $\{|\uparrow\, 00\, \downarrow\rangle,\ |0\uparrow 0\downarrow\rangle,\ |\uparrow 0\downarrow 0\rangle,\ |0\uparrow\downarrow 0\rangle\}$ for the FM case (antiferromagnetic). The arrows refer to the spin of the hole, where the first and the fourth labels in each configuration represent Ni1 and Ni2, while the second and the third labels represent p_z and p_x orbitals on the oxygen. It is quite simple now to obtain the energies of the AF and FM states of the two holes and take the difference to yield the exchange energy

$$J = E_{\uparrow\downarrow} - E_{\uparrow\uparrow}. \tag{4.3}$$

Consider the FM case with the parallel alignment of the two e_g electrons. The two spin-down holes are distributed among the four spin up states of oxygen and nickel. Of the total six configurations $(^4C_2)$, there are only four that are relevant for the ground state, viz., $\{|\uparrow\, 00\, \uparrow\rangle,\ |0\uparrow 0\uparrow\rangle,\ |\uparrow 0\uparrow 0\rangle,\ |0\uparrow\uparrow 0\rangle\}$. The remaining $|\uparrow\uparrow\, 00\rangle$ and $|00\,\uparrow\uparrow\rangle\}$ configurations don't mix, because there is no possibility of hole transfer between the two Ni atoms. They are therefore not considered as part of the working Hilbert space. The arrows here refer to the spin of the hole, where the first and the fourth labels in each configuration represent Ni1 and Ni2, while the second and the third labels represent p_z and p_x orbitals on the oxygen. Similarly, we only have the four relevant configurations $\{|\uparrow\, 00\, \downarrow\rangle,\ |0\uparrow 0\downarrow\rangle,\ |\uparrow 0\downarrow 0\rangle,\ |0\uparrow\downarrow 0\rangle\}$ for the AF case.

The Hamiltonians are then written as

$$H = \begin{pmatrix} 0 & t & t' & 0 \\ t & \Delta & 0 & t' \\ t' & 0 & \Delta & t \\ 0 & t' & t & \Delta' \end{pmatrix} \quad (4.4)$$

where $\Delta' = 2\Delta + U_p - J_H$ for the FM case and $\Delta' = 2\Delta + U_p$ for the AF case. It is obvious from the structure of the Hamiltonian why the FM state will have the lower energy. The only difference between the two Hamiltonians is the on-site energy Δ', which is lower in the FM case and hence a larger gain of the hybridization energy by configuration mixing.

Quantitatively, the ground-state energies for the FM and AF configurations are computed using the standard fourth-order non-degenerate perturbation theory[17] and taking the off-diagonal part of the Hamiltonian as the perturbation. Applying this to the Hamiltonians Eq. (4.4), we obtain the intra-layer exchange (denoted commonly by J_F for this compound) to be

$$J_F = 2 \times \frac{V_{pd\sigma}^4}{\Delta^2} \left(\frac{1}{U_p + 2\Delta - J_H} - \frac{1}{U_p + 2\Delta} \right), \quad (4.5)$$

where the factor of two comes from the fact that there are two 90° Ni−O−Ni paths on the square plaquette. The result is consistent with the expression given by Mostovoy and Khomskii[43] and is weakly ferromagnetic in agreement with one of the Goodenough-Kanamori-Anderson rules, which states that: "A 90°-exchange between half-filled orbitals is ferromagnetic and weak".[12]

The basic physical mechanism of the ferromagnetic coupling is simple. For the FM alignment of the Ni spins, the two-hole state on oxygen has the same spins, whose energy is lower by J_H (Hund's energy on the oxygen site) as compared to the energy of the two-hole state with opposite spins. The latter is relevant for virtual hopping in the case of the AF alignment of the Ni spins. Virtual hopping therefore produces a larger gain of energy for the FM case than for the AF case. It is this difference that leads to the FM interaction as seen

explicitly from the perturbation-theory result of Eq. (4.5). Within our model, the magnetic exchange would be zero if there was no Hund's energy on the oxygen site.

It is clear from Eq. (4.5) that the interaction is always ferromagnetic, irrespective of the Hamiltonian parameters. However, as usual, the strength of the interaction is obviously quite sensitive to the magnitude of the parameters. Taking typical parameters: $V_{pd\sigma} = 1$ eV, $\Delta = 4$ eV, $U_p = 5$ eV, and $J_H = 1$ eV, we find the value for $J_F \approx 10$ K, which is of the same order of magnitude as the measured value of 13 K.[1]

4.3.2   Inter-layer Exchange

We now turn to the inter-layer exchange coupling, which is experimentally anti-ferromagnetic and in view of it, is denoted by the symbol J_{AF}. The superexchange path is the Ni-O-Na-O-Ni path as shown in Fig. 1 and also in Fig. 4. Similar paths that connect the Ni atoms on the adjacent layers but with a 90° bend at the Na atom (see Fig. 4) will have less contribution to exchange, because of the type of orbital ordering of the half-filled Ni(e_g) orbitals. Unoccupied Ni(e_g) orbitals have higher energy and will contribute much less to the exchange because of the larger energy denominator and are omitted in the model Hamiltonian like in the previous section.

We examine the magnetic exchange based on a simple three site model schematically shown in Fig. 4.6, where the electrons hop between the two Ni(e_g) orbitals located on the adjacent layers via the intermediate Na(s). In reality the Ni-Na hopping takes place via the intermediate O(p) orbitals, but for the sake of simplicity we have considered only the *effective* Ni-Na hopping t.

It is more convenient for the inter-layer case to write the Hamiltonian for the electrons rather than for the holes. There are two electrons in the system and, again, our goal is to calculate the AF-FM energy difference to determine the magnetic exchange. The Hamiltonian

reads

$$H_{el} = \sum_{\langle i,j \rangle \sigma} t_{ij} (c_{i\sigma}^{\dagger} c_{j\sigma} + \text{h.c.}) + \sum_i \varepsilon_i n_i + U_i n_{i\uparrow} n_{i\downarrow} \qquad (4.6)$$

where $c_{i\sigma}^{\dagger}$'s denote the creation operators for the electrons, t is the effective Ni-Na hopping, ε_i is the on-site energy at site i, where $i = 1, 2, 3$ are, respectively, Ni(1), Na, and Ni(2) atoms, and U_i's are the on-site Coulomb interactions on the Ni ($U_1 = U_3 = U_d$) and Na sites ($U_2 = U_s$). Note that for simplicity, we do not include in the model Hamiltonian the Jahn-Teller split e_g^2 orbital ("$x^2 - y^2$") because of its higher energy. In the present section, the hopping between Ni and Na is fixed $t_{ij} = t$; however it will be dependent on the atom positions when we include the electron-phonon coupling in a latter section.

The Hamiltonian for the FM state below is given in the basis set: $\{|110\rangle, |101\rangle, |011\rangle\}$, in that order, while the basis set used for the AF state is: $\{|100; 001\rangle, |100; 010\rangle, |100; 100\rangle, |010; 001\rangle, |010; 010\rangle, |010; 100\rangle, |001; 001\rangle, |001; 010\rangle, |001; 100\rangle\}$, where the first three numbers in each configuration correspond to the occupations of the spin $\uparrow$ orbitals on the Ni(1), Na, and Ni(2) atoms, respectively, while the remaining three numbers correspond to the occupation of the corresponding spin $\downarrow$ orbitals.

With these basis sets, the Hamiltonians read

$$H_{\uparrow\uparrow} = \begin{pmatrix} \Delta & t & 0 \\ t & 0 & t \\ 0 & t & \Delta \end{pmatrix}$$

and
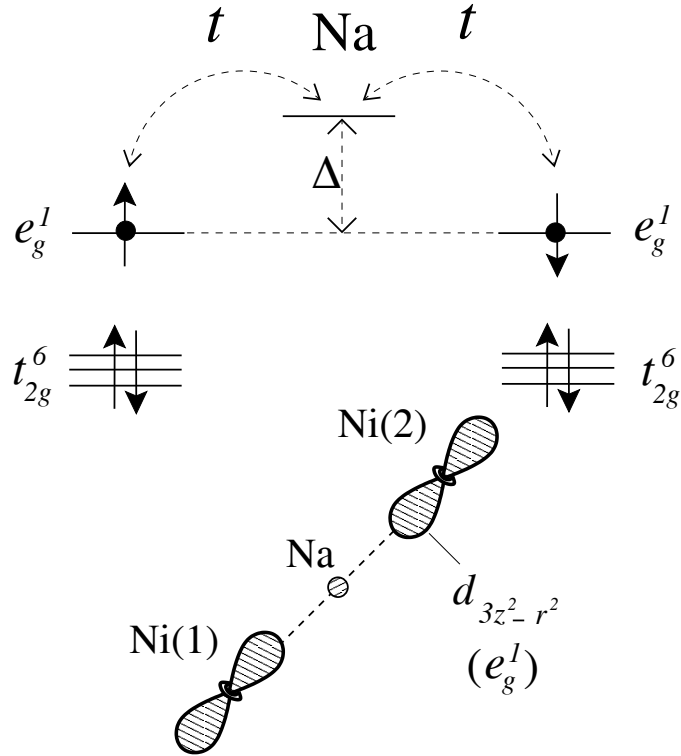
Figure 4.6: A three-site model for the magnetic exchange between the layers. The virtual hopping between nickel and sodium occurs via the intermediate oxygen atom, which is replaced in the model by an effective direct hopping between the nickel and the oxygen sites.

$$H_{\uparrow\downarrow} \;=\; \begin{pmatrix} 0 & t & 0 & t & 0 & 0 & 0 & 0 & 0 \\ t & \Delta & t & 0 & t & 0 & 0 & 0 & 0 \\ 0 & t & U_d & 0 & 0 & t & 0 & 0 & 0 \\ t & 0 & 0 & \Delta & t & 0 & t & 0 & 0 \\ 0 & t & 0 & t & U_s + 2\Delta & t & 0 & t & 0 \\ 0 & 0 & t & 0 & t & \Delta & 0 & 0 & t \\ 0 & 0 & 0 & t & 0 & 0 & U_d & t & 0 \\ 0 & 0 & 0 & 0 & t & 0 & t & \Delta & t \\ 0 & 0 & 0 & 0 & 0 & t & 0 & t & 0 \end{pmatrix}. \tag{4.7}$$

The Ni-Na charge-transfer energy cost Δ is given by

$$\Delta = \varepsilon_s - \varepsilon_d + \frac{1}{2}\Delta_{JT}, \tag{4.8}$$

where ε_s and ε_d are the Na and Ni on-site energies, respectively, and Δ_{JT} is the Jahn-Teller splitting between the two e_g orbitals as seen in Fig. 4.3, so that half of it is the JT energy gain for the electron.

First of all, we can conclude from the structure of the two Hamiltonians that the ground-state energy for the parallel configuration is higher than that of the anti-parallel configuration, for the simple reason that $H_{\uparrow\uparrow}$ forms a diagonal subblock of $H_{\uparrow\downarrow}$, so that the variational principle dictates the latter to have the lower ground-state energy, leading thus to an anti-ferromagnetic exchange.

For a quantitative result, we need to obtain the ground-state energies correct to the fourth-order in the perturbation theory. For the FM case, the exact ground-state energy is given by

$$E_{\uparrow\uparrow} = (\Delta - \sqrt{\Delta^2 + 8t^2})/2. \tag{4.9}$$

For the AF case, the exact expression for the ground-state energy is rather complicated and also the fourth-order (degenerate) perturbation theory is quite involved, unless the degeneracy is removed in a low order in the perturbation,[44] which is not the case here. Often in the literature, non-degenerate perturbation theory is applied erroneously in such cases, leading to a wrong prediction of the prefactor of the fourth-order term.

In the present case, fortunately, the symmetry present in $H_{\uparrow\downarrow}$ allows us to compute the ground-state energy $E_{\uparrow\downarrow}$ in the following manner. We first compute the eigenvalues numerically and find that the exact ground-state eigenfunctions have the symmetric form $|1, \alpha, \beta, \alpha, \gamma, \alpha, \beta, \alpha, 1>$. This can also be easily seen from the symmetry of the Hamiltonian 4.7. We then operate the Hamiltonian $H_{\uparrow\downarrow}$ (Eq. 4.7) on it, and solve the time-independent Schröedinger equation. As a result, we find that the ground-state eigenvalue λ satisfies the following transcendental equation:

$$\lambda^{-1} = (2U_d + U_s + 2\Delta - 3\lambda)(U_d - \lambda)^{-1}(U_s + 2\Delta - \lambda)^{-1} - (\Delta - \lambda)/(2t^2) \quad (4.10)$$

which we solve by an iterative method by starting with the initial guess $\lambda^{(0)} = 0$, which is the unperturbed energy, and iterating the expression (4.10) until convergence is achieved to the fourth order in the perturbation t. The result is

$$E_{\uparrow\downarrow} = -\frac{2t^2}{\Delta} + \frac{4t^4}{\Delta^3} - \frac{4t^4}{\Delta^2}\left(\frac{1}{U_d} + \frac{2}{U_s + 2\Delta}\right) + O(t^6) \quad (4.11)$$

Taking the energy difference between the FM and the AF configurations from Eqs. (4.9) and (4.11), we get the inter-layer exchange to be[45]

$$J_{AF} = -\frac{4t^4}{\Delta^2}\left(\frac{1}{U_d} + \frac{2}{U_s + 2\Delta}\right). \quad (4.12)$$

It is clear that the interaction is always antiferromagnetic, irrespective of the magnitudes of the Hamiltonian parameters. If we take as typical parameters: $t = 0.1$ eV, $\Delta = 1$ eV, and
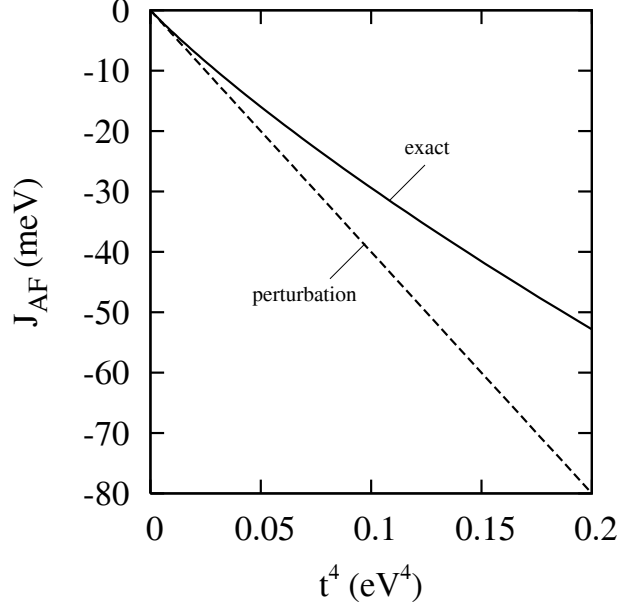
Figure 4.7: Comparison of the results of the perturbation theory Eq. (4.12) with the exact results, obtained by the diagonalization of Eq. (4.7), for the intra-layer exchange J_{AF}. Parameters are: $U_d = U_s = 5$ eV and $\Delta = 1$ eV.

$U_d = U_s = 5$ eV, we find $J_{AF} \approx -2.3$ K from Eq. (4.12), which is about the same order of magnitude as the experimental value of -1 K.[1]

If the orbital ordering is different from the one shown in Fig. (4.6), which might occur in LaNiO$_2$, the hopping integral between Ni(1) and Na will be different from that between Ni(2) and Na. Taking them as t and t', respectively, the above expression for J_{AF} becomes modified to

$$J_{AF} = -\frac{4t^2 t'^2}{\Delta^2} \left(\frac{1}{U_d} + \frac{2}{U_s + 2\Delta} \right).$$ (4.13)

For the orbital orientation shown in Fig. (4.8), Harrison's scaling gives us $t = V_{sd\sigma}$ and $t' = -t/2$, so that J_{AF} is reduced by a factor of four.
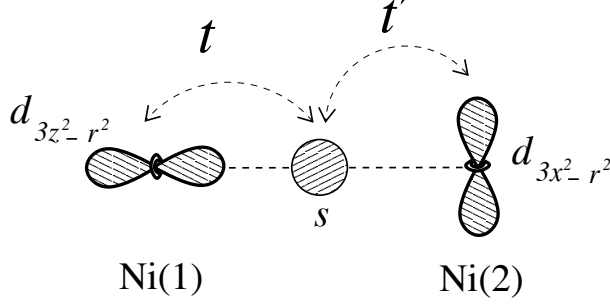
Figure 4.8: Model for inter-site superexchange with orbital ordering different from the ordering for $NaNiO_2$.

4.4 Effect of Electron-Phonon Coupling on Magnetism

4.4.1 The Electron-Phonon Hamiltonian

Since one of the differences between $NaNiO_2$ and $LiNiO_2$ is the atomic mass of the intervening alkali atom (Na or Li) through which the inter-layer superexchange is mediated, we examine the effect of this mass on the magnetic exchange. This will also allow us to predict the effect of sodium isotope substitution on the magnetic exchange.

To this end, we introduce a model electron-phonon Hamiltonian starting from a simple physical picture of the inter-layer electron hoping and the resulting NiO_6 distortions as indicated in Fig. 4.9. The total Hamiltonian is now

$$H = H_{el} + H_{e-ph}, \qquad (4.14)$$

where the electronic part of the Hamiltonian H_{el} is given by Eq. 4.6 and the electron-phonon coupling part H_{e-ph} is developed below.

For the H_{e-ph} part, consider the following argument. First of all, we have the two e_g^1 electrons hopping between the three sites in our model. Now, as shown by our DFT calculations, the Ni (d) orbitals have a nominal valence of $t_{2g}^6 e_g^1$ such that the Ni ion is in a low-spin configuration with a half-filled e_g orbital. When the e_g electron hops from the Ni

51
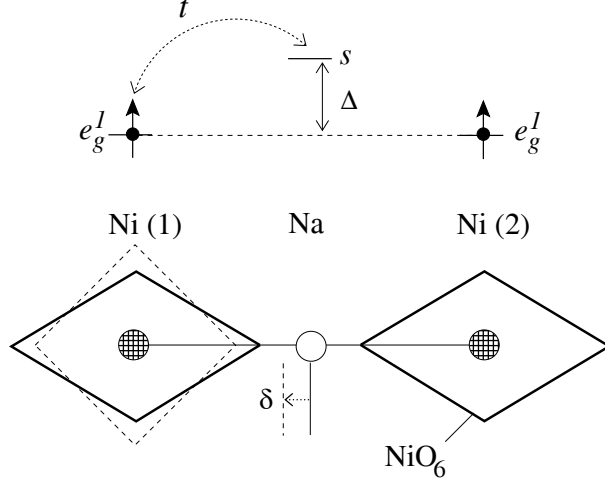
Figure 4.9: Fluctuating Jahn-Teller distortion of the NiO_6 octahedra and the consequent displacement of the Na ion. The dashed square around Ni (1) indicates the undistorted NiO_6 octahedron when the e_g orbital on that site is empty, while the solid squares indicate the Jahn-Teller distorted octahedra when the Ni atoms are occupied by one e_g electron each. The fluctuating distortions of the NiO_6 octahedra in turn induce the motion of the intermediate sodium atom, which is modeled by the electron-phonon Hamiltonian H_{e-ph} as discussed in the text.

site, the JT distortion of the NiO_6 octahedron is relaxed - Ni is t_{2g}^6 now with no degeneracy to produce the JT distortion - causing a displacement of the intermediate Na ion. For example, if the Ni(2) (e_g) and Na(s) sites are both occupied by an electron each, the NiO_6 octahedron on the Ni (1) site will be undistorted, causing a net displacement of the Na ion to the left as shown in Fig. 4.9. The different electronic occupations of the Ni-Na-Ni complex will give rise to different distortions as shown in Table 4.2. For instance, if $n_1 = 0$, $n_2 = 1$, and $n_3 = 1$, we have an equilibrium displacement of $-\delta$ for the Na ion. As seen from the Table, the equilibrium position of the Na atom for all possible electron configurations is given by the simple expression

$$x_0 = \Gamma\delta, \tag{4.15}$$

with

$$\Gamma = (1 + n_2)(n_1 - n_3)/2 \tag{4.16}$$

and n_1, n_2, and n_3 being, respectively, the electron occupations of the Ni (1), Na, and the

Ni (2) sites.

This leads to the coupling of the ionic motion to the electronic degrees of the freedom, which we describe by the displaced harmonic oscillator

$$H_{e-ph}^{(1)} = \frac{p^2}{2m} + \frac{K}{2}(x - x_0)^2, \tag{4.17}$$

where the mass of the Na atom is denoted by m, $K = m\omega^2$ is the lattice spring constant, and ω is the frequency of the phonon mode.

There is a second part to the coupling as a result of the dependence of the electronic hopping on the distance between the atoms, which was the main ingredient of the Su-Schrieffer-Heeger (SSH) model[46, 47] of the soliton. The hopping between Ni(1) and Na is a function of the distance between the two atoms and can be approximated by keeping the linear term, so that

$$t_{12} = t(|x_{Ni_1} - x_{Na}|) \approx t - t'x, \tag{4.18}$$

where t is the hopping with Na fixed at the center $(x = 0)$ between Ni(1) and Ni(2) and x is the deviation of the Na atom from this position. Similarly, hopping between Ni(2) and Na is

$$t_{23} = t(|x_{Ni_2} - x_{Na}|) \approx t + t'x. \tag{4.19}$$

The constant term in hopping reproduces the electronic part H_{el} (Eq. 4.6), while the linear term adds the electron-phonon coupling part

$$H_{e-ph}^{(2)} = -t'x \sum_\sigma (c_{1\sigma}^\dagger c_{2\sigma} - c_{2\sigma}^\dagger c_{3\sigma}) + \text{h.c.} \tag{4.20}$$

The total Hamiltonian now reads

$$H = H_{el} + H_{e-ph}^{(1)} + H_{e-ph}^{(2)}, \tag{4.21}$$

where H_{el} is given by Eq. 4.6. At this point we make use of the second quantization formalism for the lattice degrees of freedom, and a quick calculation shows

$$
\begin{aligned}
H_{e-ph}^{(1)} &= \frac{p^2}{2m} + \frac{m\omega^2}{2}x^2 - m\omega^2\delta\Gamma x + \frac{m\omega^2}{2}\delta^2\Gamma^2 \\
&= \hbar\omega(b^\dagger b + \frac{1}{2}) - \sqrt{\frac{\hbar}{2m\omega}}m\omega^2\delta\Gamma(b + b^\dagger) + \frac{m\omega^2}{2}\delta^2\Gamma^2 \\
&= \hbar\omega(b^\dagger b + \frac{1}{2}) - \sqrt{\frac{\hbar\omega}{2m\omega^2}}m\omega^2\delta\Gamma(b + b^\dagger) + \frac{m\omega^2}{2}\delta^2\Gamma^2 \\
&= \hbar\omega(b^\dagger b + \frac{1}{2}) - \left(\hbar\omega\frac{m\omega^2}{2}\delta^2\right)^{1/2}\Gamma(b + b^\dagger) + \frac{m\omega^2}{2}\delta^2\Gamma^2.
\end{aligned}
$$

where $b^\dagger$ and b are respectively the phonon creation and annihilation operators, and $\lambda = (\hbar\omega\epsilon)^{1/2}$ is the effective electron-phonon coupling constant , with $\epsilon = K\delta^2/2$. The SSH part of the electron-phonon Hamiltonian in second-quantization is

$$
\begin{aligned}
H_{e-ph}^{(2)} &= -t'\left(\frac{\hbar}{2m\omega}\right)^{1/2}\left[\sum_\sigma(c_{1\sigma}^\dagger c_{2\sigma} - c_{2\sigma}^\dagger c_{3\sigma}) + \text{h.c.}\right](b + b^\dagger) \\
&= -\eta(b^\dagger + b)\sum_\sigma(c_{1\sigma}^\dagger c_{2\sigma} - c_{2\sigma}^\dagger c_{3\sigma}) + \text{h.c.} \quad\quad\quad (4.22)
\end{aligned}
$$

where

$$
\eta = t'\left(\frac{\hbar}{2m\omega}\right)^{1/2}. \quad\quad\quad (4.23)
$$

The electron-phonon Hamiltonian in second-quantized form is then given as

$$
\begin{aligned}
H_{e-ph} &= (b^\dagger b + 1/2)\hbar\omega - \lambda\Gamma(b + b^\dagger) + (\hbar\omega)^{-1}\lambda^2\Gamma^2 \\
&\quad - \eta(b^\dagger + b)\sum_\sigma(c_{1\sigma}^\dagger c_{2\sigma} - c_{2\sigma}^\dagger c_{3\sigma}) + \text{h.c.} \quad\quad\quad (4.24)
\end{aligned}
$$

The parameters that determine H_{e-ph} are the phonon frequency $\hbar\omega$ and the strength of the electron-phonon coupling λ. There are two main parameters in the problem: the energy ratio $t/\hbar\omega$ and the dimensionless coupling strength $\lambda/\hbar\omega$, as may be seen by scaling the Hamiltonians Eqs. (4.6) and (4.24) by $\hbar\omega$.

Table 4.2: Dependence of the equilibrium position x_0 of the sodium atom on the electronic occupations of the Ni (1), Na, and the Ni (2) sites, denoted by n_1, n_2, and n_3, respectively. The orbitals involved are e_g for the nickels and the s orbital for sodium.

n_1	n_2	n_3	Γ	x_0
1	0	1	0	0
0	1	1	-1	$-\delta$
1	1	0	1	$+\delta$

The main parameters that determine H_{e-ph} are the energy ratio $t/\hbar\omega$ and the dimensionless coupling strengths $\lambda/\hbar\omega$ and $\eta/\hbar\omega$, as may be seen by scaling the Hamiltonians Eqs. (4.6) and (4.24) by $\hbar\omega$.

To make a rough order of magnitude estimate of the coupling strengths, we take the force constant $K \sim 10$ eV/ Å^2, which yields $\hbar\omega \approx 13$ meV and taking the displacement $\delta \approx 0.1$ Å from the measured oxygen displacement for the NiO$_6$ octahedron, we find $\lambda \sim 45$ meV, so that the dimensionless coupling parameter $\lambda/\hbar\omega \sim 3$. Similarly, with $t \approx 0.1$ eV and using Harrison scaling[2] for t', so that $t' \approx 0.2$eV/Å, which yields $\eta \sim 10$ meV or $\lambda/\hbar\omega \sim 1$.

To make a rough order of magnitude estimate of λ, we take the force constant $K \sim 10$ eV/ Å^2 and the mass of the alkali atom $m = 23$ u, which yields

$$\hbar\omega = \hbar c \left(\frac{K}{mc^2} \right)^{1/2} = 1973 \text{ eV.Å} \left(\frac{10 \text{ eV/Å}^2}{23 \times 931.5 \times 10^6 \text{ eV}} \right)^{1/2} \approx 13 \text{ meV}$$

and taking the displacement $\delta \approx 0.1$ Å from the measured oxygen displacement for the NiO$_6$ octahedron, we find $\lambda \sim 45$ meV, so that the dimensionless coupling parameter $\lambda/\hbar\omega \sim 3$.

Note that in our model, we have not kept the vibrations of the oxygen octahedra, which of course must be considered if one is interested in the effect of the oxygen mass. In the present case, we reason that the vibrational modes of the oxygen octahedra will have much higher frequency (stronger chemical bonds) than the motion of the intervening sodium atom, so that the quantized octahedral vibrational modes will have much larger energies than the sodium vibrational mode. Coupling to the lower energy states has a larger effect because

of the energy denominator, which justifies the neglect of the coupling to the oxygen modes within the spirit of our work.

The electron-lattice coupling affects magnetism because it modifies the bare electron hopping parameters, which is the subject of study in the next section.

4.4.2   Solution of the Hamiltonian

The lattice effects may be studied either via the Lang-Firsov approach or by exact diagonalization. The former approach, although approximate, yields a physically appealing result by casting the lattice effects in terms of the renormalization of the electron hopping parameters. Within the VLF approach, [19, 48, 20] which is a variational method based on the canonical Lang-Firsov transformation[49], we introduce the unitary transformation of the Hamiltonian H'

$$
\begin{aligned}
\tilde{H} &= e^{-S} H' e^{S}, \\
S &= \alpha \frac{\lambda}{\hbar\omega} \Gamma (b^\dagger - b),
\end{aligned}
\tag{4.25}
$$

where α is a variational parameter and S is anti-Hermitian, so that the transformation described by $U = e^{-S}$ is unitary and $H' = H_{el} + H^{(1)}_{e-ph}$. Note that the transformation can diagonalize the electron-phonon part of the Hamiltonian exactly with the choice of $\alpha = -1$ (see Eqs. 4.33 and 4.30), but the electronic part becomes modified, with the phonon operators entering the electronic Hamiltonian Eq. (4.33). The variational parameter α is a measure of the phonon "dressing" of the electron, the so-called Lang-Firsov small polaron.

Although the transformation is designed to work well in the strong coupling limit, we find that it works quite well in our case, where the coupling $\lambda/\hbar\omega$ is not that high. A better but more involved Lang-Firsov transformation[19, 20] consists of three consecutive variational transformations defined by S, $S' = \beta(b^\dagger - b)$, and $S'' = \gamma(b^\dagger b^\dagger - bb)$, where α, β, and γ are variational parameters, each designed to work well in the high, low, and intermediate

coupling regimes respectively. In the "Methods" section we have discussed the transformation of the Hamiltonian Eq. 4.14 under the full unitary transformation

$$U = e^S e^{S'} e^{S''}.\qquad(4.26)$$

In order to compute the transformed Hamiltonian, we begin by computing the transformed boson and fermion operators $\tilde{b}$ and $\tilde{c}_{i\sigma}$. Using the general expression for a transformed operator in terms of the corresponding commutators

$$\tilde{A} = e^{-S} A e^S = A + [A, S] + \frac{1}{2!}[[A, S], S] + ...,\qquad(4.27)$$

it is necessary to compute the commutators $[b, S]$ and $[c_{i\sigma}, S]$. The first commutator is given by

$$[b, S] = \alpha \frac{\lambda}{\hbar\omega}\Gamma\,[b, b^\dagger] = -\alpha\frac{\lambda\Gamma}{\hbar\omega}\qquad(4.28)$$

which gives the transformed boson operator as

$$\tilde{b} = b - \alpha\frac{\lambda\Gamma}{\hbar\omega}.\qquad(4.29)$$

As a result the transformed electron-phonon Hamiltonian is given by

$$
\begin{aligned}
\tilde{H}_{e-ph} &= \hbar\omega(b^\dagger b + \frac{1}{2}) - \alpha\frac{\lambda\Gamma}{\hbar\omega}\hbar\omega(b + b^\dagger) + \hbar\omega\left(\alpha\frac{\lambda\Gamma}{\hbar\omega}\right)^2 \\
&\quad - \lambda\Gamma\left(b + b^\dagger - 2\alpha\frac{\lambda\Gamma}{\hbar\omega}\right) + \frac{\lambda^2\Gamma^2}{\omega} \\
&= \hbar\omega\left(b^\dagger b + \frac{1}{2}\right) - (\alpha\lambda\Gamma + \lambda\Gamma)\left(b + b^\dagger\right) + \alpha^2\frac{\lambda^2\Gamma^2}{\hbar\omega} \\
&\quad + 2\alpha\frac{\lambda^2\Gamma^2}{\hbar\omega} + \frac{\lambda^2\Gamma^2}{\hbar\omega} \\
\Rightarrow \tilde{H}_{e-ph} &= \hbar\omega\left[b^\dagger b + \frac{1}{2} - (1 + \alpha)\frac{\lambda\Gamma}{\hbar\omega}\left(b + b^\dagger + (1 + \alpha)\frac{\lambda\Gamma}{\hbar\omega}\right)\right].
\end{aligned}
\qquad(4.30)
$$

In order to find the transformed Hamiltonian for the fermion operator, we compute the commutation relation

$$
\begin{aligned}
[c_{i\sigma}, S] &= -\beta[c_{i\sigma}, \Gamma](b - b^\dagger) \\
&= -\frac{\beta}{2}(b - b^\dagger)\left([c_{i\sigma}, n_2](n_1 - n_3) + (1 + n_2)[c_{i\sigma}, n_1 - n_3]\right) \\
&= -\frac{\beta}{2}(b - b^\dagger)\left(c_{2\sigma}(n_1 - n_3) + (1 + n_2)(c_{1\sigma} - c_{3\sigma})\right) \\
&= -\frac{\beta}{2}(b - b^\dagger)\left(\delta_{2i}(n_1 - n_3) + (1 + n_2)(\delta_{1i} - \delta_{3i})\right) c_{i\sigma} \\
\Rightarrow [c_{i\sigma}, S] &= B_i c_{i\sigma}
\end{aligned}
$$

which, by virtue of Eq. 4.27 gives

$$
\tilde{c}_{i\sigma} = e^{-B_i} c_{i\sigma}, \tag{4.31}
$$

where

$$
B_i = \frac{\alpha\lambda}{2\hbar\omega}(b^\dagger - b)\left[\delta_{2i}(n_1 - n_3) + (1 + n_2)(\delta_{1i} - \delta_{3i})\right].
$$

The transformed occupation numbers are then trivially computed as

$$
\begin{aligned}
\tilde{n}_i &= e^{-S} c_i^\dagger c_i e^S = e^{-S} c_i^\dagger e^S e^{-S} c_i e^S \\
&= \tilde{c}_i^\dagger \tilde{c}_i = c_i^\dagger e^{-B_i} e^{B_i} c_i = c_i^\dagger c_i \\
\Rightarrow \tilde{n}_i &= n_i. \tag{4.32}
\end{aligned}
$$

The transformed electronic Hamiltonian then reads

$$
\tilde{H}_{el} = t \sum_{\langle ij \rangle \sigma} c_{i\sigma}^\dagger e^{\frac{\alpha\lambda}{2\hbar\omega}\nu_{ij}(b^\dagger - b)} c_{j\sigma} + \text{h.c.} + \sum_i (\varepsilon_i n_i + U_i n_{i\uparrow} n_{i\downarrow}) \tag{4.33}
$$

and where $\nu_{ij} = -\nu_{ji}$, $\nu_{12} = (3/2) - n_1$, and $\nu_{23} = (3/2) - n_3$. The Hamiltonian is then averaged over the bare phonon vacuum $|\Psi_{ph}^0\rangle$. In general, the average over the phonon

vacuum of the operator $e^{x(b^\dagger - b)}$ is given by

$$
\begin{aligned}
\left\langle \Psi_{ph}^0 \right| e^{x(b-b^\dagger)} \left| \Psi_{ph}^0 \right\rangle &= \left\langle \Psi_{ph}^0 \right| e^{-xb^\dagger} e^{xb} e^{-\frac{x^2}{2}[-b^\dagger,b]} \left| \Psi_{ph}^0 \right\rangle = \left\langle \Psi_{ph}^0 \right| e^{-xb^\dagger} e^{xb} e^{-\frac{x^2}{2}[b,b^\dagger]} \left| \Psi_{ph}^0 \right\rangle \\
&= e^{-\frac{x^2}{2}} \sum_{l,m=0}^{\infty} \frac{(x)^l}{l!} \frac{(-x)^m}{m!} \left\langle \Psi_{ph}^0 \right| (b^\dagger)^l (b)^m \left| \Psi_{ph}^0 \right\rangle \\
&= e^{-\frac{x^2}{2}} + \sum_{l,m=1}^{\infty} \frac{(x)^l}{l!} \frac{(-x)^m}{m!} \underbrace{\left\langle \Psi_{ph}^0 \right| (b^\dagger)^l (b)^m \left| \Psi_{ph}^0 \right\rangle}_{=0 \ , \forall l,m \neq 0}
\end{aligned}
$$

$$
\Rightarrow \langle 0 | e^{x(b-b^\dagger)} | 0 \rangle = e^{-\frac{x^2}{2}}. \tag{4.34}
$$

which yields the fully transformed Variational Lang-Firsov Hamiltonian

$$
\begin{aligned}
\bar{H} &\approx \langle \Psi_{ph}^0 | \tilde{H} | \Psi_{ph}^0 \rangle \\
&= t \sum_{\langle ij \rangle \sigma} c_{i\sigma}^\dagger e^{-\frac{\alpha^2 \lambda^2}{8\hbar^2 \omega^2} \nu_{ij}^2} c_{j\sigma} + \text{h.c.} + \sum_i (\varepsilon_i n_i + U_i n_{i\uparrow} n_{i\downarrow}) \\
&+ \frac{\hbar \omega}{2} + (1+\alpha)^2 \frac{\lambda^2}{\hbar \omega} \Gamma^2. \tag{4.35}
\end{aligned}
$$

There is some confusion in the literature[20, 48] as to which phonon vacuum must be averaged over, the bare or transformed phonon vacuum. Reference [48] refers to the "transformed phonon vacuum", meaning by this the state of the form $U^\dagger \left| \Psi_{ph}^{(0)} \right\rangle$, while reference [20] simply refers to the phonon vacuum leaving open the possibility that the state referred to is indeed the bare phonon vacuum $\left| \Psi_{ph}^{(0)} \right\rangle$. However, it is clear from the following that if the Hamiltonian $\tilde{H} = U^\dagger H U$ is averaged over the *transformed* phonon vacuum, the result is trivially

H_{el}+constant terms :

$$
\begin{aligned}
\left(\left\langle \Psi_{\mathrm{ph}}^{(0)} \right| U \right) \tilde{H} \left(U^\dagger \left| \Psi_{\mathrm{ph}}^{(0)} \right\rangle \right) &= \left\langle \Psi_{\mathrm{ph}}^{(0)} \right| U U^\dagger H U U^\dagger \left| \Psi_{\mathrm{ph}}^{(0)} \right\rangle \\
&= \left\langle \Psi_{\mathrm{ph}}^{(0)} \right| H \left| \Psi_{\mathrm{ph}}^{(0)} \right\rangle \\
&= H_{el} + \frac{\hbar\omega}{2} + \frac{\lambda^2}{\hbar\omega}\Gamma^2.
\end{aligned}
\tag{4.36}
$$

This last Hamiltonian will show no polaronic band-narrowing and, in general, lacks any dynamical properties necessary to describe the phonon subsystem. Therefore, the average is necessarily over the bare phonon vacuum.

Note that as compared to the original electronic Hamiltonian H_{el}, the hopping parameter becomes renormalized to a lower value, which is readily seen to reduce the magnetic exchange from the fourth-order perturbation theory. Also, $\bar{H}$ will clearly yield a variational upper bound to the ground-state energy, since the Hilbert space is now restricted to the zero-phonon subspace only.

In the exact diagonalization, the ground-state wave function is simply expanded in the joint electron-phonon occupation-number basis set: $|G\rangle = \sum_i a_i |i\rangle$, and the resulting Hamiltonian matrix is diagonalized using the Lanczos method. The Hamiltonian is truncated by keeping only a finite number of phonons, making sure that convergence of the ground-state energy has been achieved as a function of the number of phonons. Typically, ten to fifty phonons are needed to achieve convergence.

Fig. 4.10 shows the calculated energies using three different methods. The results indicate that the Lang-Firsov Hamiltonian is quite accurate as far as the ground-state energy is concerned. Within the VLF approximation, the ground-state energies for the FM and AF configurations are obtained by diagonalizing the Hamiltonian Eq. (4.35) and then by minimizing the energy as a function of the variational parameters α. In general this method would give a different minimum value of α for the FM and the AF configurations, but in practice we find that the minimum in α for the FM and AF configuration are very close
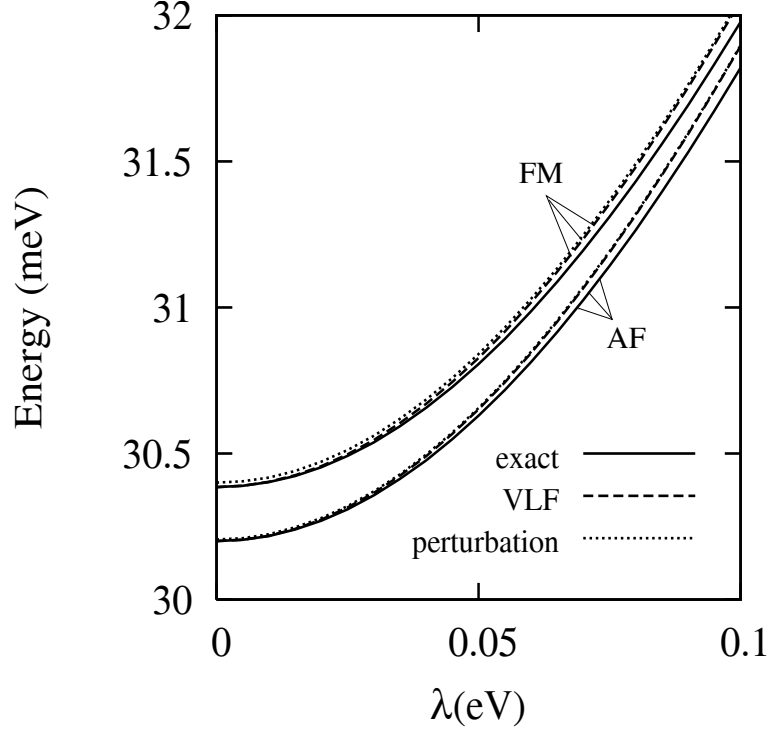
Figure 4.10: Energy of the FM and AF states using three different methods: a) Exact diagonalization of the full, untransformed Hamiltonian Eq. (4.14), b) Exact diagonalization of the Lang-Firsov Hamiltonian $\bar{H}$ (Eq. 4.35), and c) The fourth-order perturbation theory on the Lang-Firsov Hamiltonian $\bar{H}$. In the exact diagonalization method, the Hamiltonian is truncated by keeping only a finite number of phonons, making sure that convergence of the ground-state energy has been achieved as a function of the number of phonons. Often as few as only five phonons are needed. Note that the VLF energy is always above the exact energy, forming a variational lower bound to the ground-state energy. Parameters used here are: $\hbar\omega = 100$ meV, $t = 0.1$ eV, $U_d = 5$ eV, $U_s = 2$ eV, and $\Delta = 5$ eV.
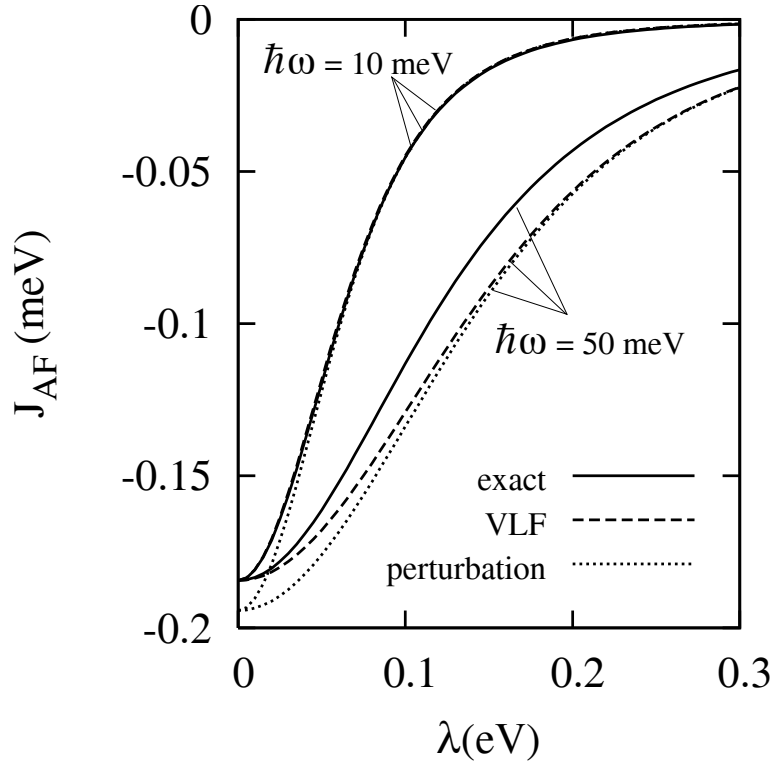
Figure 4.11: Plot of the exchange interaction J_{AF} as a function of the electron-phonon coupling. J_{AF} remains always antiferromagnetic, but its magnitude is decreased with increased strength λ of the electron-phonon coupling. Parameters used are the same as the previous figure except for $\hbar\omega$.

$\alpha_{AF} \approx \alpha_{FM} \sim 0.01$, so that we take them to be the same in writing down the perturbative result in Eq. (4.37) below.

Such a small value of α is indicative of the fact that the electron-phonon coupling does not affect the electronic system strongly. Indeed, as seen from the renormalized operators, Eq. (4.31), if α is zero, then we have just the bare electrons and phonons.

The Lang-Firsov Hamiltonian (4.35) may be written in a matrix form similar to Eq. (4.7) with modified off-diagonal hopping elements. Fourth-order perturbation theory carried out following the procedure of Section III (B) yields in the present case the following result for the inter-layer exchange:

$$
J_{AF} \approx \frac{-4t^4 e^{-5\alpha^2 \epsilon/(2\hbar\omega)}}{(\Delta + \epsilon)^2} \times \left[\frac{2e^{-2\alpha^2 \epsilon/\hbar\omega}}{U_s + 2\Delta} + \frac{1}{U_d + \epsilon} \right], \tag{4.37}
$$

where $\epsilon = \lambda^2/\hbar\omega$ as defined before. In the limit of no electron-phonon coupling, $\lambda/\hbar\omega \to 0$, this expression clearly reduces to Eq. 4.12. As indicated from the expression, the exchange remains always antiferromagnetic, however, the electron-phonon coupling diminishes the magnitude of J_{AF}. The result of the perturbation expression Eq. (4.37) together with the exact diagonalization and the Lang-Firsov results have been shown in Fig. 4.11.

The second part of the coupling $H_{e-ph}^{(2)}$ is somewhat cumbersome to treat by the Lang-Firsov approach, since it contains off-diagonal hopping terms. However, this coupling, parametrized by the strength η, also reduces the magnetic exchange, as seen from Fig. 4.12, obtained from exact diagonalization.

We now turn to the question of the dependence of the exchange interaction on the mass of the alkali atom. We have computed this by diagonalizing the full Hamiltonian, keeping all couplings. As mass is varied, the phonon frequency $\hbar\omega$ as well as the coupling strengths λ and η change, which are calculated using the parameters given in the caption of Fig. 4.13. The figure shows the result for two different values for the Ni to Na charge-transfer
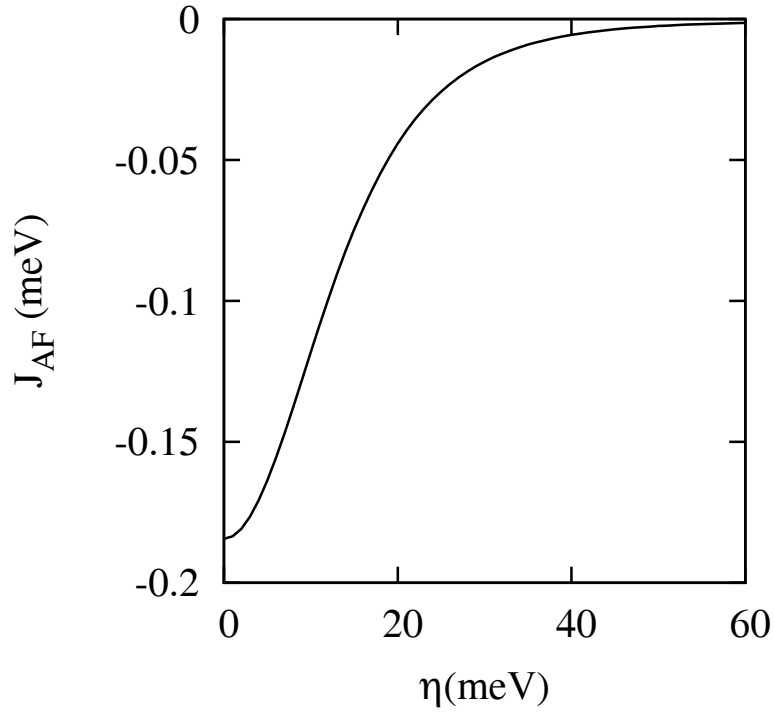
Figure 4.12: Plot of the exchange interaction J_{AF} as a function of the electron-phonon coupling strength η, with $\lambda = 0$, obtained from diagonalization of the full Hamiltonian Eq.(4.21). Parameters are: $\hbar\omega = 10$ meV, $t = 0.1$ eV, $U_d = 5$ eV, $U_s = 5$ eV, and $\Delta = 1$ eV.
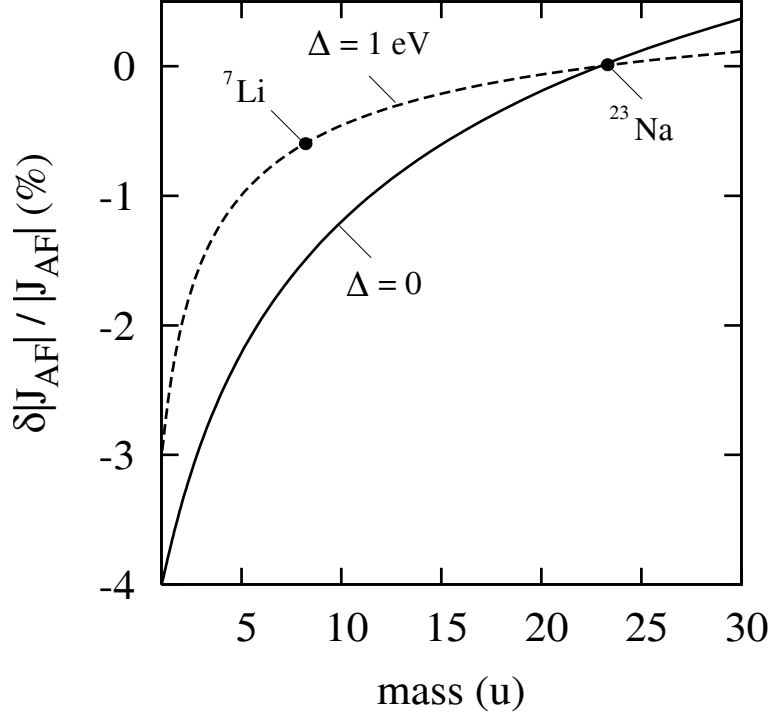
Figure 4.13: Dependence of the magnitude of the inter-planar exchange J_{AF} on the mass of the intermediate alkali atom for the parameters: $\hbar\omega = 10$ meV, $t = 0.1$ eV, $U_d = 5$ eV, and $U_s = 5$ eV. Δ is the Ni to Na charge transfer energy and $\delta|J_{AF}|/|J_{AF}| \equiv [|J_{AF}(m)| - |J_{AF}(Na)|] \times |J_{AF}(Na)|^{-1}$. A smaller Δ increases the fluctuation in Γ, thus enhancing the lattice effects on magnetism as discussed in the text.

energy Δ. Although the measured $J_{AF} \approx -1$ K is already quite small for $NaNiO_2$, we find a reduction of J_{AF} by only a small amount in going from ^{23}Na to ^{7}Li. We thus conclude that the difference in mass alone can not describe the differences in the magnetic behavior between the two compounds $NaNiO_2$ and $LiNiO_2$.

A further reduction in J_{AF} could come from changes in the electronic structure in going from $NaNiO_2$ to $LiNiO_2$. For example, neutron scattering experiments[5] have shown that unlike $NaNiO_2$, no long-range orbital ordering exists in $LiNiO_2$. An orbital ordering different from $NaNiO_2$ would diminish J_{AF} as indicated in the last part of Section III B, as would also a variation in the electronic parameters in the Hamiltonian.

4.5   Conclusion

We have studied the electronic structure and the exchange interaction in the Nickelate compound $NaNiO_2$. The density-functional results showed a ferrodistorsive orbital ordering with all $Ni(e_g)$ orbitals in the crystal pointed along the Ni-O bond, i.e., along the same crystallographic direction.

Both the intra- and the inter-layer exchange interactions are weak because of different reasons. The intra-layer exchange is mediated via the 90° Ni-O-Ni superexchange and is weakly ferromagnetic, consistent with the Goodenough-Kanamori-Anderson rules, while the inter-layer exchange is even weaker and antiferromagnetic due to the long Ni-O-Na-O-Ni superexchange path.

Finally, we studied the effect of the electron-phonon coupling on the magnetic exchange by solving a simple model Hamiltonian from exact diagonalization, variational Lang-Firsov, and perturbation theoretic approaches. While we found that the inter-layer exchange is indeed diminished by coupling to the lattice, this effect alone is not large enough to alter the magnetic behavior in going from $NaNiO_2$ to $LiNiO_2$. What is happening is that the inter-layer superexchange, which is especially small in this class of compounds owing to the long

Ni-O-Na-O-Ni superexchange path, becomes enhanced in $NaNiO_2$ due to orbital ordering (Ni orbitals pointed along Ni-O facilitating electron hopping, which in turn enhances the magnetic exchange). The J_{AF} (measured value ~ 1 K), although still relatively weak, is nevertheless strong enough to support magnetism between the layers and hence in the entire 3D structure. Within this scenario, what is suggested is that the weak magnetism in $NaNiO_2$ is the result of the specific type of orbital ordering in the compound, which allows for a strong enough exchange between the planes.

Chapter 5

Self-trapped magnetic polaron in the electron-doped CaMnO$_3$

Recent experiments have suggested that magnetic polarons may be present in the electron-doped Ca$_{1-x}$La$_x$MnO$_3$ with small x. In this work we study the problem of an electron in an antiferromagnetic (AF) cubic lattice as appropriate for the manganites. The effects of the various interactions are examined through a model Hamiltonian that includes both the nearest and the next-nearest neighbor hopping, the Anderson-Hasegawa double-exchange between the core spins and the conduction electron, as well as the electron-phonon coupling due to the static Jahn-Teller (JT) effect. We compute the ground state of the system using a variational technique and by solving exactly the resulting set of self-consistent equations. The energetics, size, and magnetic moment of the polaron are studied both with and without the JT coupling. While we show that the next-nearest-neighbor hopping significantly reduces the binding energy of the magnetic polaron, this reduction is not enough to destabilize the self-trapped state. We find the ground-state of the spin lattice to be close to a seven-site ferromagnetic cluster, where one core spin is turned by 180° and the doped electron is more or less confined to this cluster. The resulting net magnetic moment is approximately 7 μ_B/Mn ion in qualitative agreement with experiments.

5.1 Introduction

The magnetic polaron consists of an itinerant electron plus a local ferromagnetic (FM) region that it nucleates via exchange interaction in an otherwise antiferromagnetic lattice of local spins as indicated in Fig. 5.1. A distinction is made between the bound magnetic polaron (BMP), where the electron is bound to a defect center and polarizes the localized magnetic moments in its neighborhood, and the self-trapped magnetic polaron (STMP), where the electron is trapped in the magnetic potential well that it produces via the exchange interaction with the local moments. Analogous to the case of the lattice polaron (electron plus lattice distortion), the magnetic polaron must carry the magnetic distortion along with it, as it moves from site to site in the lattice. There are important differences in the conduction properties of the BMP and STMP. While the BMP should always show activated conductivity, the STMP should have metallic conductivity in the weak coupling limit, with a modified effective mass, and an activated conductivity in the strong coupling limit.

The BMP have been established in the magnetic semiconductors, where they lead to a number of novel properties such as the giant red shifts in the band gap and the spectacular metal-insulator transition in EuO. The STMP is believed to exist in the antiferromagnetic (AF) semi-conductors such as EuSe and EuTe as well as the Gd-doped family of materials $Eu_{1-x}Gd_xSe$ and $Eu_{1-x}Gd_xTe$.[50, 51, 52, 53] Their existence is however not conclusively established. Recent experiments[54] have suggested the existence of the STMP in the manganites, where measurements of the saturation magnetization of $Ca_{1-x}La_xMnO_3$ at low doping levels $(0.0 < x < 0.2)$ are consistent with the presence of local FM regions in the globally AF lattice. This was attributed by the authors to the stabilization of a STMP state in low electron-doped $CaMnO_3$.7

Theoretical work on the STMP dates back to the early seventies with the pioneering work of Kasuya[55], Mott[56], and Nagaev[57]. More recently, Pathak *et. al.* studied the problem in the continuous limit as well as for a lattice [58] using variational methods. Previous theories, however, did not approach the problem of the STMP with the manganites in mind.

As such, significant effects that determine the physics in these materials are neglected by many authors. Such effects as orbital degeneracy, JT coupling, and next-nearest-neighbor hopping are known to lead to important phenomena in the manganites. Recently, Chen and Allen[59] developed a model describing the magnetic polaron in the manganites, but neglected the next-nearest neighbor electron hopping which plays a crucial role in determining the energy of the STMP state. In this work we examine the energetics and the
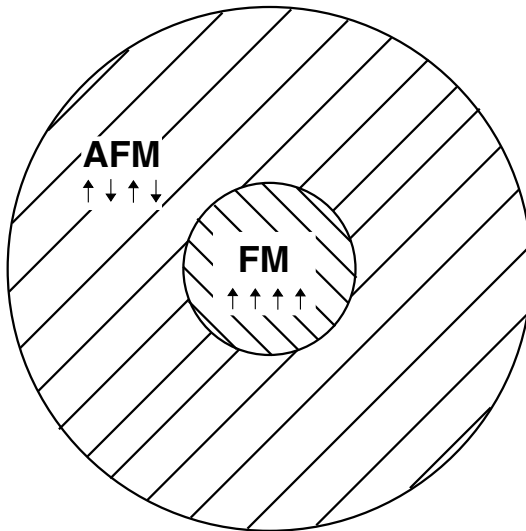
Figure 5.1: Schematic representation of the magnetic polaron. The continuous lattice is entirely AF except for a FM core. The core is spherical of radius R, and the electron is trapped inside by an infinite confinement potential of spherical symmetry.

formation of the self-trapped magnetic polaron in $Ca_{1-x}La_xMnO_3$ in the light doing limit, i.e., for small lanthanum concentration. In particular, we will consider what happens when a single electron is introduced into the AF lattice of $CaMnO_3$. Our model takes into account the coupling between the electronic, lattice, and spin degrees of freedom. A variational approach is adopted to study the ground state of the system within our model, the results of which are compared to density-functional calculations for selected cases.

Our conclusions may be summarized as follows. *1.* We find that the Jahn-Teller interaction increases the binding energy of the STMP only marginally, while the second-nearest-neighbor hopping has a much larger effect. *2.* This effect however is not strong enough to

destabilize the STMP state completely, leading to a polaron binding energy in the range of 100 meV or so. 3. The configuration of the lattice spins in the ground state with the added electron is generally a seven-site ferromagnetic cluster (central site plus the six nearest neighbors on the cubic lattice), formed by flipping the central spin. This is consistent with the experimental observation (Neumeier) as well as earlier theory work of Chen and Allen. 4. And, finally, we argue that the STMP in the electron doped $CaMnO_3$ should show activated conductivity and we estimate the activation energy for the hopping of the magnetic polaron.

The chapter is organized as follows. In section II we discuss the basic physics of the self-trapped magnetic polaron within the simple model of Mott. Section III introduces a model Hamiltonian appropriate to the magnetic polaron in $CaMnO_3$, while section IV describes the method used to find the ground state. In section V, we discuss the results of the model calculation and argue that the polaron conductivity should be activated type as observed in the experiments.

5.2 The Mott Polaron

Before studying the magnetic polaron in $CaMnO_3$, we discuss the Mott model which, despite its simplicity, captures many features of the magnetic polaron physics. We consider an AF lattice where the lattice spins interact through an anti-ferromagnetic Heisenberg-like exchange of the form $J\vec{S}_i.\vec{S}_j$ ($J > 0$ is the exchange coupling constant). When a single excess electron of mass m is introduced into the AF background, it will interact with the spins of the lattice via a ferromagnetic interaction. This interaction will tend to polarize a FM region of radius R around the site occupied by the excess electron (see Fig. 5.1).

If the energy cost to turn a single lattice spin from AF to FM is $2JS^2$ (the energy of the AF bond is by definition zero) then the energy required to form a polaron of radius R is $(\nu/2)2JS^2\frac{4\pi}{3}(R/a)^3$. If we refer to the number of nearest-neighbors (NN) around the site occupied by the excess electron as ν, then the number of site inside the FM core is

$\frac{4\pi}{3}\left(R/a\right)^3$. In addition, the electron is confined inside the FM region since hopping between AF sites is energetically unfavorable. In the limit where the Hund's rule coupling is infinite, the electron is forbidden to leave the FM core and is trapped inside an infinite potential well with a confinement energy $\hbar^2\pi^2/2mR^2$. The energy of the system is

$$E = \frac{\hbar^2\pi^2}{2mR^2} + \nu JS^2\frac{4\pi}{3}\left(\frac{R}{a}\right)^3 - 3t \tag{5.1}$$

where the last term is the band energy of the electron with t being the hopping constant $(t > 0)$. In the following we use the tight-binding approximation where the band-mass of the electron is such that $\frac{1}{m} = \frac{1}{\hbar^2}\frac{\partial^2 E}{\partial k_i^2}$. It can easily be shown that for a two bands model we have necessarily

$$\frac{\hbar^2}{m} = ta^2. \tag{5.2}$$

Using the above in Eq. (5.1), we eliminate the mass of the electron and minimize the Mott energy with respect to the radius R of the core. The radius and energy minima as a function of the dimensionless coupling constant $\alpha = t/JS^2$ are given by

$$R = \left(\frac{\pi\alpha}{4\nu}\right)^{1/5} a$$
$$E_{Mott}/t = A\alpha^{-2/5} - 3 \tag{5.3}$$

where $A \approx 18.55$ for a simple cubic lattice. The above equation shows that the energy of the Mott polaron as well as its size depend only on the ratio t/JS^2. This shows a competition between two interactions: the spin-spin interactions that favor an AF arrangement of the lattice spins, and the electronic hopping that favors a FM lattice. The latter will tend to increase the radius of the polaron, while the former will tend to reduce it. If we define the binding energy of the magnetic polaron as the energy gained by forming a FM core starting from an AF lattice

$$E_B^{Mottt} = E_{AF} - E_{Mott}, \tag{5.4}$$

then for parameters appropriate to CaMnO$_3$[31, 6, 60], $t = 0.5 - 0.75$ eV, and $JS^2 = 5$ meV,

we find a polaron radius $R \approx 1.81a$, and a binding energy varying from $E_B^{Mottt} = 0.03 - 0.38$ eV and increasing linearly as a function of t.

Jahn-Teller coupling– In order to describe the physics of the Jahn-Teller effect in this system, we wish to extend the above model to include the electron-phonon coupling. In manganites with perovskite structure, six oxygens form an octahedron around the manganese ions which have a Mn^{+4} valence (Fig. 5.2).
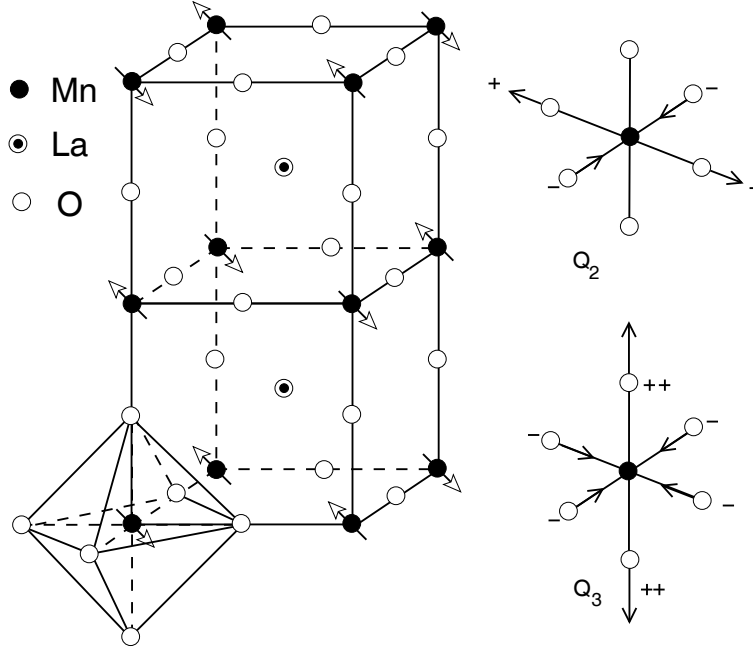
Figure 5.2: Type-G magnetic structure of $CaMnO_3$ and schematic description of the relevant normal modes of the MnO_6 octahedra. When the itinerant electron occupies an e_g orbital on the Mn ion, the Jahn-Teller effect causes the octahedron to distort. The arrows show the Jahn-Teller modes considered in this work.

When an excess electron occupies one of the Mn d orbitals, thus changing the valence from Mn^{+4} to Mn^{+3}, the MnO_6 octahedra will distort in order to lower the energy of the system via Jahn-JT coupling Teller coupling. in $CaMnO_3$ the JT coupling is of type $e \otimes E$, coupling the e_g electrons to the E_g normal modes of the isolated single octahedron. The Hamiltonian due to this JT effect may be written

$$H_{JT} = \frac{K}{2} \sum_{i=1}^{3} Q_i^2 - g(\sigma_x Q_2 + \sigma_z Q_3) \tag{5.5}$$

where Q_1, Q_2, and Q_3 are respectively the uniform, in-plane, and apical stretching modes of the isolated MnO$_6$ octahedron. The pseudo-spins σ_x, and σ_z are introduced to describe the coupling of the lattice to the orbital degrees of freedom. The lattice stiffness and electron-lattice coupling constants are denoted K and g.

It can then be shown[61] that the energy gain by JT effect is of the form $\frac{1}{2}K(Q_1^2 + Q_2^2 + Q_3^2) \pm g\sqrt{Q_2^2 + Q_3^2}$. This is the well-known "Mexican hat" potential for which the minimum in terms of the lattice distortions is given by $E_{JT}^{(1)} = -g^2/2K$, with an optimal distortion $Q_{min} = g/K$.

In our case however, the electronic wave function is spread out over the entire spherical FM region, thus "diluting" the electron-lattice coupling. Therefore the energy gained by distorting a single octahedron at a site a distance r from the center of the magnetic polaron is given by

$$E(r) = \frac{K}{2}Q^2 \pm gQn(r), \tag{5.6}$$

where $n(r)$ is the number of electrons at site r, and $Q(r)$ is the lattice displacement from equilibrium. The optimal lattice displacement Q_{min} is found by solving $\partial E/\partial Q = 0$ for Q, which gives

$$Q_{min} = \frac{g}{K}n(r) \tag{5.7}$$

and a minimum energy

$$E_{JT}(r) = -\frac{g^2}{2K}n^2(r). \tag{5.8}$$

The electron density $n(r)$ at site r is calculated as follows; if the electron is considered trapped by an infinite potential of spherical symmetry, its wave function is a solution to the classic electron-in-an-infinite-spherical-potential problem

$$\psi(r) = \left(\frac{\pi}{2R^3}\right)^{1/2} j_0\left(\frac{\pi r}{R}\right) = \left(\frac{1}{2\pi R}\right)^{1/2} \frac{\sin(\pi r/R)}{r}. \tag{5.9}$$

We assume the electron distribution to be uniform around a given site r and consider a

spherical shell of radius r and thickness dr; then the number of electrons at site r is $n(r) = a^3 |\psi(r)|^2$, while the number of MnO$_6$ octahedra in the shell is $\frac{4\pi r^2}{a^3} dr$. The correction to the Mott energy due to the JT distortion is then

$$
\begin{aligned}
E_{JT} &= \int_0^R E_{JT}(r) dr \\
&= -\int_0^R \frac{g^2}{2K} n^2(r) \frac{4\pi r^2}{a^3} dr \\
&= -\frac{g^2}{2K} c_0 \left(\frac{a}{R}\right)^3
\end{aligned}
\tag{5.10}
$$

where

$$
c_0 = \int_0^\pi \frac{\sin^4 x}{x^2} dx = 0.6721.
\tag{5.11}
$$

Therefore, in the presence of the JT interaction, the total energy of the Mott-like magnetic polaron is modified to

$$
E_{Mott} = -3t + \frac{t\pi^2 a^2}{2R^2} + \frac{4\pi\nu JS^2 R^3}{3a^3} - \frac{\Gamma t c_0 a^3}{2R^3}
\tag{5.12}
$$

where we have defined the dimensionless constant $\Gamma = g^2/Kt$.

Eq. (5.12) shows that the qualitative effect of the JT coupling in this system is to increase the binding energy of the magnetic polaron. Finding the minimum of E'_{Mott} using analytical methods is not simple, so we have used a numerical method in order to minimize Eq. (5.12) with respect to the magnetic polaron radius R for different values of the effective electron phonon coupling constant Γ. The results are shown in Fig.5.3. The two lines shown in the figure correspond to the Mott energy as a function of the polaron radius, with two different values of the electron phonon coupling constant Γ.

The solid line correspond to parameters appropriate to CaMnO$_3$(with $g = 2$ eV/Å, and $K = 10 - 20$ eV/Å^2) and its minimum gives a binding energy of $E_B^{Mottt} \approx 0.48$ eV and a polaron radius of $R = 1.8a$. These values are close to the ones found for the Mott polaron without JT effect, which shows that the effect of the JT distortion on the magnetic polaron
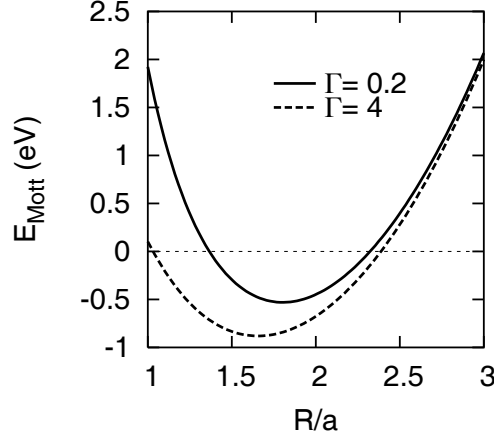
Figure 5.3: The total energy in the Mott approximation. The solid line correspond to $\Gamma = g^2/Kt \approx 0.67$, while the dotted and dashed lines correspond respectively to $\Gamma = 0$ and $\Gamma = 4$. This shows that the JT effect increases the binding energy of the magnetic polaron while reducing its size. The curve for $\Gamma = 0$ is not significantly different from the one for $\Gamma = 0.67$: the correction due to the JT distortion has a small effect on the magnetic polaron.

energy and radius is quantitatively small. The dashed curve shows the Mott energy for a much larger value of Γ, and demonstrates the qualitative effect of the JT distortion. The total energy is lowered by the JT gain $E_{JT} = \frac{\Gamma}{2}t\left(\frac{a}{R}\right)^3$, while the radius of the FM core is slightly reduced.

5.3 Hamiltonian for the Magnetic Polaron

In $CaMnO_3$ the valence of the Mn ions is 4+, with 3 electrons of parallel spin occupying the lower t_{2g} orbitals while the e_g orbitals $|3z^2 - r^2\rangle$ and $|x^2 - y^2\rangle$ are unoccupied and higher in energy due to the crystal field splitting. The t_{2g} and e_g orbitals of opposite spin are lifted higher in energy by the Hund's rule exchange as shown in Fig. 5.4. A single excess electron introduced in the system through light doping will thus occupy the lowest e_g orbital, with its spin parallel to that of the t_{2g} electrons, and will cause the degeneracy of the e_g orbitals to be lifted via cooperative JT effect.[62]

In order to study the formation and stability of the STMP state in a 3-dimensional $CaMnO_3$ cubic lattice, we have constructed a model that includes both the nearest and next-
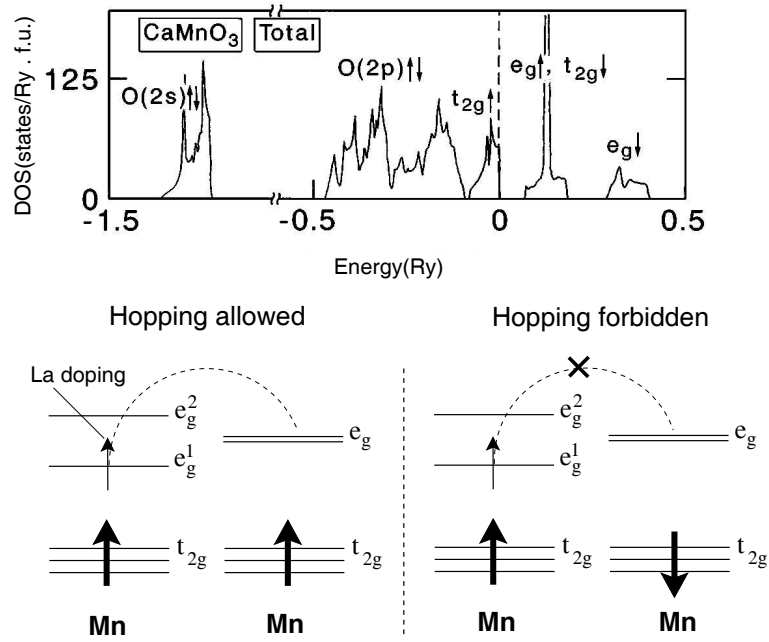
Figure 5.4: Density of state, and electron hopping between Mn ions in $CaMnO_3$. The Hund's rule exchange being infinite, the Mn-Mn electron hopping is forbidden when the spins of the $Mn(t_{2g})$ electrons are AF. The site occupied by the itinerant electron has a valence Mn^{+3}, which causes the degeneracy of the two e_g orbitals to be lifted due to the Jahn-Teller effect.

nearest neighbor electron hopping, the $t_{2g} - t_{2g}$ exchange interaction between local spins, as well as a static JT coupling between lattice and electron degrees of freedom. We also include the Hund's rule exchange coupling below, but it is assumed infinite as is customary in the manganites. However, in order to take the limit $I \to \infty$, where I is the Hund's exchange constant, we express the different terms of the total Hamiltonian

$$H = H_{el} + H_{spin} + H_{JT} \tag{5.13}$$

in a basis where the electronic spin quantization axis is parallel to the total t_{2g} spin $\vec{S}_i$ at each site i. The first and second terms Eq.(5.13) are the electronic hopping and $t_{2g} - t_{2g}$ exchange terms respectively, the third is the Hund's rule exchange coupling, and the last term is the electron-lattice coupling contribution to the total Hamiltonian H of the system.

In the following we derive the Hamiltonian and discuss the parameters used for the variational solution to the problem. The electronic hopping takes place between two sites for which the spins $\vec{S}_i$ and $\vec{S}_j$ are in general not parallel. If the electron spin-quantization axis is parallel to the global z direction, the hopping term is expressed as

$$H_{el} = \sum_{\langle ij \rangle} \sum_{\alpha\beta,\sigma} (t_{ij}^{\alpha\beta} a_{i\alpha\sigma}^{\dagger} a_{i\beta\sigma} + \text{H.c.}) + H_{Hund}. \tag{5.14}$$

The Koster-Slater matrix elements $t_{ij}^{\alpha\beta}$ shown in table 5.1 represent the hopping between orbitals α and β on sites i and j . $a_{i\alpha\sigma}^{\dagger} (a_{i\alpha\sigma})$ are the creation (annihilation) operators when the single excess electron with spin σ occupies the orbital α and site i, and H_{Hund} is the Hund's rule coupling term.

With the above choice of creation/annihilation operators the Hund's rule term will depend on the relative angles between the itinerant electron and lattice spins, which unnecessarily complicates the problem. Therefore, we choose to express the spin of the electron such that the spin-quantization axis is along the local lattice spin.

We define a new set of creation/destruction operators $(c_{i\alpha\sigma}^{\dagger}, c_{i\alpha\sigma})$ such that the quantiza-

Direction	$\langle e_g^1 \vert H_{el} \vert e_g^1 \rangle$	$\langle e_g^1 \vert H_{el} \vert e_g^2 \rangle$	$\langle e_g^2 \vert H_{el} \vert e_g^2 \rangle$
$\hat{x}$	$\frac{1}{4}V_\sigma$	$-\frac{\sqrt{3}}{4}V_\sigma$	$\frac{3}{4}V_\sigma$
$\hat{y}$	$\frac{1}{4}V_\sigma$	$\frac{\sqrt{3}}{4}V_\sigma$	$\frac{3}{4}V_\sigma$
$\hat{z}$	V_σ	0	0
$\hat{x}+\hat{y}$	$\frac{1}{4}V'_\sigma$	0	V'_π
$\hat{y}+\hat{z}$	$\frac{1}{16}V'_\sigma+\frac{3}{4}V'_\pi$	$\frac{\sqrt{3}}{16}V'_\sigma-\frac{\sqrt{3}}{4}V'_\pi$	$\frac{3}{16}V'_\sigma+\frac{1}{4}V'_\pi$
$\hat{z}+\hat{x}$	$\frac{1}{16}V'_\sigma+\frac{3}{4}V'_\pi$	$-\frac{\sqrt{3}}{16}V'_\sigma+\frac{\sqrt{3}}{4}V'_\pi$	$\frac{3}{16}V'_\sigma+\frac{1}{4}V'_\pi$

Table 5.1: The Koster -Slater hopping matrix elements between nearest and next-nearest neighbors e_g orbitals as calculated in [2]. $\vert e_g^1 \rangle$ and $\vert e_g^2 \rangle$ refer respectively to $\vert 3z^2 - r^2 \rangle$ and $\vert x^2 - y^2 \rangle$ d states, while $(V_\sigma,\ V_\pi)$ and $(V'_\sigma,\ V'_\pi)$are the first and second NN tight-binding hopping parameters.

tion axis is parallel to the net t_{2g} spin. As a consequence, the electronic hopping amplitudes will depend on the relative angle between the lattice spins. This considerably simplifies the expression of the Hund's rule coupling

$$H_{Hund} = -\frac{IS\hbar}{2}\sum_{i\alpha}(c^\dagger_{i\alpha\uparrow}c_{i\alpha\uparrow} - c^\dagger_{i\alpha\downarrow}c_{i\alpha\downarrow}) \tag{5.15}$$

where I is the Hund's rule exchange coupling constant. Replacing $a^\dagger_{i\alpha\sigma}(a_{i\alpha\sigma})$ by the new set of creation/annihilation operators $c^\dagger_{i\alpha\sigma}(c_{i\alpha\sigma})$ in Eq. (5.14) and taking the limit $I \to \infty$ the electronic part of the Hamiltonian becomes

$$H_{el} = \sum_{ij,\alpha\beta} t^{\alpha\beta}_{ij}\cos\frac{\chi_{ij}}{2}c^\dagger_{i\alpha}c_{j\beta} + \text{H.c.}, \tag{5.16}$$

where χ_{ij} is the angle difference between the spin angles θ_i and θ_j of two neighboring t_{2g} spins, and is defined such that

$$\chi_{ij} = \theta_j - \theta_i. \tag{5.17}$$

At each site i there are three angle differences corresponding to the three bonds in the positive x, y, z directions.

The magnetic interaction H_{spin} between lattice spins appearing in Eq. (5.13) is Heisenberg-like and is given by

$$H_{spin} = J \sum_{\langle i,j \rangle} \vec{S}_i . \vec{S}_j. \qquad (5.18)$$

Taking the spins to be classical and redefining the zero of energy such that the AF alignment of neighboring spins has zero energy, H_{spin} becomes

$$H_{spin} = JS^2 \sum_{\langle i,j \rangle} (1 + \cos \chi_{ij}). \qquad (5.19)$$

The last term in Eq. (5.13) is the electron-lattice coupling due to the JT effect. As the electron moves around the lattice, the valence of the Mn ions changes from 4+ to 3+. The MnO_6 octahedron seeks to reduce its energy by distorting itself, which leads to the splitting of the two e_g orbitals into $|3z^2 - r^2\rangle$ and $|x^2 - y^2\rangle$. The isolated MnO_6 octahedron has 12 normal modes of which we only consider the two giving rise to the above splitting. Throughout this work we have chosen to ignore the breathing mode Q_1, whose effect on the JT coupling is merely to shift the total energy. This coupling between the distortion of the lattice and the motion of the excess electron is described by the Hamiltonian

$$
\begin{aligned}
H_{JT} &= \sum_i \frac{K}{2} (Q_{1i}^2 + Q_{2i}^2 + Q_{3i}^2) \\
&- g [\, c_{i2}^\dagger \,\, , c_{i3}^\dagger \,] \begin{pmatrix} Q_{3i} & Q_{2i} \\ Q_{2i} & -Q_{3i} \end{pmatrix} \begin{bmatrix} c_{i2} \\ c_{i3} \end{bmatrix}.
\end{aligned}
\qquad (5.20)
$$

This is the same as Eq. (5.5), but we know sum over all lattice sites as well. The constants K and g have been defined earlier, and Q_{2i} and Q_{3i} refer respectively to the in-plane and apical stretching modes as defined in References [29, 28].

The nearest and next nearest neighbor hopping parameters are designated by $t_{1NN} = |V_{dd\sigma}|$ and $t_{2NN} = |V'_{dd\sigma}|$, and their values are obtained from the band-width estimates of

density functional theory (DFT) calculations as: [6] $t_{1NN} = 0.5-0.75$ eV and $t_{2NN} = 0.2-0.3$ eV. Note that we make use of the Harrison scaling[2] $V'_{dd\pi} \approx -0.54 V'_{dd\sigma}$ for the next-nearest neighbors inter-atomic matrix elements.

The remaining parameters are the $t_{2g} - t_{2g}$ exchange constant J, which is such that $JS^2 \approx 5$ meV[63, 64, 65], and the lattice elasticity and JT coupling constants which are estimated from *ab initio* DFT calculations[31] of LaMnO$_3$ to be $K = 10 - 20$ eV/Å^2 and $g = 2$ eV/Å.

5.4   Method of solution

The most general ground-state wave function is given by

$$|\Psi\rangle \;=\; |\psi_e\rangle \otimes |Q\rangle \otimes |\theta\rangle \tag{5.21}$$

where $|Q\rangle$ and $|\theta\rangle$ are the lattice and angle states in configuration space, and $|\psi_e\rangle = \sum_{i\alpha} \psi_{i\alpha} c^\dagger_{i\alpha} |0\rangle$ is the electronic wave function, with $\psi_{i\alpha}$ variational parameters. Using the pseudo-spins τ_x and τ_z to describe the different e_g orbitals, the total energy corresponding to the Hamiltonian Eq. (5.13) is given by

$$\begin{aligned}
E \;=\;& \sum_{ij}\sum_{\alpha\beta} t^{\alpha\beta}_{ij} \cos\frac{\chi_{ij}}{2} \psi^*_{i\alpha}\psi_{j\beta} \\
&+\; JS^2 \sum_{\langle i,j\rangle}(1+\cos\chi_{ij}) + \frac{K}{2}\sum_i Q^2_i \\
&-\; g\sum_i\sum_{\alpha\beta} \psi^*_{i\alpha}\psi_{i\beta}\left(\tau^{\alpha\beta}_x Q_{2i} + \tau^{\alpha\beta}_z Q_{3i}\right).
\end{aligned} \tag{5.22}$$

The problem is then to find the global minimum of the total energy (5.22) as a function of the variational parameters subject to the constraint that the wave function is normalized.

In order to do so we define the functional

$$F = E - \Lambda(\sum_{i\alpha} 1 - |\psi_{i\alpha}|^2).$$

The minima conditions are given by $\partial F/\partial \psi_{i\alpha} = 0$, $\partial F/\partial Q_{2i} = 0$, $\partial F/\partial Q_{3i} = 0$, and
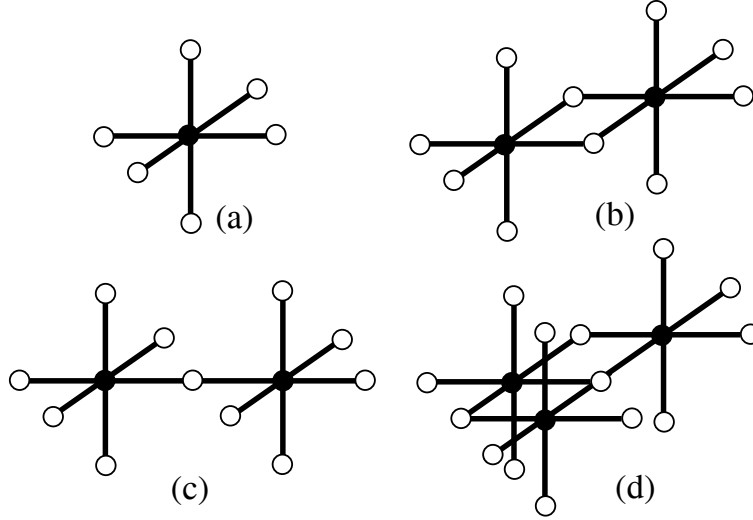
Figure 5.5: Ferromagnetic clusters used in optimizing the total energy in terms of the t_{2g} angles. These are formed by turning one to three spins by 180°. These clusters are labeled (a)seven-site FM, (b)twelve-site FM, (c)thirteen-site FM, and (d) seven-site FM. The particular spins flipped to form the clusters are shown in black. All circles represent Mn sites with same spin, while the remainder of the lattice is not shown and is anti-ferromagnetic of type G.

$\partial F/\partial\theta_i = 0$, which give the following set of non-linear equations

$$\sum_{j\beta} t_{ij}^{\alpha\beta} \cos\frac{\theta_i - \theta_j}{2}\psi_{j\beta} - \Lambda\psi_{i\alpha}$$

$$-\sum_{\beta} g(\tau_x^{\alpha\beta}Q_{2i} + \tau_z^{\alpha\beta}Q_{3i})\psi_{i\beta} = 0 \tag{5.23}$$

$$KQ_{2i} - g\sum_{\alpha\beta}\tau_x^{\alpha\beta}\psi_{i\alpha}^*\psi_{i\beta} = 0 \tag{5.24}$$

$$KQ_{3i} - g\sum_{\alpha\beta}\tau_z^{\alpha\beta}\psi_{i\alpha}^*\psi_{i\beta} = 0 \tag{5.25}$$

$$A\sin\frac{\theta_i}{2} + C\sin\theta_i$$

$$-B\cos\frac{\theta_i}{2} - D\cos\theta_i = 0 \tag{5.26}$$

where we have defined A, B, C, and D such that

$$A = \sum_j \varepsilon_{ij}\cos\frac{\theta_j}{2} \quad , \quad B = \sum_j \varepsilon_{ij}\sin\frac{\theta_j}{2}$$

$$C = \sum_j \varepsilon_{ij}\cos\theta_j \quad , \quad D = \sum_j \varepsilon_{ij}\sin\theta_j$$

and $\varepsilon_{ij} = \sum_{\alpha\beta} t_{ij}^{\alpha\beta}\psi_{i\alpha}^*\psi_{j\beta}$. The above set of coupled equations is then solved self-consistently by taking an initial guess of the angles θ then computing the lattice distortions Q_2 and Q_3, followed by the wave function ψ at each step. New angles θ are then computed by finding the roots of Eq. (5.26).

We compute the ground-state energy of the system and study the binding energy (BE) in terms of NN and NNN hoppings t_{1NN} and t_{2NN} as well as in terms of the electron-phonon coupling g. The binding energy E_B of the magnetic polaron is defined as the energy gained in forming a magnetic polaron state from a type-G AF arrangement of the t_{2g} lattice spins

$$E_B = E_{AF} - E_P.$$

The AF energy E_{AF} is calculated as the ground state energy of the system when the t_{2g}

spins are fixed in the AF type G configuration. This amounts to solving Eqs.(5.23-5.26) with the angles θ fixed in the AF type G configuration. The polaron energy E_P is the minimum found from the same set of equations but with the angles θ now allowed to vary between 0 and 2π.

The nature of the ground-state to which the above algorithm will converge is strongly dependent on the initial guess, in particular, the initial guess for the angles θ. In order to avoid convergence to a local minimum (meta-stable state), this guess must be chosen appropriately. We have chosen as such starting guesses the clusters shown in Fig. 5.5, formed by turning one or more spin.

5.5   Results
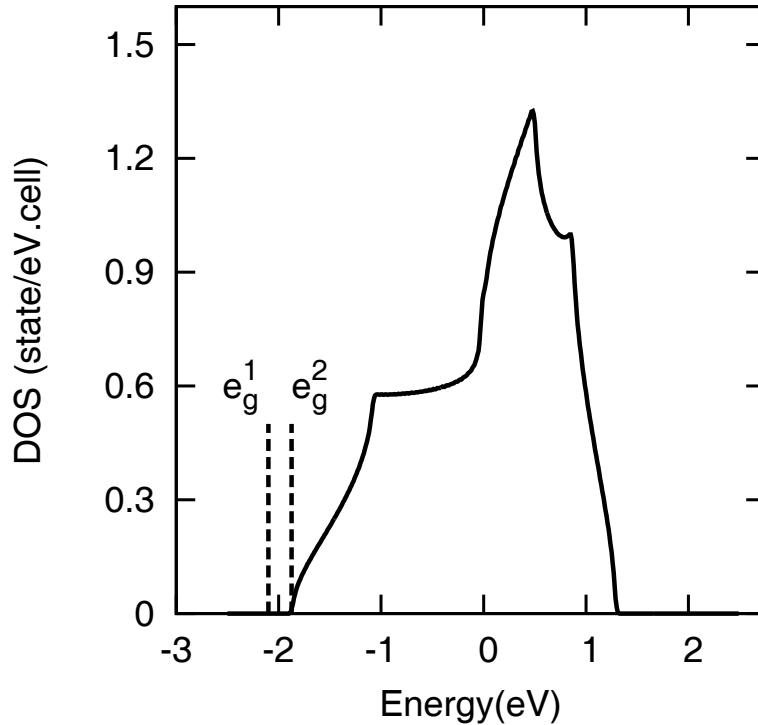
Figure 5.6: Density of States of CaMnO$_3$ corresponding to the Hamiltonian Eq. (5.16). when the t_{2g} spins are in the in the AF type G. The solid line corresponds to the undoped CaMnO$_3$(AF lattice), while the dashed lines shows the one-electron energies after doping one electron. The parameters are such that $t_{1NN} = -0.5$eV, $t_{2NN} = -0.25$ eV, and $g = 0$.

Tight-binding density of state of the STMP – To get a simple picture of the energetics of the system we consider a tight-binding model for the AF type G and STMP states.

In the case of the perfectly AF lattice for $CaMnO_3$ the NN hopping is forbidden by the infinite Hund's rule exchange, because the hopping term between NN sites has the form $t \cos \theta_{ij}/2$, where θ_{ij} is the angle between two neighboring classical lattice spins. In the case of the AF type G, the angle θ_{ij} between NN lattice spins is always 180° which gives zero coupling. Therefore, in the case where the magnetic structure is AF type G and the Hund's exchange is infinite, hopping only occurs across second and further nearest neighbors sites.

We have computed the band structure of the electron due to the second nearest neighbor hopping, via the Hamiltonian Eq. (5.14) by keeping only the NNN hopping matrix elements given in Table 5.1. The corresponding density of state shown in Fig. 5.6 is then computed in the simple tight-binding approximation, and is found to correctly reproduce the band-width of the e_g levels ($\sim$0.2 Ry) as computed by Satpathy *et. al.* [13]. In the case of the Type G AF magnetic structure, the Hamiltonian Eq. (5.16) corresponds to the total energy of the system because in that case $H_{spin} = 0$ and $H_{JT} = 0$.

If an electron is doped into the AF lattice, it will occupy the bottom of the conduction band, that is the orbital e_g^1. Let's for example consider a seven-site cluster where the central spin is turned by 180° and compute its energy. Since turning one spin breaks the spatial symmetry, it is not possible to make use of the Bloch theorem. Instead we have computed the one-electron energies of the e_g states by direct diagonalization of the Hamiltonian Eq. (5.14) on a finite lattice (of size 7^3). In addition to the kinetic energy gained by hopping there are magnetic and elastic energy costs resulting in the net energy

$$\varepsilon = E_P - JS^2 \sum_{\langle i,j \rangle} 1 + \cos \chi_{ij} - \frac{K}{2} \sum_{ia} Q_{ia}^2 \tag{5.27}$$

which is shown in dashed lines in Fig. 5.6.

When an electron is doped in the AF lattice of $CaMnO_3$ and if a STMP state is formed,
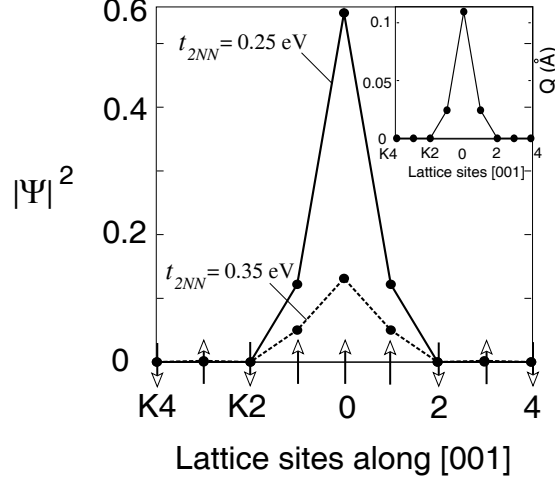
Figure 5.7: Wave function of the doped electron along the [001] direction of the simple cubic lattice for different values of the second-nearest neighbor hopping. The arrows represent the spin orientation of the classical lattice spins. The inset shows the magnitudes of the total lattice distortion $Q = \sqrt{Q_2^2 + Q_3^2}$ in the same direction. The solid line corresponds to $g = 3$ eV/Å, while the dashed and dotted lines are for $g = 0$ eV/Å. The nearest-neighbor hopping is always taken $t_{1NN} = 0.75$ eV and the remaining parameters are shown in the label boxes.

it will seek to lower its energy via hopping and by way of distorting the lattice. We therefore expect to find the energy of the e_g states to be lowered as compared to the DOS of the AF lattice. Furthermore, the e_g^1 and e_g^2 will be split by the JT effect. These states are shown as dashed lines in Fig. 5.6.

The doped electron will occupy the e_g^1 state which has lowest energy as shown in Fig. 5.4. This state is a combination of $3z^2 - r^2$ and $x^2 - y^2$ states, the particular mixture depending on the parameters.

Typical ground-state of the STMP – We consider the seven-site FM cluster configuration (Fig. 5.5a), and begin the discussion by studying the electronic wave function and the typical lattice distortions obtained by solving Eqs. (5.23-5.26).

The wave function of the doped electron along the [001] direction is shown in Fig. 5.7. The total wave function shown is the sum of the contributions from both the $3z^2 - r^2$ and $x^2 - y^2$ orbitals. For the set of parameters chosen these two contributions are comparable

in magnitude. The solid and dashed lines represent the total wave function of the electron for two different values of the nearest-neighbor hopping. For parameters appropriate for CaMnO$_3$, the wave function of the electron is localized to the central site, and drops rapidly away from the center. This is consistent with a seven-site FM cluster configuration, where only the lattice spin at the central site is turned.

The dashed line corresponds to a higher value of the NNN hopping t_{2NN}. This will cause the electron to spread more in the lattice, thus lowering the magnitude of its wave function on the central site, while simultaneously increasing it on sites away from the center.

The inset in Fig. 5.7 shows the total distortion $Q = \sqrt{Q_2^2 + Q_3^2}$ of the lattice along the [001] direction. This distortion is more prominent in the center of the STMP and decreases rapidly on sites away from the center. This is to be expected, the JT energy gain being proportional to $-g^2/2K\,|\psi|^2$ as previously discussed in the context of the Mott polaron.

In the case where the angles of the lattice spins are freely varied, a competition between the different interactions in the system will determine the exact nature of the ground-state of the magnetic polaron. The competition between the various interactions is discussed in the next section.

Effect of t_{1NN}**,** t_{2NN}**, and** g — In a FM cluster where the central spin is turned by 180°, as the nearest neighbor hopping t_{1NN} is increase the electron will gain kinetic energy and its wave function will tend to delocalize, as schematically shown by the arrows in Fig. 5.7. This situation is similar to what happens in the Mott limit. In fact, our model reduces exactly to the Mott model in the large t_{1NN} limit and $t_{2NN} = 0$.

The next-nearest neighbor hopping also causes a delocalization of the wave function, but its contribution is in direct competition with the NN hopping. As one turns a lattice spin in an otherwise AF lattice, the twelve NNN which were initially parallel to the central spin are now anti-parallel to it , thus causing a large kinetic energy loss. This will have a destabilizing effect on the STMP state, where, unlike in the Mott limit, the magnetic polaron is only stable
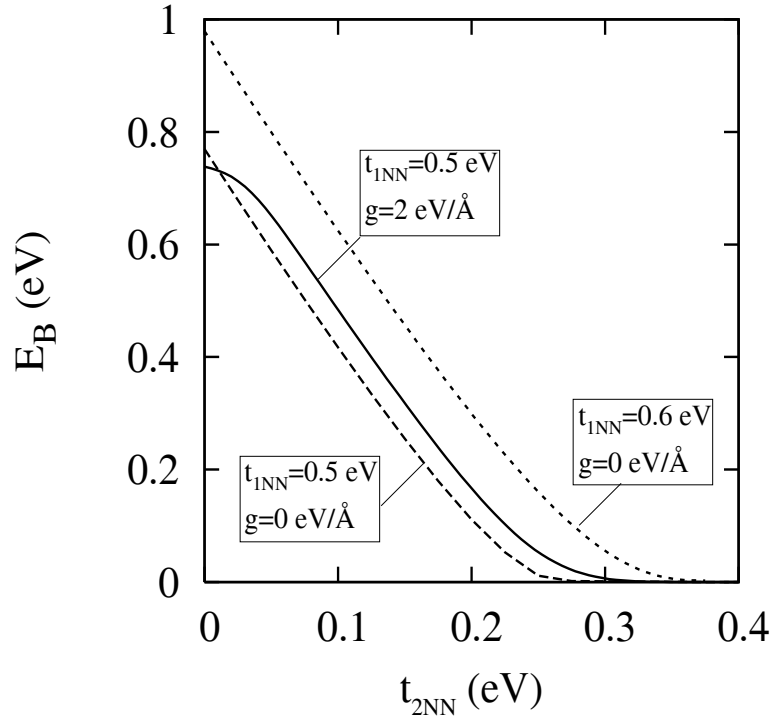
Figure 5.8: Binding energy of the magnetic polaron as a function of the next-nearest neighbor hopping. The binding energy is defined as above; the dashed lines are for $g = 2$ eV/Å ($t_{1NN} = 0.6$ eV or $t_{1NN} = 0.5$ eV) and the solid lines for $g = 2$ eV/Å and $t_{1NN} = 0.6$ eV.

for values of t_{2NN} less than a critical value.

The electronic wave function also shows this competition between nearest and next-nearest neighbor hopping (Fig. 5.7) where the electronic wave function is broadened when the second NN hopping is increased.

The electron-phonon coupling will either lower or raise the energy of the STMP state, depending on how well the electron wave function is localized. If the electronic wave function is strongly localized, the energy gain will be close to that of the isolated octahedron: $-g^2/2K$. If, on the other hand, the electron is more spread out through the lattice, this energy gain is lowered, turning eventually into an energy *cost*. This is shown in Fig. 5.8, where the binding energy is plotted in terms of the NNN hopping parameters. For small values of t_{2NN}, the BE is lowered by the electron-lattice interaction, while beyond a value of about 0.07 eV, it is enhanced by this coupling.

Energetics of different ferromagnetic clusters − So far in our discussion, we have only considered the case of the seven-site FM cluster. There are however other possible spin configurations which may, depending on the parameters, have a lower energy than the seven-site configuration.

Chen *et al.*[59] considered such clusters in their work on the magnetic polaron in $_3$. However, they have failed to include the next-nearest neighbor hopping which , as we shall show in the following, has important consequences on the nature of the ground-state.

In order to form a FM cluster, one has to flip one or more spins, thus gaining NN hopping at the cost of losing NNN hopping energy. Therefore clusters with more than a few flipped spins are too expensive energetically. In addition to the AF type G configuration, we choose four different spin configurations with one, two, or three spins flipped, and study the energetics of the STMP. The different FM clusters discussed in this chapter are shown in Fig. 5.5.

The seven-site FM cluster is formed by flipping one spin, and has the lowest kinetic
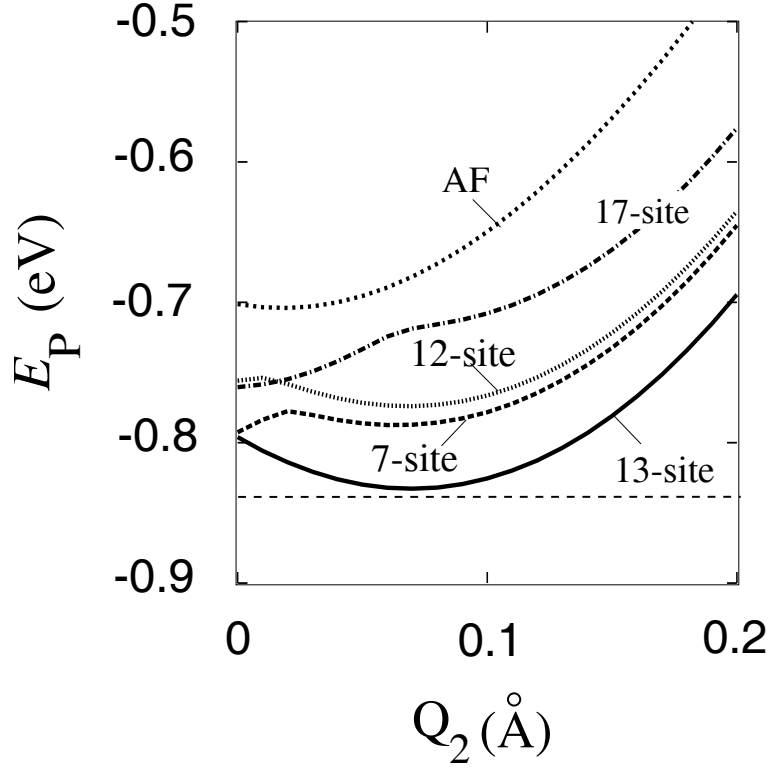
Figure 5.9: Energy of the magnetic polaron for different FM clusters (as shown in Fig. 5.5) as a function of the dominant lattice distortion mode Q_2. The dashed horizontal line corresponds to the global variational minimum. The parameters are $t_{1NN} = 0.5$ eV, $t_{2NN} = 0.2$ eV, $g = 2$ eV/Å, and $K = 10$ eV/Å^2.
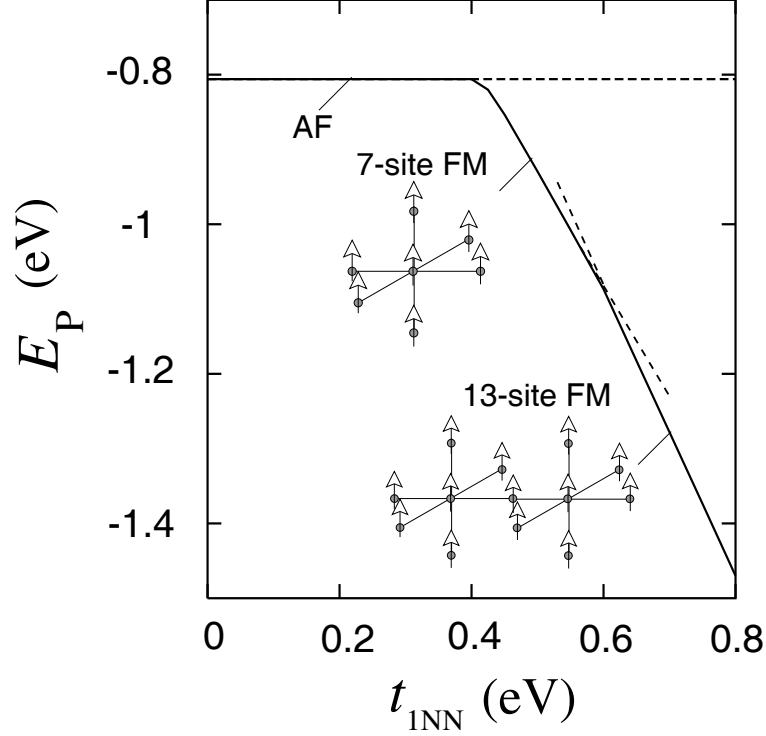
Figure 5.10: Total energy of the magnetic polaron as obtained by the global optimization as a function of the NN hopping t_{1NN}. The short dashed lines correspond to the energies of the seven-site FM and thirteen-site FM clusters, while the horizontal dashed line is the AF energy. Below $t_{1NN} = 0.4$ eV, the magnetic polaron state is not stable, while above 0.4 eV the seven-site FM, and later the thirteen-site FM, have lowest energy. The parameters are $t_{2NN} = 0.25$ eV, $g = 2$ eV/Å, and $K = 10$ eV/Å^2
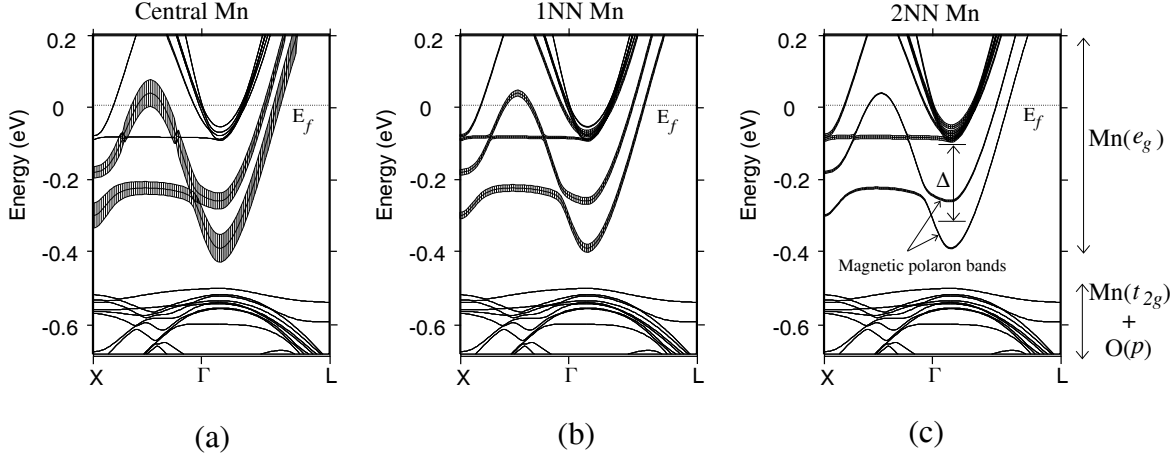
Figure 5.11: Energy bands of the $(La_xCa_{1-x}MnO_3)_N$ super cell around the Fermi level as obtained by Density Functional Theory(DFT) calculations of reference [6]. The parameters of the DFT calculation are such that $N = 32$ formula units, and $x = 1/32 \approx 3\%$. The fat bands' thickness is proportional to the occupation of the e_g^1 and e_g^2 bands for the (a) central Mn atom, the (b) first nearest neighbor and (c) second nearest neighbor Mn atoms. We are thankful to T.S. Dasgupta for communication of these results.

energy gain via NN hopping. This cluster, however, also has the lowest net energy cost due to magnetic energies and NNN hopping. The next most energy-favorable FM cluster is the thirteen-site FM cluster, where the two spins flipped are along the [110] of the simple cubic lattice. These two spin arrangements are very close in energy in the range $t_{1NN} = 0.4-0.7$ eV (Fig. 5.10), with the thirteen-site becoming more favorable as the NN hopping is increased.

The other spin clusters are energetically too expensive for a parameter range valid for CaMnO$_3$ as shown by Fig. 5.9. It is not excluded, however, that in a different material (for a different set of parameters) these other clusters may be more energetically favorable.

Note that because of the competition between NN and NNN hopping, the system does not always find it energetically favorable to form a STMP state. This is clearly shown in Fig, 5.10, where the AF type G is the lowest energy state for values of $t_{1NN} \leq 0.4$ eV, which shows that forming the magnetic polaron is not favored in that range.

Global optimization −   We have used the different clusters discussed above as starting guesses in the numerical optimization. In fact, because of the large number of variables,

there are many local minima. This makes it necessary to consider small angle deviations at the central, first and second NN sites for each of these clusters. The results of the global optimization are shown in Figs. 5.10 and 5.8.

The BE as a function of the NNN hopping parameter t_{2NN} shows a sharp decrease, which is easily understood since the NNN hopping favors the FM alignment of the second NN t_{2g} spins. In the limit of large t_{2NN} the STMP is unstable, and the ground-state of the system has the AF type G configuration.

The JT effect mostly increases the stability of the magnetic polaron, although this effect is rather small (Fig. 5.8, solid line). The STMP state is thus further enhanced by the lattice polaron effect caused by the electron-phonon coupling. In the small t_{2NN} limit, however, the BE is weakened by the JT coupling. The reason being that, in that limit, electron hopping is almost completely suppressed (AF lattice) and the NNN hopping is small, causing a strong localization of the electronic wave function. This gives rise to a large JT energy gain close to that of the isolated site[61] $-g^2/2K$.

Density-functional results $-$ The above model is missing several important features such as the higher order order hopping or the finite Hund's rule coupling. In order to describe the seven-site cluster solution using a more realistic theory we have performed a *ab initio* DFT calculation of the band structure of $La_xCa_{1-x}MnO_3(x=3\%)$.

A super-cell method was used to model the low electron-doping with the super-cell consisting of thirty two formula units of $CaMnO_3$ with one Ca^{2+} replaced by La^{3+}. This introduces one doped electron per super-cell into the conduction band and corresponds to a La doping of about 3%. Two separate magnetic calculations were performed: one for the type-G AF magnetic structure, and another where a central $Mn(t_{2g})$ spin was flipped, thus forming the seven site FM cluster.

The main feature of the band structure is the introduction of two bands in the gap, which we interpret as being due to the formation of a STMP state in the $Ca_{1-x}La_xMnO_3$

super-cell. The binding energy as calculated from the DFT work is found to be about 0.1 eV, which agrees with the value found by our variational method. The higher order hopping or Hund's rule coupling seem then to only have a qualitative effect on the BE of the magnetic polaron. Furthermore, the wave-function of the itinerant electron is shown to rapidly drop as one moves away from the center of the magnetic polaron as can be seen from Fig. 5.11, and this is also what comes out of the variational model. A more detailed discussion of this work may be found in Ref. [6].
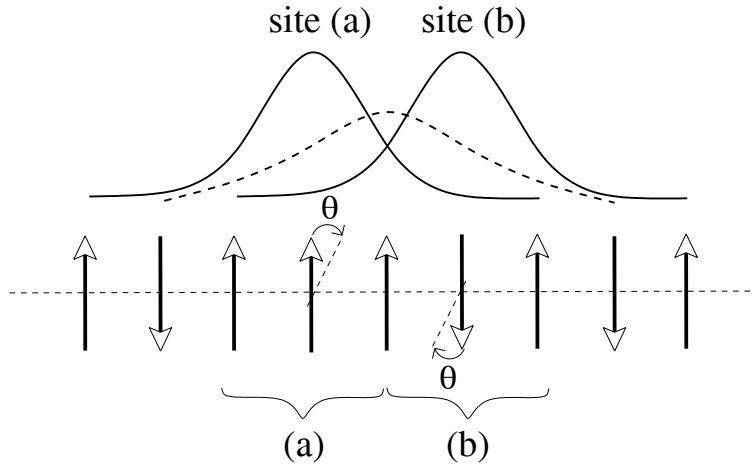
Figure 5.12: Activated hopping of the self-trapped magnetic polaron. The angle θ represents the deviation of the angle from the ideal seven-site cluster configuration for the central spin and one of its NNN along the [100] direction

Conductivity in low-doped manganites −   We now examine the issue of transport of the STMP in low-doped $CaMnO_3$. While in the case where the magnetic polaron is bound to an ionic center we expect the system to be an insulator, it is not clear whether the conductivity of the STMP should be activated or metallic. To shed some light on the issue we have used a method inspired from studies of small lattice polaron[66] to estimate the activation energy.

In the small polaron limit, the transport takes place via hopping of an electron from one site to the next while it carries the lattice distortion with it. Since the lattice distortion

must move with the electron as it hops in the lattice, there might be an activation energy E_A involved. "Authors" et al. [66] calculated this activation energy by considering an intermediate state, putting half the charge of the electron on each of the two sites involved in the hopping process. A full lattice relaxation for the intermediate state is then carried out to compute E_A.

In the case of the magnetic polaron we follow a similar line of reasoning, with the lattice distortion replaced by the exchange-induced distortion of the lattice spins. We assume the conduction to take place via hopping of the excess electron which carries the spin distortion with it. The starting configuration is the seven-site FM cluster, and the final state is one where the center of the seven-site cluster has moved to the NNN. The intermediate state is formed by turning the central lattice spin and its NNN by 90° in the same direction as shown in Fig. 5.13.

The total energy is computed as a function of the cant-angle θ, and the activation energy E_A is defined as

$$E_A = E_P(\theta = \pi/2) - E_p(\theta = 0).$$

We find the activation energy to be $E_A \approx 40$ meV or roughly half the binding energy E_B which is what we expect if transport takes place via activated hopping.

It is interesting that experiments [54] do indeed show an activated conductivity with an activation energy of $50 - 80$ meV. This may be interpreted as the barrier energy of the intermediate configuration as indicated in Fig. 5.13

5.6   Conclusion

We have studied the problem of the self-trapped magnetic polaron in the manganites using several methods. The Mott approximation valid in the large polaron limit found that the magnetic polaron is stable for all values of the parameters, and that the influence the JT effect on the dimension of the magnetic polaron is small to negligible. In addition, we have
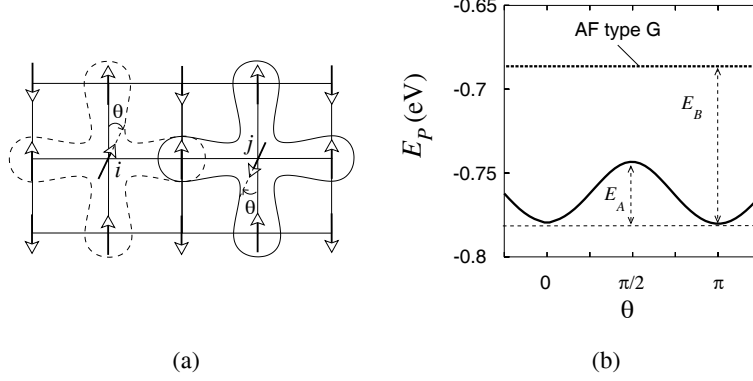
Figure 5.13: (a) Energy of the self-trapped magnetic polaron as a function of the angle .
(b)The angle θ is the angle varied to change the initial configuration with the magnetic
polaron at site i (solid lines), to the final configuration where the polaron has moved to site
j (dashed lines).

performed an *ab initio* calculation of the electronic structure of $Ca_{1-x}La_xMnO_3$ ($x = 0.03$)
using a super-cell method, and used the parameters thus obtained in a model appropriate
to the manganites.

A variational method was used in conjunction with a model appropriate to the particular
physics of the manganites to compute the ground state of the self-trapped magnetic polaron.
It is found that the double exchange, mechanism mediated by the nearest-neighbor hopping,
is in competition with the Heisenberg-like exchange interaction: while the former strongly
increases the binding energy, the latter tends to favor an AF arrangement of the lattice, thus
lowering E_B.

Also, we find that the next-nearest interaction has a major effect on the stability of the
STMP state, sharply reducing the binding energy by as much as a factor of three in the case
of $CaMnO_3$.

This, however, is not enough to destroy the self-trapped stated, and we found the polaron
to be stable with a binding energy of 0.1 meV. This is agrees with the energy gain of $E_B = 0.1$
meV found by the DFT calculation. The effect of the JT coupling is small with an optimal
distortion of $Q = 0.1$ Å, comparable to the distortion in $LaMnO_3$. The magnetic moment
$\mu \approx 7$ μ_B/Mn for the seven-site ferromagnetic solution, where one t_{2g} is turned by 180°,

96

agrees well with the value of the magnetic moment found experimentally by Neumeier *et al.*[54].

Chapter 6

Concluding Remarks

In conclusion, I shall summarize the main results of this dissertation this thesis as well as suggest new directions of research for the issue of the interaction between lattice and electrons in solids.

The second chapter is devoted to the discussion of the various methods that were used to obtain the main results of the work. In particular, density functional theory and the variational Lang-Firsov method were discussed in some detail, as well as the "*Cluster*" computer program used he to compute the exchange interaction in several instances. In chapter three we discuss the electron-phonon coupling in a two-site system. It was found that the coupling significantly reduces the magnetic exchange from the $t \cos \theta / 2$ Anderson-Hasegawa limit. The magnitude of the oxygen isotope effect was estimated and the isotope exponent was found to agree with experiment.

The effect of the electron-phonon coupling on the magnetic interaction in oxides was, in general, to dramatically decrease the strength of the coupling. This decrease comes as a result of two separate effects: the first is due to the reduced hopping due to the lengthening of the chemical bond. This has been considered by Su, Schrieffer, and Heeger in their celebrated papers.[46, 47] A second, and this is the predominant effect in most transition oxides, is the cooperative dynamical Jahn-Teller effect. The Jahn-Teller effect gives rise to some of

the more interesting properties of the TM oxides and is discussed in great detail in many references. For a good source see reference [62].

Other consequences of the electron-phonon coupling that we discuss in this study is the isotope effect of which we have seen examples in both chapters three and four. The isotope effect may be described simply as the shift, as a result of the variation of the oxygen mass, of the critical temperature T_c at which the Metal-Insulator transition takes places. This effect was observed to be unusually large in several manganites.[25, 67].

Another example of an isotope effect was also discussed in the nickelates (chapter four), where it was found that decreasing the mass of the intermediate Na ion *increased* the magnetic exchange. This effect was found to be small, but more importantly, to be opposite to that in the manganites. This is found to be caused by the nature of the electron-phonon coupling which takes place vi a long Ni-O-Na-O-Ni superexchange path.We have also estimated the effect of the electron-phonon coupling on the magnetic exchange and found that the exchange is not significantly modified by this coupling. We conclude from this result that it is unlikely that the electron-phonon coupling is the cause of the unusual magnetic properties of the isostructural $LiNiO_2$.

The fifth chapter was devoted to the study of the magnetic polaron in low-doped $CaMnO_3$, where again we study the effect of electron-phonon coupling. This effect increases the binding energy of the magnetic polaron and localizes the electronic wavefunction. In addition the effect of the next-nearest-neighbor hoping we found to have a destabilizing effect on the magnetic polaron.

Appendix A

Summary of often-used relations

This appendix hopes to be an important addendum to the main body of the dissertation as well as a useful reference for the reader. It covers some very basic topics such as commutation relations, as well as some more arcane subjects such as the Lanczos diagonalization scheme and the "fermion-sign" issue.

A.1   Koster-Slater Inter-atomic Matrix Elements

The Slater and Koster (1954) inter-atomic matrix elements as a function of the direction cosines l, m, n between the two atoms involved in the hopping are given by

$$E_{s,s} = V_{ss\sigma}$$

$$E_{s,x} = lV_{sp\sigma}$$

$$E_{x,x} = l^2 V_{pp\sigma} + \left(1 - l^2\right) V_{pp\pi}$$

$$E_{x,y} = lm V_{pp\sigma} + lm V_{pp\pi}$$

$$E_{x,z} = ln V_{pp\sigma} + ln V_{pp\pi}$$

$$E_{s,xy} = \sqrt{3} lm V_{sd\sigma}$$

$$E_{s,x^2-y^2} = \frac{\sqrt{3}}{2} \left(l^2 - m^2\right) V_{sd\sigma}$$

$$E_{s,3z^2-r^2} = \left[n^2 - \frac{\left(l^2 + m^2\right)}{2}\right] V_{sd\sigma}$$

$$E_{x,xy} = \sqrt{3} l^2 m V_{pd\sigma} + m \left(1 - 2l^2\right) V_{pd\pi}$$

$$E_{x,yz} = \sqrt{3} lmn V_{pd\sigma} - 2lmn V_{pd\pi}$$

$$E_{x,zx} = \sqrt{3} l^2 n V_{pd\sigma} + n \left(1 - 2l^2\right) V_{pd\pi}$$

$$E_{y,xy} = \sqrt{3} m^2 l V_{pd\sigma} + l \left(1 - 2m^2\right) V_{pd\pi}$$

$$E_{y,yz} = \sqrt{3} m^2 n V_{pd\sigma} + n \left(1 - 2m^2\right) V_{pd\pi}$$

$$E_{y,zx} = \sqrt{3} lmn V_{pd\sigma} - 2lmn V_{pd\pi}$$

$$E_{z,xy} = \sqrt{3} lmn V_{pd\sigma} - 2lmn V_{pd\pi}$$

$$E_{z,yz} = \sqrt{3} n^2 m V_{pd\sigma} + m \left(1 - 2n^2\right) V_{pd\pi}$$

$$E_{z,zx} = \sqrt{3} n^2 l V_{pd\sigma} + l \left(1 - 2n^2\right) V_{pd\pi}$$

$$E_{x,x^2-y^2} = \frac{\sqrt{3}}{2}l\left(l^2 - m^2\right)V_{pd\sigma} + l\left(1 - l^2 + m^2\right)V_{pd\pi}$$

$$E_{y,x^2-y^2} = \frac{\sqrt{3}}{2}m\left(l^2 - m^2\right)V_{pd\sigma} + m\left(1 - l^2 + m^2\right)V_{pd\pi}$$

$$E_{z,x^2-y^2} = \frac{\sqrt{3}}{2}n\left(l^2 - m^2\right)V_{pd\sigma} - n\left(l^2 - m^2\right)V_{pd\pi}$$

$$E_{x,3z^2-r^2} = l\left[n^2 - \frac{1}{2}\left(l^2 + m^2\right)\right]V_{pd\sigma} - \sqrt{3}ln^2V_{pd\pi}$$

$$E_{y,3z^2-r^2} = m\left[n^2 - \frac{1}{2}\left(l^2 + m^2\right)\right]V_{pd\sigma} - \sqrt{3}mn^2V_{pd\pi}$$

$$E_{z,3z^2-r^2} = n\left[n^2 - \frac{1}{2}\left(l^2 + m^2\right)\right]V_{pd\sigma} + \sqrt{3}n\left(l^2 + m^2\right)V_{pd\pi}$$

The V's are taken from the solid-state table in reference [2] and are given by

$$V_{ll'm} = \eta_{ll'm}\frac{\hbar^2}{md^2} \quad V_{ldm} = \eta_{ldm}\frac{\hbar^2 r_d^{3/2}}{md^{7/2}} \quad V_{ddm} = \eta_{ddm}\frac{\hbar^2 r_d^3}{md^5}$$

$$\eta_{ss\sigma} = -1.40 \qquad \eta_{sd\sigma} = -3.16 \qquad \eta_{dd\sigma} = -16.2$$

$$\eta_{sp\sigma} = 1.84 \qquad \eta_{pd\sigma} = -2.95 \qquad \eta_{dd\pi} = 8.75$$

$$\eta_{pp\sigma} = 3.24 \qquad \eta_{pd\pi} = 1.36 \qquad \eta_{dd\delta} = 0$$

$$\eta_{pp\pi} = -0.81$$

$$V_1 = \frac{\varepsilon_p - \varepsilon_s}{4}, \quad V_2 = 2.16\frac{\hbar^2}{md^2} \quad V_3 = \frac{\varepsilon_p^c - \varepsilon_p^a}{2}$$

$$V_2^h = 4.37\frac{\hbar^2}{md^2} \quad W_d = 6.83\frac{\hbar r_d^3}{mr_0^5}$$

A.2 Fourth Order Non-Degenerate Perturbation Theory

We write The total Hamiltonian as $H = diag(H) * 1_u + V$ where $diag(V) \equiv 0$. That is the perturbation is the off-diagonal of the Hamiltonian. The perturbative corrections of the

lowest energy state up to fourth order are then

$$
\begin{aligned}
E_n^1 &= V_{nn} \\
E_n^2 &= \sum_{i \neq n} \frac{|V_{ni}|^2}{E_n^0 - E_i^0} \\
E_n^3 &= \sum_{i,j \neq n} \frac{V_{ni} V_{ij} V_{jn}}{\left(E_n^0 - E_i^0\right)\left(E_n^0 - E_j^0\right)} - \sum_{i \neq n} V_{nn} \frac{|V_{ni}|^2}{\left(E_n^0 - E_i^0\right)^2} \\
E_n^4 &= \sum_{i,j,k \neq n} \frac{V_{ni} V_{ij} V_{jk} V_{kn}}{\left(E_n^0 - E_i^0\right)\left(E_n^0 - E_j^0\right)\left(E_n^0 - E_k^0\right)} \\
&\quad - \sum_{i,j \neq n} \frac{|V_{ni}|^2 |V_{jn}|^2}{\left(E_n^0 - E_i^0\right)\left(E_n^0 - E_j^0\right)} \frac{1}{E_n^0 - E_i^0} \\
&\quad + \sum_{i \neq n} \frac{|V_{nn}|^2 |V_{ni}|^2}{\left(E_n^0 - E_i^0\right)^3} \\
&\quad - \sum_{i,j \neq n} \frac{V_{ni} V_{ij} V_{jn} \cdot V_{nn}}{\left(E_n^0 - E_i^0\right)\left(E_n^0 - E_j^0\right)} \left[\frac{1}{E_n^0 - E_i^0} + \frac{1}{E_n^0 - E_j^0}\right]
\end{aligned}
$$

A.3   Lanczos Diagonalization Scheme

The goal of this method is to reduce a large symmetric matrix to tridiagonal form, then diagonalize the resulting matrix in a sub-space of lower dimension. We start by choosing a vector $|\Psi\rangle$ such that

$$
|\Psi\rangle = \sum_{j=1}^{N} c_{1,j} |\phi_j\rangle
$$

where $\{|\phi_j\rangle\}_{j=1,N}$ is a complete basis set. Then, sequentially, we calculate the first few Lanczos numbers

$$g_{1,k} = \sum_{j=1}^{N} c_{1,j} H_{k,j}$$

$$d_1 = \sum_{i,j=1}^{N} c_{1,i} c_{1,j} H_{i,j}$$

$$f_2 = \left[\sum_{j=1}^{N} (g_{1,j} - d_1 c_{1,j})^2 \right]^{1/2}$$

$$c_{2,j} = \frac{1}{|f_2|} (g_{1,j} - d_1 c_{1,j})$$

The next $k+1$ numbers are calculated as such

$$g_{k,j} = \sum_{l=1}^{N} c_{k,l} H_{j,l}$$

$$f_{k+1} = \left[\sum_{j=1}^{N} (g_{k,j} - f_k c_{k-1,j} - d_k c_{k,j})^2 \right]^{1/2}$$

$$c_{k+1,j} = \frac{1}{|f_{k+1}|} (g_{k,j} - f_k c_{k-1,j} - d_k c_{k,j})$$

$$d_{k+1} = \sum_{i,j=1}^{N} c_{k+1,i} c_{k+1,j} H_{i,j}$$

A.4   Fermion sign "problem".

When computing matrix elements in the occupation number representation it is necessary to take the commutation relations of the fermion operators into account. This issue is similar to that of the normal-ordering of operators when computing the time-evolution of a many-body Hamiltonian. In what follows we derive a formula to compute the fermion sign for an arbitrary pair of states in the occupation number representation.

Consider two states in the many-body Hilbert space $|\psi\rangle$ and $|\phi\rangle$ such that

$$
\begin{aligned}
|\psi\rangle &= c_{i1}^{\dagger} c_{i2}^{\dagger} \cdots c_{i_S}^{\dagger} |0\rangle \\
|\phi\rangle &= c_{j1}^{\dagger} c_{j2}^{\dagger} \cdots c_{j_S}^{\dagger} |0\rangle
\end{aligned}
$$

If the $\{i_k\}$ and $\{j_k\}$ are all equal except one pair (as would occur in the case of an electron hopping between two states), then there exists a pair (M, N) such that

$$
\langle\phi| c_M^{\dagger} c_N |\psi\rangle = \pm 1 \tag{A.1}
$$

The sign of the cross product depends on the precise order of the pair (M, N) as well as on the occupation of the kets $|\psi\rangle$ and $|\phi\rangle$. In fact it is possible to derive a formula to determine such a sign for all states and all pairs (M, N). We find

$$
\begin{aligned}
\langle\phi| c_M^{\dagger} c_N |\psi\rangle &= \langle\phi| c_M^{\dagger} c_N c_{i1}^{\dagger} c_{i2}^{\dagger} \cdots c_{i_S}^{\dagger} |0\rangle \\
&= (-1)^1 \langle\phi| c_N c_M^{\dagger} c_{i1}^{\dagger} c_{i2}^{\dagger} \cdots c_{i_S}^{\dagger} |0\rangle \\
&= (-1)^{i_k+1} \langle\phi| c_N c_{i1}^{\dagger} c_{i2}^{\dagger} \cdots c_{i_k}^{\dagger} c_M^{\dagger} \cdots c_{i_S}^{\dagger} |0\rangle \\
&= (-1)^{\sum_{j=1}^{M} \psi(j)} \langle\phi| c_N c_{i1}^{\dagger} c_{i2}^{\dagger} \cdots c_{i_k}^{\dagger} c_M^{\dagger} \cdots c_{i_S}^{\dagger} |0\rangle \\
&= (-1)^{\sum_{j=1}^{M} \psi(j)} \times \langle\phi| c_{i_S} \cdots c_{i_k} \cdots c_{i_2} c_{i_1} c_{i_N} c_{i1}^{\dagger} c_{i2}^{\dagger} \cdots c_{i_k}^{\dagger} c_M^{\dagger} \cdots c_{i_S}^{\dagger} |0\rangle \\
&= (-1)^{\sum_{j=1}^{M} \psi(j)} (-1)^{\sum_{j=1}^{N-1} \phi(j)} \times \\
&\quad \langle\phi| c_{i_S} \cdots c_{i_N} c_{i_k} \cdots c_{i_2} c_{i_1} c_{i1}^{\dagger} c_{i2}^{\dagger} \cdots c_{i_k}^{\dagger} c_M^{\dagger} \cdots c_{i_S}^{\dagger} |0\rangle
\end{aligned}
$$

If we define S_l such that:

$$
S_l(\psi) = \sum_{k=1}^{l} \psi(k)
$$

The hopping term is then

$$
\left\langle\phi \left| c_M^{\dagger} c_N \right| \psi\right\rangle = (-1)^{S_M(\psi) + S_{N-1}(\phi)} \tag{A.2}
$$

A.5 "Cluster" computer program listing

```
1    PROGRAM RUN_CLUSTER
2    USE VARIABLES
3    implicit none
4    INTEGER::Niter=3 ! Number values +1 of angles between pi/2 and pi
5    INTEGER::NLCZ ! Maximum Number of Lanczos steps
6    INTEGER::INFO
7    INTEGER::SUCCESS ! Status of convergence(y=>1,n=>0)
8    REAL*8::delta     ! Radius of convergence of the Lanczos
9    REAL*8::theta     ! Mn−O−Mn bond angle
10   REAL*8::dtheta    ! Bond angle increment
11   REAL*8::Ndt       ! Number of increments to add to pi/2
12   REAL*8::Xhund   ! Strength of the Hund's exchange coupling
13   REAL*8::EGrFM ! FM ground state energy
14   REAL*8::EGrAF ! AF ground state energy
15   REAL*8::Vpds     ! Strength of the hopping
16   character(LEN=1)::EXACT
17   open(33,file='REPORT') ! The Lanczos results are stored here
18   open(133,file='RESULT') ! The Lanczos results are stored here
19   Ndt=Niter        ! This impose theta=pi
20   EXACT='Y'
21   NLCZ=100000
22   Xhund=1.0d0
23        print*, 'Give the hopping'
24        read*, Vpds
25   lambda=−0.0
```

BIG FAT WARNING:
The values of the Hund's exchange on each atom are defined in the *Jh* array. **You should change this for your specific problem**

```
26   Jh=(/ Xhund,0.0d0,Xhund/)
27   dtheta=Ndt*pi/(2*Niter)      ! See above
28   theta=pi !/2 + dtheta          ! See above
29   Nmiss=1 !Number of missing orbitals from each Mn site.(See doc.tex)
```

Ferro

```
30   MAGTYP='FM'
31   ! The FM Hamiltonian is formed by CLUSTER and the
32   ! result outputed to 'MNOFM'
33   CALL CLUSTER(theta,Vpds,'MN.TPfm','MN_IN','MNOFM')
34   NZMAX=MAXVAL(NZ) !Max number of non−zero matrix elements per line in H
35   ! The GS energy is calculated by Lanczos diagonalization
36   CALL DLANCZOSMETH('MNOFM',NDIM,NZ,NZMAX,NLCZ,EgrFM,INFO,SUCCESS,delta)
37   !Interupts if The Lanczos hasn't converged
38   if(SUCCESS/=1)then
39      stop'The Lanczos did not converge yet'
40   end if
41   !Output the results of the Lanczos run in unit 33(REPORT)
42   write(33,*)MAGTYP
43   write(33,*)'The number of Lanczos steps is: ',INFO
44   write(33,*)'The radius of convergence is: ',delta
45   deallocate(NZ)
```

Anti-Ferro

```
46   MAGTYP='AF'
47   CALL CLUSTER(theta,Vpds,'MN.TPaf','MN_IN','MNOAF')
48   NZMAX=MAXVAL(NZ)!Max number of non−zero matrix elements per line in H
49   !The GS energy is calculated by Lanczos diagonalization
50   CALL DLANCZOSMETH('MNOAF',NDIM,NZ,NZMAX,NLCZ,EgrAF,INFO,SUCCESS,delta)
51   !Interupts if The Lanczos hasn't converged
52   if(SUCCESS/=1)then
53      stop'The Lanczos did not converge yet'
```

```fortran
54        end if
55        !Output the results of the Lanczos run in unit 33(REPORT)
56        write(33,*)MAGTYP
57        write(33,*)'The number of Lanczos steps is: ',INFO
58        write(33,*)'The radius of convergence is: ',delta
59        deallocate(NZ)
60        !FINAL results
61        write(*,'(4f12.5)')theta,EGrFM,EGrAF,(EGrFM-EGrAF)*1000
62        write(*,'(4a12)')"Vpds","EGrFM","EGrAF","Jex (meV)"
63        write(*,'(4f12.5)')Vpds,EGrFM,EGrAF,(EGrAF-EGrFM)*1000
64        open(10,file="energies.dat")!,access='append')
65        write(10,'(4a20)')'Vpds','EGrFM','EGrAF','EAF-EFM (meV)'
66        write(10,'(4f20.5)')Vpds,EGrFM,EGrAF,(EGrAF-EGrFM)*1000
67        close(10)
68        close(33)
69   END PROGRAM RUN_CLUSTER
70   SUBROUTINE editinput(theta,Vpds,INPUT_FILE,OUTPUT_FILE)
71        USE Variables
72        IMPLICIT NONE
73        integer,parameter::Nline=1000,Nhopp=8,Natoms=3 !eg'-eg'
74        INTEGER,DIMENSION(NHopp)::AT1,AT2,OR1,OR2
75        REAL*8::theta
76        REAL*8,DIMENSION(Nhopp)::t
77        CHARACTER(LEN=7) ::INPUT_FILE
78        CHARACTER(LEN=5) ::OUTPUT_FILE
79        CHARACTER(LEN=50)::characs
80        CHARACTER(LEN=50),DIMENSION(Nline)::ASCI
81        REAL*8:: Vpds,Vpdp
82        Vpdp=-lambda*Vpds
83        print*,&
84        "Did you remember to edit the file edit.f90 for this particular problem?"
```

$e'_g - e'_g$

```fortran
85        AT1=(/1,1,1,1,3,3,3,3/) ! Left Atom
86        OR1=(/1,2,3,4,1,2,3,4/) ! Orbital of Left Atom
87        AT2=(/2,2,2,2,2,2,2,2/) ! Right Atom
88        OR2=(/1,1,2,3,1,1,2,3/) ! Orbital of Right Atom
89        ! These are the Koster Slater matrix elements
90        t(1)  =Vpds*sqrt(3.0)/2
91        t(2)  =Vpds*-1.0/2
92        t(3)  =Vpdp
93        t(4)  =Vpdp
94        t(5)  =Vpds*sqrt(3.0)/2
95        t(6)  =Vpds*-1.0/2
96        t(7)  =Vpdp
97        t(8)  =Vpdp
98        OPEN(77,FILE=INPUT_FILE)
99        OPEN(55,FILE=OUTPUT_FILE)
100       i=0
101       DO k=1,10*Nline
102          i=i+1
103          READ(77,'(a50)',END=100)ASCI(i)
104          WRITE(55,'(a50)')ASCI(i)
105          IF(INDEX(ASCI(i),'*20:')/=0)THEN
106             READ (77,'(a50)')characs
107             WRITE(55,'(a50)')characs
108             WRITE(55,'(i4)')Nhopp
109             DO j=1,NHopp
110                WRITE(55,'(4i8,f15.3)')AT1(j),OR1(j),AT2(j),OR2(j),t(j)
111             END DO
112             READ (77,'(a50)')characs
```

```fortran
113            WRITE(55,'(a50)')characs
114            WRITE(55,'(i4)')Nhopp
115            DO j=1,NHopp
116                WRITE(55,'(4i8,f15.3)')AT1(j),OR1(j),AT2(j),OR2(j),t(j)
117            END DO
118          ELSE IF(INDEX(ASCI(i),'*50:')/=0)THEN
119            DO j=1,Natoms
120                WRITE(55,'(i10,f10.3)')j,Jh(j)
121            END DO
122          END IF
123        END DO
124   100 CONTINUE
125      CLOSE(55);CLOSE(77)
126    END SUBROUTINE editinput
```

This essentially checks for errors and only keep as a basis vector the vectors satisfying $\sum_{i\alpha\sigma} \psi_{i\alpha\sigma} = N_e$

```fortran
127    SUBROUTINE BASIS_FORM(Ns,Ne,Nd,Basis_Set)
128        IMPLICIT NONE
129        INTEGER:: Ns,Ne,Nd
130        INTEGER::i,j,k,p,check,index
131        INTEGER,DIMENSION(Ns)::Vector
132        INTEGER,DIMENSION(Nd,Ns+1)::Basis_Set
133        Basis_Set=0;index=0
134        bin_loop:DO i=1,2**Ns
135            print*,i
136            Vector=0
137            CALL conv_binary(i,Ns,Vector)
138            IF(SUM(Vector)/=Ne)CYCLE bin_loop
139            index=index+1
140            Basis_Set(index,1)=index
141            Basis_Set(index,2:Ns+1)=Vector
142        END DO bin_loop
143        RETURN
144    END SUBROUTINE BASIS_FORM
```

Converts any integer into binary format, for book-keeping of the vectors of the basis sets

```fortran
145    SUBROUTINE conv_binary(input,Ns,output)
146        IMPLICIT NONE
147        INTEGER :: m,l,Ns,rank,input
148        INTEGER,DIMENSION(Ns) :: output
149        IF(Ns<=1)THEN
150            WRITE(*,*)'CONV_BINARY the no. of sites is too small'
151            RETURN
152        END IF
153        rank=0;output=0
154        IF(input==1)THEN
155            output(1)=1
156            RETURN
157        ELSEIF(input==2)THEN
158            output(2)=1
159            RETURN
160        ELSEIF(input==3)THEN
161            output(1)=1;        output(2)=1
162            RETURN
163        ENDIF
164        l=input;      m=INT(l/2)
165        DO WHILE(m>1)
166            rank=rank+1
167            m=INT(l/2)
168            output(rank)=MOD(l,2)
169            l=INT(l/2)
170        END DO
171        rank=rank+1;    output(rank)=1
```

```fortran
172     RETURN
173 END SUBROUTINE conv_binary
174 SUBROUTINE CLUSTER(theta,Vpds,INPUT_0,INPUT_FILE,OUTPUT_FILE)
175     USE Variables
176     !Calculate the non−zero matrix elements of the Hamiltonian
177     !of a small cluster, and outputs the result in OUTPUT_FILE.
178     !
179     !   theta:      REAL*8. Used as input for the EDITINPUT
180     !               subroutine. It corresponds to the Mn−O−Mn
181     !               bond angle(see the file "doc.tex").
182     !
183     !   Vpds:       REAL*8. Used as input for the EDITINPUT
184     !               subroutine. It is the dtrength of the hopping
185     !               (see the file "doc.tex").
186     !
187     !   INPUT_0:    CHARACTER(LEN=7). This the user−supplied
188     !               template file. Use the file MN.TP in the
189     !               template directory to buid it.
190     !
191     !   INPUT_FILE: CHARACTER(LEN=5). This file is produced by
192     !               EDITINPUT subroutine based on the supplied
193     !               template(INPUT_0).
194     !
195     !   OUTPUT_FILE: CHARACTER(LEN=5). This is the outpout file
196     !                containing the non−zero matrix elements with
197     !                their indices
198     IMPLICIT NONE
199     REAL*8::x
200     CHARACTER(LEN=7)::INPUT_0 !User−provided template file
201     CHARACTER(LEN=5)::INPUT_FILE !Created by EDITINPUT
202     CHARACTER(LEN=5)::OUTPUT_FILE !Created by EDITINPUT
203     REAL*8::theta                 !Mn−O−Mn bond angle
204     INTEGER::Natoms               !Number of atoms
205     REAL*8::Vpds                  !p−d Hopping
206     !Modifies the template file 'INPUT_0' to account for the theta
207     !dependance of the hopping and writes the result to 'INPUT_FILE'.
208     CALL EDITINPUT(theta,Vpds,INPUT_0,INPUT_FILE)
209     !Reads the parameters from the 'INPUT_FILE'.
210     CALL READATA(INPUT_FILE)
211     !This line checks that the Coulomb interaction
212     !is  the same for up and down spins
213     IF(SUM(U_UP−U_DN)>1.e−7)THEN
214         STOP'CHECK␣THE␣COULOMB␣DEFINITION␣IN␣MN_IN.'
215     END IF
216     !The Number of Up and Down atoms are assumed to be the same
217     ! all the time.
218     Natoms=NatomsUP
219     NdimUP=COMB(NsiteUP,NeUP)
220     NdimDN=COMB(NsiteDN,NeDN)
221     Ndim=NdimUP*NdimDN
222     ALLOCATE(HUP(NdimUP,NdimUP) ,HDN(NdimDN,NdimDN),NZ(NDIM))
223     ! SPIN UP
224     !form the UP Basis Set
225     ALLOCATE(BasisSetUP(NdimUP,NsiteUP+1) )
226     CALL BASIS_FORM(NsiteUP,NeUP,NdimUP,BasisSetUP)
227     Nsite=NsiteUP
228     ALLOCATE(E0(Nsite),T_h(Nsite,Nsite) ,U(Nsite,Nsite) ,BasisSet(NdimUP,Nsite+1) )
229     E0=E0UP
230     T_h=T_hUP
231     BasisSet=BasisSetUP
232     U= U_UP
233     CALL form_offd_H(NdimUP,HUP)
234     CALL form_diag_H(NdimUP,HUP)
235     DEALLOCATE(E0,T_h,U,BasisSet
236     ! SPIN DOWN
```

109

```
237    !form the DN Basis Set
238    ALLOCATE(BasisSetDN(NdimDn,NsiteDN+1) )
239    CALL BASIS_FORM(NsiteDN,NeDN,NdimDN,BasisSetDN)
240    Nsite=NsiteDN
241    ALLOCATE(E0(Nsite),T_h(Nsite,Nsite),U(Nsite,Nsite),BasisSet(NdimDN,Nsite+1) )
242    E0=E0DN
243    T_h=T_hDN
244    BasisSet=BasisSetDN
245    U=U_DN
246    !Symetricity:
247    ! If the UP and DOWN dimensions are the same,
248    !the off−diagonal elements of HUP & HDN will
249    !be identical . In that case there is no need to
250    ! recalculate the off−diagonal terms of HDN
251    IF (NdimUP/=NdimDn)THEN
252        CALL FORM_offd_H(NdimDN,HDN)
253    ELSE
254        HDN=HUP
255    END IF
256    CALL FORM_diag_H(NdimDN,HDN)
257    DEALLOCATE(E0,T_h,BasisSet,U)
258    !Form The total Basis Set − Needed to calculate
259    !the Coulomb & Hund's rule couplings
260    ALLOCATE(BasisSet(Ndim,1+NsiteUP+NsiteDN) )
261    k=1
262    DO i=1,NdimUP
263        DO j=1,NdimDN
264            BasisSet(k,1)=k
265            BasisSet(k,2:NsiteUP+1)=BasisSetUP(i,2:)
266            BasisSet(k,2+NsiteUP:)=BasisSetDN(j,2:)
267            k=k+1
268        END DO
269    END DO
270    !
271    ! At this Point we deviate from the small Cluster Method:
272    ! Instead of forming the full HAMILTON and storing in memory,
273    ! we only determine which elements are Non−Zero from the
274    ! HUP & HDN matrices, calculate only those, and output the
275    ! results to a file .
276    CALL TENSPROD(NdimUP,NdimDN,HUP,HDN)
277    DEALLOCATE(BasisSet,BasisSetUP,BasisSetDN,OrbDensUP,OrbDensDN,phi,psi,HUP,HDN,EHund,T_hUP,T
278 CONTAINS
279    SUBROUTINE TENSPROD(N,M,A,B)
280        ! This is similar to the FUNCTION TENSPROD,
281        ! However this SUBROUTINE version takes the
282        ! A x B (i,j) element and stores it in a
283        ! file instead of in an array
284        !
285        CHARACTER(LEN=5)::OUTPUT
286        INTEGER,INTENT(in)::N,M
287        INTEGER::i1,j1,k,l
288        REAL*8,DIMENSION(N,N),INTENT(in)::A
289        REAL*8,DIMENSION(M,M),INTENT(in)::B
290        REAL*8,DIMENSION(N,N)::ONE_N
291        REAL*8,DIMENSION(M,M)::ONE_M
292        REAL*8::AxB,y
293        OPEN(99,FILE=OUTPUT_FILE)
294        OPEN(88,FILE='COUNTS')
295        ALLOCATE(psi(Nsite),phi(Nsite))
296        ONE_N=0.0;ONE_M=0.0
297        DO i=1,N
298            ONE_N(i,i)=1.0
299        END DO
300        DO i=1,M
```

110

```
301            ONE_M(i,i)=1.0
302         END DO
303         NZcount=0
304         NZ=0.0
305         iloopUP:DO k=1,N
306            iloopDN:DO i=1,M
307               jloopUP:DO l=1,N
308                  IF(A(k,l)==0.0 .AND. k/=l)THEN
309                     CYCLE jloopUP
310                  END IF
311                  !            iloopDN:DO i=1,M
312                  jloopDN:DO j=1,M
313                     IF(B(i,j)==0.0 .AND. j/=i)THEN
314                        CYCLE jloopDN
315                     END IF
316                     ! From the indices of HUP & HDN
317                     ! we calculate the corresponding i1,j1
318                     i1=(k-1)*M+i ;    j1=(l-1)*M+j
319                     AxB=A(k,l)*ONE_M(i,j)+ONE_N(k,l)*B(i,j)
320                     IF(i1==j1)THEN
321                        !-site Coulomb interaction*************
322                        ! For each DIAGONAL state, count the number
323                        ! of electrons in each atom and add the
324                        ! Coulomb and Hund's exchange energies
325                        psi=BasisSet(i1,2:NsiteUP+1)   !Up electrons
326                        phi=BasisSet(i1,NsiteUP+2: )   !Down "
327                        DO atom1=1,Natoms
328                           NelUp=0;NelDN=0
329                           ! This is to account for the
330                           ! missing Hund's exchange when
331                           ! some of the orbitals are not
332                           ! explicitly included.
333                           IF(MAGTYP=='FM')THEN
334                              IF(atom1==1)NelUP=Nmiss;NelDN=0
335                              IF(atom1==3)NelUP=Nmiss;NelDN=0
336                           ELSE
337                              IF(atom1==1)THEN
338                                 NelUP=Nmiss;NelDN=0
339                              END IF
340                              IF(atom1==3)THEN
341                                 NelUP= 0  ;NelDN=Nmiss
342                              END IF
343                           END IF
344                           Nelec=0
345                           DO orb1=1,OrbDensUP(atom1)
346                              ! From the atom and orbital indices,
347                              !find the site index
348                              CALL find_site(Nsite,OrbDensUP,atom1,orb1,n1)
349                              !Calculate the number of electrons from
350                              !the occupation of the state
351                              Nelec=Nelec+psi(n1)+phi(n1)
352                              NelUP=NelUP+psi(n1)
353                              NelDN=NelDN+phi(n1)
354                           END DO
355                           CALL find_site(Nsite,OrbDensUP,atom1,1,n2)
356                           AxB=AxB+ U_UP(n2,n2)*Nelec*(Nelec-1)/2 &
357                                + NelUP*NelDN*EHund(atom1)
358                           y=NelUP*NelDN*EHund(atom1)
359                        END DO
360                     END IF
361                     IF (AxB/=0.0.OR.i1==j1)THEN
362                        NZcount=NZcount+1
363                        WRITE(99,*)i1,j1,AxB
364                        NZ(i1)=NZ(i1)+1
```

111

```fortran
365              END IF
366          END DO jloopDN
367        END DO jloopUP
368      END DO iloopDN
369    END DO iloopUP
370    WRITE(88,*)NZcount,Ndim,NdimUP,NdimDN
371    WRITE(88,'(i5)')NZ
372    NZMAX=MAXVAL(NZ)
373    CLOSE(99);CLOSE(88)
374  END SUBROUTINE TENSPROD
375  SUBROUTINE FORM_offd_H(Ndim,H)
376    INTEGER,INTENT(IN)::Ndim
377    REAL*8,DIMENSION(Ndim,Ndim),INTENT(OUT)::H
378    INTEGER::sgn
379    ! Calculates T_he first two terms of the Hamiltonian:
380    !     The on-site energies term
381    !         +
382    !       the Hopping term
383    ! This is done simply by calculating the following term:
384    !        H(i,j)=SUM_{l,m}[T(l,m) <i|c+_{l}c_{m}|j>]
385    H=0.0
386    DO i=1,Ndim
387      !Hopping energy term
388      DO j=i+1,Ndim
389        H(i,j)=0.0
390        DO m=1,Nsite
391          DO n=1,Nsite
392            IF(n==m)CYCLE
393            sgn=-(-1)**( SUM(BasisSet(j,2:n))+SUM(BasisSet(i,2:m)) )
394            !<i|c+_{n}c_{m}|j>*T(n,m)
395            H(i,j)=H(i,j)+sgn*DOT(Nsite,BasisSet(i,2:Nsite+1),&
396                Creates(Nsite,n,&
397                Destroy(Nsite,m,BasisSet(j,2:Nsite+1)) )   )*T_h(n,m)
398          END DO
399        END DO
400        H(j,i)=H(i,j)
401      END DO
402    END DO
403  END SUBROUTINE FORM_OFFD_H
404  SUBROUTINE FORM_diag_H(Ndim,H)
405    INTEGER,INTENT(IN)::Ndim
406    REAL*8,DIMENSION(Ndim,Ndim),INTENT(OUT)::H
407    DO i=1,Ndim
408      !On-site energy: SUM_{i}[ E(k)<psi(i)|n(k)|psi(i)> ]
409      H(i,i)=0.0
410      DO l=1,Nsite
411        H(i,i)=H(i,i)+BasisSet(i,1+l)*E0(l)
412      END DO
413    END DO
414  END SUBROUTINE form_diag_H
415  INTEGER FUNCTION FSIGN(k,l)RESULT(sgn)
416    INTEGER::k,l
417    sgn=0
418    IF(l==1)THEN
419      sgn=0
420      RETURN
421    END IF
422    sgn=SUM(BasisSet(k,2:l))
423  END FUNCTION FSIGN
424  SUBROUTINE READATA(INPUT_FILE)
425    INTEGER::Natoms,n
426    REAL*8::t,E,Ucoul
427    CHARACTER(LEN=5)::INPUT_FILE
```

```fortran
428     OPEN(10,FILE=INPUT_FILE)
429     DO i=1,10000
430       READ(10,'(a)',END=100)inline
431       IF(INDEX(inline,'*00')/=0)THEN
432          ! Reads the number of atoms in the cluster
433          READ(10,*)NatomsUP,NatomsDN
434          ! Allocate the dimension of the orbital density arrays
435          ALLOCATE(OrbDensUP(NatomsUP),OrbDensDN(NatomsDN))
436          OrbDensUP=0;OrbDensDN=0
437       ELSEIF(INDEX(inline,'*01')/=0)THEN
438          ! Reads the orbital density matrices
439          READ(10,'(a)')inline
440          IF(INDEX(inline,'UP')/=0)THEN
441             ! Spin Up Density Matrix:
442             DO k=1,NatomsUP
443                READ(10,*)OrbDensUP(k)
444             END DO
445             READ(10,'(a)')inline
446             ! Spin Down Density Matrix:
447             DO k=1,NatomsDN
448                READ(10,*)OrbDensDN(k)
449             END DO
450          END IF
451       ELSEIF(INDEX(inline,'*02')/=0)THEN
452          READ(10,'(a)')inline
453          ! Reads the no. of electrons with spin UP/DOWN
454          IF(INDEX(inline,'UP')/=0)THEN
455             READ(10,*)NeUP ! no. of Up e-
456             READ(10,'(a)')inline
457             READ(10,*)NeDN ! no. of Down e-
458          END IF
459       END IF
460     END DO
461 100 CONTINUE
462     ! At this point all the information about the structure
463     ! of the cluster has been gathered from the input file(s)
464     ! In the next section we read the hopping matrix elements
465     ! Calculate the no. of sites by adding up all the orbitals
466     ! accessible to the itinerant e-'s:
467     NsiteUP=SUM(OrbDensUP); NsiteDN=SUM(OrbDensDN)
468     ! Calculate the TOTAL no. of possible hopping paths
469     ! for Up & Down spins.
470     NhoppsUP=COMB(NsiteUP,2); NhoppsDN=COMB(NsiteDN,2)
471     ! The Koster Slater Mat. elements
472     ALLOCATE(T_hUP(NsiteUP,NsiteUP) ,T_hDN(NsiteDN,NsiteDN) ,U_UP (NsiteUP,NsiteUP),U_DN (Nsi
473     T_hUP=0.0 ;   T_hDN=0.0 ;    U_UP=0.0 ;    U_DN=0.0
474     ! On-site energies
475     ALLOCATE(E0UP(NsiteUP) ,E0DN(NsiteDN) )
476     E0UP =0.0 ; E0DN=0.0
477     ! Read the matrix elements from "CU_IN".
478     REWIND(10)
479     DO i=1,1000
480       READ(10,'(a)',END=200)inline
481       IF(INDEX(inline,'*10')/=0)THEN
482          !Read the Up on-site energies
483          READ(10,'(a)')inline
484          DO j=1,NsiteUP
485             READ(10,*)i_atom,i_orb,E
486             CALL find_site(NatomsUP,OrbDensUP,i_atom,i_orb,n)
487             E0UP(n)=E
488          END DO
489          !Read the Down on-site energies
490          READ(10,'(a)')inline
```

113

```
491        DO j=1,NsiteDN
492           READ(10,*)i_atom,i_orb,E
493           CALL find_site(NatomsDN,OrbDensDN,i_atom,i_orb,n)
494           E0DN(n)=E
495        END DO
496     END IF
497     IF(INDEX(inline,'*20')/=0)THEN
498        READ(10,'(a)')inline !ReadtThe Up K.S. hopping elements
499        READ(10,*)M
500        DO j=1,M
501           READ(10,*)atom1,orb1,atom2,orb2,t
502           CALL find_site(NatomsUP,OrbDensUP,atom1,orb1,n1)
503           CALL find_site(NatomsUP,OrbDensUP,atom2,orb2,n2)
504           T_hUP(n1,n2)=t
505           T_hUP(n2,n1)=t
506        END DO
507        READ(10,'(a)')inline
508        READ(10,*)M   !Read the Down K.S. hopping elements
509        DO j=1,M
510           READ(10,*)atom1,orb1,atom2,orb2,t
511           CALL find_site(NatomsDN,OrbDensDN,atom1,orb1,n1)
512           CALL find_site(NatomsDN,OrbDensDN,atom2,orb2,n2)
513           T_hDN(n1,n2)=t
514           T_hDN(n2,n1)=t
515        END DO
516     END IF
517     ! Find The on−site Coulomb interaction terms
518     IF(INDEX(inline,'*30')/=0)THEN
519        READ(10,'(a)')inline
520        DO j=1,NatomsUP
521           READ(10,*)i_atom,Ucoul
522           DO k=1,OrbDensUP(i_atom)
523              DO l=1,OrbDensUP(i_atom)
524                 CALL find_site(NsiteUP,OrbDensUP,i_atom,k,n1)
525                 CALL find_site(NsiteUP,OrbDensUP,i_atom,l,n2)
526                 U_UP(n1,n2)=Ucoul
527              END DO
528           END DO
529        END DO
530        READ(10,'(a)')inline
531        DO j=1,NatomsDN
532           READ(10,*)i_atom,Ucoul
533           DO k=1,OrbDensDN(i_atom)
534              DO l=1,OrbDensDN(i_atom)
535                 CALL find_site(NsiteDN,OrbDensDN,i_atom,k,n1)
536                 CALL find_site(NsiteDN,OrbDensDN,i_atom,l,n2)
537                 U_DN(n1,n2)=Ucoul
538              END DO
539           END DO
540        END DO
541     END IF
542     ! Read The inter−atomic Coulomb interaction terms
543     IF (INDEX(inline,'*40')/=0)THEN
544        READ(10,'(a)')inline
545        READ(10,*)Ncoul
546        IF(Ncoul == 0)EXIT
547        DO j=1,Ncoul
548           READ(10,*)atom1,atom2,Ucoul
549           DO k=1,OrbDensUP(atom1)
550              DO l=1,OrbDensUP(atom2)
551                 CALL FIND_SITE(NsiteUP,OrbDensUP,atom1,k,n1)
552                 CALL FIND_SITE(NsiteUP,OrbDensUP,atom2,l,n2)
```

```fortran
553                    U_UP(n1,n2)=Ucoul
554                    U_UP(n2,n1)=Ucoul
555                END DO
556              END DO
557            END DO
558            READ(10,'(a)')inline
559            READ(10,*)Ncoul
560            DO j=1,Ncoul
561              READ(10,*)atom1,atom2,Ucoul
562              DO k=1,OrbDensDN(atom1)
563                DO l=1,OrbDensDN(atom2)
564                  CALL FIND_SITE(NsiteDN,OrbDensDN,atom1,k,n1)
565                  CALL FIND_SITE(NsiteDN,OrbDensDN,atom2,l,n2)
566                  U_DN(n1,n2)=Ucoul
567                  U_DN(n2,n1)=Ucoul
568                END DO
569              END DO
570            END DO
571          END IF
572        END DO
573   200  CONTINUE
574        ALLOCATE(EHUND(NatomsUP))
575        REWIND(10)
576        DO i=1,1000
577          READ(10,'(a)',END=300)inline
578          ! Read Hund's rule energy
579          IF (INDEX(inline,'*50:')/=0)THEN
580            DO j=1,NatomsUP
581              READ(10,*)atom1,EHund(atom1)
582            END DO
583          END IF
584        END DO
585   300  CONTINUE
586        CLOSE(10)
587      END SUBROUTINE READATA
```

$C_{i\alpha\sigma}^{\dagger}$ function

```fortran
588      FUNCTION CREATES(Nsite,i_site,psi) RESULT(phi)
589        ! The Creation operator acting on a state vetor: c+|psi>
590        !  As input:
591        !   * Nsite     : T_he dimension of the state
592        !                 [i.e. the total no. of
593        !               sites =sum(OrbDens)]
594        !   * i_site: T_he site at which the function operates
595        !  As output:
596        !   * psi    : T_he resulting vector = c+|psi>
597        INTEGER,INTENT(IN)::i_site
598        INTEGER,INTENT(IN)::Nsite
599        INTEGER,DIMENSION(Nsite),INTENT(IN)::psi
600        INTEGER,DIMENSION(Nsite)::phi
601        IF(psi(i_site)==1)THEN
602          phi=-20
603        ELSE IF(psi(i_site)==0)THEN
604          phi=psi
605          phi(i_site)=1
606        END IF
607      END FUNCTION Creates
```

$C_{i\alpha\sigma}$ function

```fortran
608      FUNCTION DESTROY(Nsite,i_site,psi) RESULT(phi)
609        ! The Destruction operator acting on a state vetor: c|psi>
610        !  As input:
611        !   * Nsite     : T_he dimension of the state
```

```
612    !                      [i.e. the total no. of
613    !                  sites =sum(OrbDens)]
614    !     * i_site: T_he site at which the function operates
615    !   As output:
616    !     * psi    : T_he resulting vector = c|psi>
617    INTEGER,INTENT(IN)::i_site
618    INTEGER,INTENT(IN)::Nsite
619    INTEGER,DIMENSION(Nsite),INTENT(IN)::psi
620    INTEGER,DIMENSION(Nsite)::phi
621    IF(psi(i_site)==0)THEN
622        phi=20
623    ELSE IF(psi(i_site)==1)THEN
624        phi=psi
625        phi(i_site)=0
626    END IF
627  END FUNCTION DESTROY
628  !    DOT Product
629  FUNCTION DOT(Ns,phi,psi) RESULT(x)
630    INTEGER,INTENT(IN)::Ns
631    INTEGER,INTENT(IN),DIMENSION(Ns)::phi,psi
632    INTEGER::x,i
633    x=1
634    DO i=1,Ns
635        IF(phi(i)/=psi(i)) x=0
636    END DO
637  END FUNCTION DOT
638  SUBROUTINE FIND_SITE(Natoms,Orb_Dens,i_atom,i_orb,i_site)
639  ! Given Atomic and Orbital indices this calculates the Site index
640  !    * N_atoms : T_he no. of atoms
641  !    * Orb_Dens: An array of dimension N_atoms such that
642  !          Orb_Dens(i) is the number of orbitals in the i−th atom
643  !    * i_atom : T_he given atomic index
644  !    * i_orb   : T_he given orbital index
645  !    * i_site     : T_he site index
646  !   See notes for method of calculation
647    INTEGER,DIMENSION(Natoms),INTENT(IN)::Orb_Dens
648    INTEGER,INTENT(OUT)::i_site
649    IF(i_atom==1)THEN
650        i_site=i_orb
651    ELSE IF(i_atom>1)THEN
652        i_site=SUM(Orb_Dens(1:i_atom−1))+i_orb
653    ELSE
654        STOP 'You␣entered␣an␣invalid␣atomic␣index'
655    END IF
656  END SUBROUTINE FIND_SITE
657  INTEGER FUNCTION COMB(n,m) RESULT(bino)
658    INTEGER,INTENT(IN)::N,M
659    INTEGER::i
660    REAL*8::L1=0,L2=0
661    L1=0.0
662    DO i=M+1,N
663        L1=L1+LOG(1.0*i)
664    END DO
665    L2=0.0
666    DO i=1,N−M
667        L2=L2+LOG(1.0*i)
668    END DO
669    bino=NINT(EXP(L1−L2))
670  END FUNCTION COMB
671  RECURSIVE FUNCTION FACTORIAL(N) RESULT(N_Fact)
672    INTEGER, INTENT(IN)::N
673    INTEGER :: N_Fact
674    IF (N>0)THEN
```

116

```
675          N_Fact = N * factorial(N−1)
676        ELSE
677          N_Fact=1
678        END IF
679      END FUNCTION FACTORIAL
680    END SUBROUTINE CLUSTER
681    !* This module is used to declare common variables *!
682    MODULE Variables
683      IMPLICIT NONE
684      CHARACTER(LEN=40)::inline
685      CHARACTER(LEN=2) ::MAGTYP
686      INTEGER::NatomsUP,NatomsDN,NeUP,NeDN,Nmiss
687      INTEGER::Nsite,NsiteUP,NsiteDN,NZcount,NZMAX
688      INTEGER::Nhopps,NhoppsUP,NhoppsDN,NdimUP,NdimDN,Ndim
689      INTEGER::i_atom,i_orb,Ncoul,Nelec,NelUP,NelDN,icount
690      INTEGER::atom1,atom2,orb1,orb2
691      INTEGER::i,j,k,l,m,n,n1,n2
692      INTEGER,ALLOCATABLE,DIMENSION(:,:)::BasisSet,BasisSetUP,BasisSetDN
693      INTEGER,ALLOCATABLE,DIMENSION(:)::OrbDensUP,OrbDensDN
694      INTEGER,ALLOCATABLE,DIMENSION(:)::phi,psi,NZ
695      REAL*8::lambda
696      REAL*8,DIMENSION(3)::Jh
697      REAL*8,ALLOCATABLE,DIMENSION(:,:):: HUP,HDN,HAMILTON
698      REAL*8,ALLOCATABLE,DIMENSION(:,:):: T_h,T_hUP,T_hDN
699      REAL*8,ALLOCATABLE,DIMENSION(:,:):: U,U_UP,U_DN
700      REAL*8,ALLOCATABLE,DIMENSION(:)::E0,E0UP,E0DN,EHund
701      REAL*8::Elow,E1,E2,E3,E4
702     REAL*8,PARAMETER::pi=3.141592653589793d0
703    END MODULE VARIABLES
704    SUBROUTINE DLANCZOSMETH(FILE,NDIM,NZ,NZMAX,NLCZ,E0,INFO,SUCCESS,Delta)
705      IMPLICIT NONE
```

Read The Non zero matrix elements and their indices from the file "INPUTFILE" and compute the ground state energy using the Lanczos diagonalization scheme.

```
706      INTEGER::i,j,k,l,m,n,p,q,INFO,LDZ,LWORK !integer dummy variables
707      INTEGER,INTENT(IN)::NDIM !dimension of the Hilbert space
708      INTEGER,INTENT(IN)::NZMAX !Max. number of non−zero elements per row
709      INTEGER,INTENT(IN),DIMENSION(NDIM)::NZ ! Number of n−z elements in each row
710      INTEGER,INTENT(IN)::NLCZ ! The Number of Lanczos iterations
711      INTEGER,INTENT(OUT)::SUCCESS !=1 if covergence is acheived, =0 otherwise
712      INTEGER,DIMENSION(NDIM,NZMAX)::JD !index of n−z elements in each row.
713      CHARACTER(LEN=5),INTENT(IN)::FILE
714      CHARACTER(LEN=1)::JOBZ='N'
715      real*8,parameter::toler=1.e−6 !radius of convergence criterion
716      REAL*8::E_OLD=0.0,qdrng,x !real dummy variables
717      REAL*8,INTENT(OUT)::E0 !Ground−state energy
718      REAL*8,INTENT(OUT)::Delta !convergence radius
719      REAL*8,DIMENSION(NLCZ)::D
720      REAL*8,DIMENSION(NLCZ+1)::F
721      REAL*8,DIMENSION(NDIM)::g
722      REAL*8,DIMENSION(2,NDIM)::c
723      REAL*8,DIMENSION(NDIM)::cTMP
724      REAL*8,DIMENSION(NDIM,NZMAX)::HD
725      REAL*8,ALLOCATABLE,DIMENSION(:)::LANCZ_DIAG,LANCZ_OFFD,ZWORK
726      REAL*8,ALLOCATABLE,DIMENSION(:,:)::ZDUM
727      JD=0.0;HD=0.0
728      E0=−17.
729      OPEN(10,file=FILE)
730      ! Read The Non−zero matrix elements and their
731      ! indices from FILE
732      DO k=1,NDIM
733        DO l=1,NZ(k)
734          READ(10,*)i,JD(i,l),HD(i,l)
```

117

```fortran
735         END DO
736       END DO
737       CLOSE(10)
738       E_OLD=qdrng()! Take a random guess of the energy
739       ! Start the run by calculating
740       ! F(1),{c(1,j)},{g(1,j)},D(1),F(2) and {c(2,j)}
741       F(1)=0.0d0;C=0.0d0;G=0.0d0;D=0.0d0
742       DO i=1,NDIM
743          c(1,i)=qdrng()  ! Random guess of the initial Gram-Schmidt vector
744       END DO
745       c(1,:)=c(1,:)/SQRT(SUM(c(1,:)**2)) !Normalize {c(1,j)}
746       !First diagonal element
747       D(1)=0.0d0
748       DO i=1,NDIM !Cycles over all rows
749          DO j=1,NZMAX ! Cycles over non-zero elements in each row
750             IF(JD(i,j)==0)CYCLE
751             D(1)=D(1)+c(1,i)*c(1,JD(i,j))*HD(i,j)
752          ENDDO
753       ENDDO
754       !First   intermediate vector in the Gram-Schmidt orthogonalization
755       g=0.0
756       DO j=1,NDIM
757          DO l=1,NZMAX
758             IF(JD(j,l)==0)CYCLE
759             g(j)=g(j)+c(1,JD(j,l))*HD(j,l)
760          ENDDO
761       ENDDO
762       !First  off-diagonal element
763       F(2)=0.0
764       DO i=1,NDIM
765          F(2)=F(2)+( g(i)-D(1)*c(1,i) )**2
766       END DO
767       F(2)=SQRT(F(2))
768       !2ND Gram-Schmidt vector
769       DO j=1,NDIM
770          c(2,j)=(g(j)-D(1)*c(1,j))/ABS(F(2))
771       ENDDO
772       !Compute the remaining Lanczos numbers
773       DO K=2,NLCZ
774          LDZ=NLCZ
775          !The K-th diagonal
776          D(k)=0.0d0
777          DO i=1,NDIM
778             DO j=1,NZMAX
779                IF(JD(i,j)==0 )EXIT
780                D(k)=D(k)+c(2,i)*c(2,JD(i,j))*HD(i,j)
781             ENDDO
782          ENDDO
783          !k-th intermediate vector in the Gram-Schmidt orthogonalization
784          g=0.0d0
785          DO j=1,NDIM
786             DO l=1,NZMAX
787                IF(JD(j,l)==0)EXIT
788                g(j)=g(j)+c(2,JD(j,l))*HD(j,l)
789             ENDDO
790          ENDDO
791          !The K-th off-diagonal
792          F(k+1)=0.0
793          DO i=1,NDIM
794             F(k+1)=F(k+1)+( g(i)-F(k)*c(1,i)-D(k)*c(2,i) )**2
795          END DO
796          F(k+1)=SQRT(F(k+1))
797          !(k+1)-th Gram-Schmidt vector
798          cTMP(:)=c(2,:)
```

118

```
799      DO j=1,NDIM
800         c(2,j)=(g(j)−F(k)∗c(1,j)−D(k)∗c(2,j) )/ABS(F(k+1))
801      ENDDO
802      c(1,:)=cTMP(:)
803      !Diagonalization of the Lanczos Matrix
804      ALLOCATE (LANCZ_DIAG(K),LANCZ_OFFD(K−1),ZDUM(K,K),ZWORK(2∗K−2))
805      LDZ=K
806      LANCZ_DIAG(:)=D(1:K)
807      LANCZ_OFFD(:)=F(2:K+1)
808      ZDUM=0.0
809      !Subroutine to diagonalize a tri−diagonal matrix from the LAPACK
810      !library. Type 'man dstev' at the prompt for more details.
811      CALL DSTEV (JOBZ, K, LANCZ_DIAG, LANCZ_OFFD, ZDUM,LDZ, ZWORK, INFO)
812      x=LANCZ_DIAG(1)
813      Delta=abs(x−E_OLD)
814      ! Check the convergence at the k−th iteration
815      if(Delta<toler)then ! If successfull
816         SUCCESS=1       ! =1 if successfull
817         INFO=K          ! Number of Lanczos iterations
818         E0=x            ! ground−state energy
819         DEALLOCATE (LANCZ_DIAG,LANCZ_OFFD,ZDUM,ZWORK)
820         goto 100
821      else
822         SUCCESS=0       ! =0 if unsuccessfull
823         E_OLD=x         ! The old energy becomes the new one
824         E0=−19          ! To check if the energy has converged after NLCZ steps.
825      end if
826      DEALLOCATE (LANCZ_DIAG,LANCZ_OFFD,ZDUM,ZWORK)
827      ENDDO
828  100 continue
829      RETURN
830  END SUBROUTINE DLANCZOSMETH
```

QUICK AND DIRTY Random Number Generator (From Numerical Recipes)

```
831  FUNCTION qdrng()
832  INTEGER,PARAMETER::a=9301,m=233280,c=49297
833  INTEGER::jran=233267
834  REAL∗8::qdrng
835  jran=MOD(jran∗a+c,m)
836  qdrng=float(jran)/float(m)
837  END FUNCTION qdrng
```

Bibliography

[1] E. Chappel, M. D. Núñez Regueiro, G. Chouteau, O. Isnard, and C. Darie, "Study of the ferrodistorsive orbital ordering in nanio$_2$ by neutron diffraction and submillimeter wave ESR," *Eur. Phys. J. B*, vol. 17, p. 615, 2000.

[2] E. A. Harrison, *Electronic Structure and the Properties of Solids*. San Francisco: Freeman, 1980.

[3] E. Chappel, M. D. Núñez Regueiro, F. Dupont, G. Chouteau, C. Darie, and A. Sulpice, "Antiferromagnetic resonance and high magnetic field properties of NaNiO$_2$," *Eur. Phys. J. B*, vol. 17, p. 609, 2000.

[4] L. D. Dyer, D. S. Borie, Jr., and G. P. Smith, "Alkali metal-nickel oxides of the type MNiO$_2$," *J. Am. Chem. Soc.*, vol. 76, p. 1499, 1954.

[5] J.-H. Chung, T. Proffen, A. M. Ghorayeb, L. Croguennec, W. Tian, B. Sales, R. Jin, D. Mandrus, and T. Egami, "Local structure of LiNiO$_2$ studied by neutron diffraction," *Phys. Rev. B*, vol. 71, p. 064410, 2005.

[6] H. Meskine, T. Saha-Dasgupta, and S. Satpathy, "Is the self-traped polaron energetically stable in the electron-doped manganites?," *Phys. Rev. Lett.*, vol. 92, p. 056401, 2004.

[7] A. J. Millis, "Double exchange alone does not explain the resistivity of La$_{1-x}$Sr$_x$MnO$_3$," *Phys. Rev. Lett.*, vol. 74, 1995.

[8] M. B. Salamon and M. Jaime, "The physics of manganites: Structure and transport," *Rev. Mod. Phys.*, vol. 73, p. 583, 2001.

[9] G. Jonker and J. van Santen, "Ferromagnetic compounds of manganese with perovskite structure," *Physica*, vol. 16, p. 337, 1950.

[10] E. O. Wollan and E. C. Koehler, "Neutron diffraction study of the magnetic properties of the series of perovskite-type compounds $La_{1-x}Ca_xMnO_3$," *Phys. Rev.*, vol. 100, p. 545, 1955.

[11] J. B. Goodenough, *Magnetism and the Chemical Bond.* New York: Interscience, 1963.

[12] D. Khomskii, *Electronic Structure, Exchange and Magnetism in Oxides.* Berlin: Springer-Verlag, 2001.

[13] S. Satpathy, Z. S. Popović, and F. R. Vukajlović, "Electronic structure of the perovskite oxides:$La_{1-x}Ca_xMnO_3$," *Phys. Rev. Lett.*, vol. 76, p. 960, 1996.

[14] J. P. Franck, I. Isaac, E. Chen, J. Chrzanowski, and J. C. Irwin, "Oxygen-isotope effect of the paramagnetic-insulating to ferromagnetic-metallic transition in $La_{1-x}Ca_xMnO_3$," *Phys. Rev. B*, vol. 58, no. 9, pp. 5189–5192, 1998.

[15] I. Isaac and J. P. Franck, "Oxygen-isotope effect on the charge-ordering transition of $La_{1-x}Ca_xMnO_3$," *Phys. Rev. B*, vol. 57, no. 10, pp. R5602–R5605, 1998.

[16] E. Dagotto, *Nanoscale Phase Separation and Colossal Magnetoresistance.* Berlin: Springer, 2002.

[17] R. D. Mattuck, *A Guide to Feynman Diagrams in the Many-Body Problem.* New York: Dover, 2nd ed., 1976.

[18] S. S. M. Wong, *Computational Methods in Physics and Engineering.* Prentice-Hall, 1992.

[19] H. Fehske, H. Röder, G. Wellein, and A. Mistriotis, "Hole-polaron formation in the two-dimensional Holstein $t - J$ model: A variational lanczos study," *Phys. Rev. B*, vol. 51, no. 23, pp. 16582–16593, 1995.

[20] H. Röder, J. Zang, and A. R. Bishop, "Lattice effects in colossal-magnetoresistance manganites," *Phys. Rev. Lett.*, vol. 76, no. 8, p. 1356, 1996.

[21] P. Hohenberg and E. Kohn, "Inhomogeneous electron gas," *Physical Review*, vol. 136, no. 3B, pp. B864–B871, 1964.

[22] E. Kohn and L. J. Sham, "Self-consistent equations including exchange and correlation effects," *Physical Review*, vol. 140, no. 4A, pp. A1133–A1138, 1965.

[23] A. J. Millis, "Cooperative Jahn-Teller effect and electron-phonon coupling in $La_{1-x}A_xMnO_3$," *Phys. Rev. B*, vol. 53, p. 8434, 1996.

[24] A. J. Millis, "Lattice effects in magnetoresistive manganese perovskitesr," *Nature*, vol. 392, p. 147, 1998.

[25] G. M. Zhao, K. Conder, and K. A. Mueller, "Giant oxygen isotope shift in the magnetoresistive perovskite $La_{1-x}Ca_xMnO_{3+y}$," *Nature*, vol. 381, p. 676, 1996.

[26] C. Zener, "Interaction between the d-shells in the transition metals. ii. ferromagnetic compounds of manganese with perovskite structure," *Phys. Rev.*, vol. 82, p. 403, 1951.

[27] P. E. Anderson and H. Hasegawa, "Considerations on double exchange," *Phys. Rev.*, vol. 100, p. 675, 1955.

[28] J. Kanamori, "Crystal distortion in magnetic compounds," *J. Appl. Phys.*, vol. 31, p. S14, 1960.

[29] J. H. Van Vleck, "Jahn-Teller effect and crystalline Stark splitting for clusters of the form XY_6, the," *Journal of Chemical Physics*, vol. 7, p. 72, 1939.

[30] H. Meskine and S. Satpathy, "Jahn-Teller coupling and double exchange in the Van Vleck-Kanamori two-site model," *J. Appl. Phys.*, vol. 85, no. 8, p. 4346, 1999.

[31] S. Satpathy and Z. Popović, "Cooperative Jahn-Teller coupling in the manganites," *Phys. Rev. Lett.*, vol. 84, no. 7, p. 1603, 2000.

[32] A. N. Das and P. Choudhury, "Stability and nature of polarons in a two-site two-electron model," *Phys. Rev. B*, vol. 49, no. 18, p. 13219, 1994.

[33] J. Chaterjee and A. N. Das, "Comparison of perturbative expansion using different phonon bases of the two-site Holstein model," *Phys. Rev. B*, vol. 61, p. 4592, 7 2000.

[34] D. Mermin and H. Wagner, "Absence of ferromagnetism or antiferromagnetism in one- or two-dimensional isotropic Heisenberg models," *Phys. Rev. Lett.*, vol. 17, p. 1133, 1966.

[35] P. C. Hohenberg, "Existence of long-range order in one and two dimensions," *Phys. Rev.*, vol. 158, p. 383, 1967.

[36] E. I. Terukov, E. Reichelt, D. Ihle, and H. Oppermann, "Isotope effect on the Verwey transition temperature of magnetite," *Phys. Status Solidi B*, vol. 95, p. 491, 1979.

[37] S. Satpathy, "Effect of electron-phonon coupling on the double-exchange interaction," *Solid State Commun.*, vol. 112, no. 4, p. 195, 1999.

[38] O. K. Andersen and O. Jepsen, "Explicit, first-principles tight-binding theory," *Phys. Rev. Lett.*, vol. 53, no. 27, pp. 2571–2574, 1984.

[39] O. K. Andersen, "Linear methods in band theory," *Phys. Rev. B*, vol. 12, no. 8, pp. 3060–3083, 1975.

[40] V. I. Anisimov, F. Aryasetiawan, and A. I. Lichtenstein, "First-principles calculations of the electronic structure and spectra of strongly correlated systems: the LDA+U method," *J. Phys.: Condens. Matter*, vol. 9, p. 767, 1997.

[41] U. Von Barth and L. Hedin, "A local exchange-correlation potential for the spin polarized case I," *J. Phys. C*, vol. 5, no. 13, pp. 1629–1642, 1972.

[42] H. Meskine and S. Satpathy, "Ferrodistorsive orbital ordering in the layered nickelate NaNiO$_2$: a density functional study," *J. Appl. Phys.*, vol. 97, p. 10A314, 2005.

[43] M. V. Mostovoy and D. I. Khomskii, "Orbital ordering in frustrated Jahn-Teller systems with 90° exchange," *Phys. Rev. Lett.*, vol. 89, no. 22, p. 227203, 2002.

[44] L. Landau *Phy. Z. Sov. Un.*, vol. 3, p. 664, 1933.

[45] The expression Eq. (4.12) for the inter-layer exchange corrects the misprint in Eq. (4) in our earlier paper,[42] where a factor of two is missing.

[46] E. P. Su, J. R. Schrieffer, and A. J. Heeger, "Solitons in polyacetylene," *Phys. Rev. Lett.*, vol. 42, p. 1698, 1979.

[47] E. P. Su, J. R. Schrieffer, and A. J. Heeger, "Soliton excitations in polyacetylene," *Phys. Rev. B*, vol. 22, p. 2099, 1980.

[48] G. Wellein and H. Fehske, "Self-trapping problem of electrons or excitons in one dimension," *Phys. Rev. B*, vol. 58, p. 6208, 1998.

[49] L. G. Lang and Y. A. Firsov *Sov. Phys. JETP*, vol. 16, p. 1301, 1963.

[50] N. F. Oliveira, S. Foner, Y. Shapira, and T. B. Reed *Phys. Rev. B*, vol. 5, p. 2634, 1972.

[51] Y. Shapira, S. Foner, N. F. Oliveira, and T. B. Reed, "EuTe. II. resistivity and hall effect," *Phys. Rev. B*, vol. 5, no. 7, p. 2647, 1972.

[52] P. Wachter, "Photoconductivity of the magnetic semiconductor EuSe," *Solid State Commun.*, vol. 8, p. 473, 1970.

[53] S. Von Molnar and S. Methfessel, "Giant negative magnetoresistance in ferromagnetic Eu$_{1-x}$Gd$_x$Se," *J. Appl. Phys.*, vol. 38, p. 959, 1967.

[54] J. J. Neumeier and J. L. Cohn, "Possible signatures of magnetic phase segregation in electron-doped antiferromagnetic $CaMnO_3$," *Phys. Rev. B*, vol. 61, p. 14319, 2000.

[55] K. T., Y. A., and T. T., "Stability condition for the paramagnetic polaron in a magnetic semiconductor," *Solid State Commun.*, vol. 8, p. 1543, 1970.

[56] N. F. Mott, *Metal-Insulator Transitions.* London: Taylor and Francis, 1974.

[57] E. L. Nagaev *Sov. Phys. Solid State*, vol. 13, p. 961, 1971.

[58] S. Pathak and S. Satpathy, "Self-trapped magnetic polaron: Exact solution of a continuum model in one dimension," *Phys. Rev. B*, vol. 63, p. 214413, 2001.

[59] Y.-R. Chen and P. B. Allen, "Spin versus lattice polaron: Prediction for electron-doped $CaMnO_3$," *Phys. Rev. B*, vol. 64, no. 6, p. 064401, 2001.

[60] T. Saha-Dasgupta and S. Satpathy, "Wannier-like functions and tight-binding parametrization for the manganese bands in $CaMnO_3$," *J. Phys.: Cond. Matt.*, vol. 15, p. 1685, 2003.

[61] B. B. I., *The Jahn-Teller Effect and Vibronic Interaction in Modern Chemistry.* New York: Plenum, 1984.

[62] K. M. D. and V. B. G., *Cooperative Phenomena in Jahn-Teller Crystal.* Plenum, 1995.

[63] G. S. Rushbrooke and P. J. Eood, "Curie points and high-temperature susceptibilities of Heisenberg-model ferromagnetics," *Mol. Phys.*, vol. 1, p. 257, 1958.

[64] G. S. Rushbrooke and P. J. Eood *Mol. Phys.*, vol. 6, p. 409, 1963.

[65] M. E. Fisher *Rep. Prog. Phys.*, vol. 30, p. 615, 1967.

[66] A. M. Stoneham, "Small polarons and polaron transitions," *J. Chem. Soc., Faraday Trans. 2*, vol. 85, p. 505, 1989.

[67] N. A. Babushkina, L. M. Beova, O. Y. Gorbenko, A. R. Kaul, A. A. Bosak, V. I. Ozhogin, and K. I. Kugel, "Metal-insulator transistion induced by oxygen isotope exchange in the magnetoresistive perovskite manganites," *Nature*, vol. 391, p. 159, 1998.

VITA

Hakim Meskine was born on July 20, 1972, in Casablanca. He graduated in June of 1996 from the University Hassan II, Casablanca with a "License de Physique", with an emphasis on solid-state theory. He joined the Department of Physics and Astronomy at the University of Missouri-Columbia in August 1996 where he began work with Dr. Satpathy in the summer of 1997. He successfully defended this dissertation and received his PhD in May 2005. He then accepted a postdoctoral fellowship at the theory department of the Fritz-Haber Institute in Berlin to study Heterogeneous Catalysis using *ab initio* methods. The FHI is part of the Max-Planck Society, and has a strong program in surface science.